UNIVERSITÀ DI PADOVA

FACOLTÀ DI INGEGNERIA

Dipartimento di Ingegneria dell'Informazione

Scuola di Dottorato di Ricerca in Ingegneria dell'Informazione
Indirizzo: Bioingegneria

XXIII CICLO

BAYESIAN ESTIMATION TECHNIQUES FOR THE EXTRACTION OF EVENT - RELATED POTENTIALS IN NEUROSCIENCE

Direttore della Scuola: Ch.mo Prof. Matteo Bertocco

Supervisore: Ch.mo Prof. Giovanni Sparacino

Dottoranda: Costanza D'Avanzo

ABSTRACT

The study of the Event-Related Potentials (ERPs) represents a classic topic in neuroscience research. In fact, as discussed in Chapter 1 of this work, ERPs measured in response to sensory, cognitive and motor stimuli are crucial in the comprehension of many aspects of neurophysiology and, since their acquisition is relatively simple and non invasive, they also have several clinical applications. On the other hand, ERPs extraction is not a trivial question: ERPs signals are embedded in background spontaneous electroencephalographic (EEG) activity with much larger amplitude and common spectral content. The approach traditionally used for ERP extraction, the so-called Conventional Averaging (CA), presents well-known limitations. In the light of this, more sophisticated methodologies have been proposed in order to improve the average estimate and to provide a single-trial description of the ERPs; in Chapter 2 some of these techniques are described. In this thesis a Bayesian approach for the improved estimation of the average ERP and for the single-trial ERPs extraction is proposed. In particular, in Chapter 3 and 4 two new methods, with different degree of sophistication, are implemented. The first method is based on a two-stage procedure. In the first stage, an average ERP is determined as the weighted average of the available sweeps, previously processed by an individual optimal filter, in which a 2^{nd} order *a priori* statistical information on the involved signals is exploited. In the second stage, single-sweep estimation is dealt with within the same framework, by using the average ERP estimated in the previous stage as *a priori* expected response. The second method is based on a one-stage multi task learning procedure. Differently from the most estimation approaches, the method provides the estimate of the average and the single-trial responses by processing just once all the available sweeps simultaneously. The unknown single-trial ERPs are treated as the “individuals” of a homogenous population and the information available for a sweep is considered informative with respect to the other ones. The method assumes that the generic sweep can be modeled as the sum of three independent stochastic processes: an average curve of

population that is common to all the sweeps, an individual shift that differentiates each sweep from the others, a background EEG noise component varying sweep by sweep. Simulated datasets with different levels of signal-to-noise ratio (SNR) have been employed in order to test the performance of the proposed approaches in estimating the average ERP and the single-trial ERPs, also by varying the number of available sweeps. Results, discussed in Chapter 5, point out that the proposed approaches provide significantly better estimates of the average ERP with respect to the CA technique, for each of the tested SNR levels. In particular, with the new approaches, the number of sweeps needed for the average ERP estimation can be reduced of about 50 %. As far as the single-trial estimation is concerned, the proposed methods provide a significantly better reconstruction of the single-trial responses in comparison with a representative literature method, while results comparable with the above-mentioned method are obtained with regard to the estimation of latency and amplitude of P300 component. In Chapter 6, the proposed methods are applied to a real data set. This data set consists of EEG signals recorded on cirrhotic and normal subjects during a Simon task, a two-choice paradigm in which the subject is required to evaluate which stimulus, between the two possible target stimuli, appears on a monitor. In particular, the availability of the single trial P300 latencies and amplitudes has allowed to better understand the causes of the reduction in cirrhosis of the CA-based P300 amplitude and it has made possible the investigation of the relationship between the variability of P300 component and the variability of the behavioral measures.

SOMMARIO

Lo studio dei potenziali evento-relati (ERPs) è uno dei temi classici della ricerca neuro-scientifica. Infatti, come discusso nel Capitolo 1 di questo lavoro di tesi, gli ERPs misurati in risposta a stimoli sensoriali, cognitivi e motori sono cruciali nella comprensione di molti aspetti della neurofisiologia e, poiché la loro acquisizione è relativamente semplice e non invasiva, essi hanno anche diverse applicazioni cliniche. D'altro canto, l'estrazione degli ERPs è spesso molto difficile in quanto essi sono completamente immersi nell'attività elettroencefalografica spontanea (EEG) che ha una maggiore ampiezza ma comune contenuto spettrale. L'approccio tradizionalmente usato per estrarre gli ERPs, la cosiddetta media convenzionale (CA), ha delle riconosciute limitazioni. Alla luce di questo, sono state proposte delle metodologie più sofisticate aventi come scopo il miglioramento della stima media fornita dalla tecnica CA e l'estrazione single-trial degli ERPs; nel Capitolo 2 è fornita una descrizione di alcune di queste tecniche. In questa tesi si propone un approccio bayesiano per la stima degli ERPs; in particolare, nei Capitoli 3 e 4, sono presentati due nuovi metodi in grado fornire sia una stima dell'ERP medio che degli ERPs single-trial. Il primo metodo è basato su una procedura a due passi. Nel primo passo viene calcolato l'ERP medio. Esso è determinato come media pesata delle epoche a disposizione, una volta che queste ultime siano state individualmente filtrate sfruttando delle informazioni note *a priori* sulla statistica del secondo ordine dei segnali coinvolti. Nel secondo passo, gli ERPs delle singole epoche vengono stimati nello stesso contesto, usando l'ERP medio stimato al passo precedente come valore atteso *a priori*. Il secondo metodo è basato su una procedura multi-task learning ad un passo. Diversamente dalla maggior parte degli approcci proposti in letteratura, il metodo fornisce delle stime della risposta media e degli ERPs single-trial considerando simultaneamente tutte le sweeps a disposizione. I segnali ERPs incogniti sono trattato come "individui" di una popolazione omogenea e l'informazione disponibile per un'epoca è considerata utile per la stima di tutte le altre. Il metodo assume che la generica epoca possa essere modellata come la

somma di tre componenti stocastiche indipendenti: una curva media di popolazione che è comune a tutte le epoche, uno shift individuale che differenzia un'epoca dalle altre, una componente di rumore EEG di fondo che varia da un'epoca ad un'altra. Dataset simulati a diversi livelli di rapporto segnale-rumore (SNR) sono stati impiegati per testare la performance degli approcci proposti nell'estrazione dell'ERP medio e degli ERPs single-trial, anche al variare del numero delle sweep a disposizione. I risultati ottenuti, discussi nel Capitolo 5, dimostrano che gli approcci proposti forniscono delle stime dell'ERP medio significativamente migliori di quelle fornite dalla tecnica CA, per ogni livello di SNR testato. In particolare, con i metodi proposti il numero di sweeps per la stima della media può essere ridotto circa del 50 %. Per quanto riguarda la stima single-trial, i metodi proposti forniscono una ricostruzione significativamente migliore delle risposte single-trial se confrontati con un metodo rappresentativo della letteratura, mentre, in merito alla determinazione della latenza e dell'ampiezza della componente P300, i risultati forniti dai metodi proposti sono paragonabili a quelli ottenuti con il suddetto metodo. Nel Capitolo 6, infine, le tecniche proposte sono state applicate a dati reali. Questi dati consistono in segnali EEG registrati su soggetti normali e su pazienti cirrotici durante un compito Simon, un paradigma a doppia scelta in cui al soggetto è richiesto di valutare quale tra due possibili stimoli target appaia su un monitor. In particolare, la disponibilità dei parametri di latenza e ampiezza della P300 a livello single-trial ha permesso di capire le cause della riduzione dell'ampiezza della P300 misurata dalla tecnica CA e ha reso possibile lo studio della relazione tra la variabilità della componente P300 e la variabilità delle misure comportamentali.

TABLE OF CONTENTS

1 THE ELECTROENCEPHALOGRAPHIC SIGNAL AND THE EVENT-RELATED POTENTIALS

The understanding of the nervous system is an intriguing challenge for science, as the control of all the functions of the human body and the interaction with the external environment are entrusted to this very complex structure. The study of the nervous system is the field of interest of neuroscience. Neuroscience works in a interdisciplinary context that embraces medicine, biology, chemistry, physics, psychology. But it is thanks to the recent development of the neuroimaging techniques and to the advancements in biomedical signal processing that the knowledge about the nervous system, and about the human brain in particular, has had a powerful impulse. So, other disciplines such as mathematics, computer science, and engineering have had a effective influence on neuroscience. Several methodologies and instrumentation have been used to discover the functionality of the human brain, employing invasive and non-invasive approaches. Among them, electroencephalography is one of the principal techniques for extracting information from the human brain for research and clinical purposes.

1.1 The electroencephalographic signal

1.1.1 Origin

The electroencephalogram (EEG) gives a measure of the difference in voltages between pairs of sites on the human head and reflects the electrical activity of the brain. From an anatomical point of view, the human brain is a complex structure constituted by three elements: cerebrum, cerebellum, and brainstem, as shown in Fig. 1.1a. The main functions of the cerebellum are the coordination of voluntary movements and balance while the brainstem regulates involuntary functions such as respiration, heart regulation, biorhythms. The cerebrum is the

center of the brain, it consists of two large and oval cerebral hemispheres. The central core of the cerebrum transfers information from and toward the surface [1], called cerebral cortex. The cerebral cortex is a highly folded mass of cells bodies that presents elevations and depressions [1]. It receives sensory information from the internal and external environments of the organism, processes this information and then gives responses. Different regions of the cerebral cortex are specialized for specific functions, such as somatic, sensory, motor and integrative cognitive functions [2].

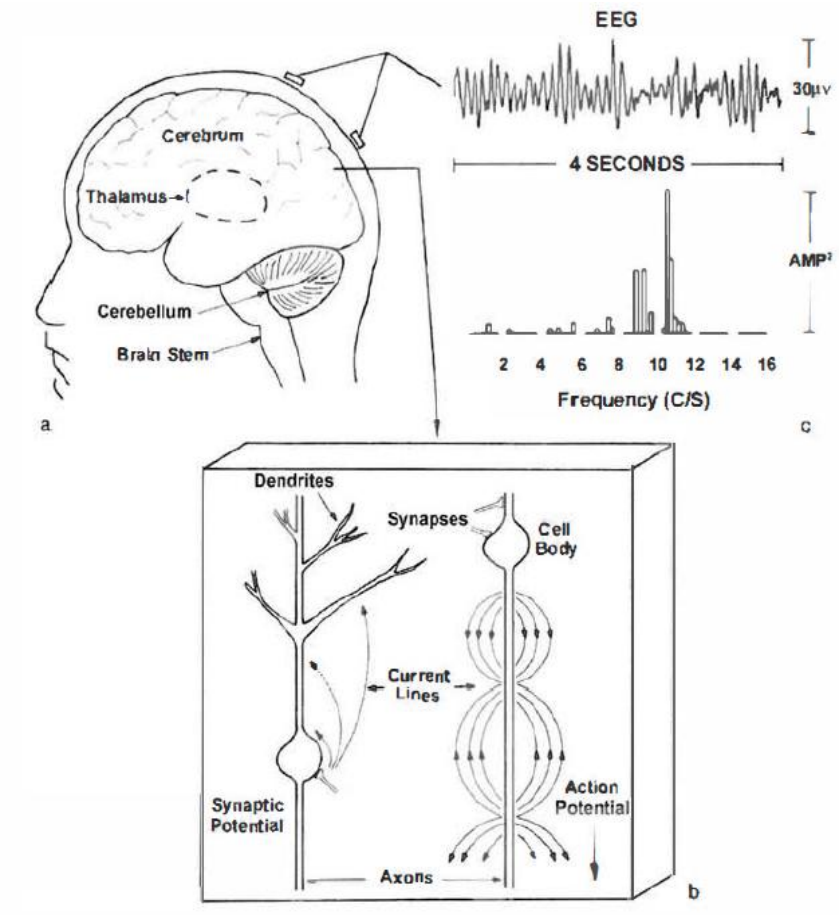

Figure 1.1. From [5]: (a) the human brain; (b) section of the cerebral cortex showing micro-current sources due to synaptic and action potentials; (c) a four-second epoch recorded by using a scalp EEG electrode and its corresponding power spectrum.

The electrical activity of the brain is due to the intrinsic characteristics of its cells that can be divided into two broad categories: nerve cells, or neurons,

andsupporting cells called neuroglia. Nerve cells represent the functional units of the central nervous system and they are specialized for electrical signaling and intercellular communication [3]. Each neuron consists of a cell body, an axon and many dendrites. In Fig.1.1b a typical neuron cell is shown. Neurons are capable of receiving, conducting, and transmitting impulses to each other as well as to muscle cells and cells of glands [1]. Typically, information is received at dendrites, conducted toward the cell body and then transmitted along the axon. Neurons communicate with each other and with other cells at synapses level [1], the terminal parts of axons and dendrites. In the human brain, each neuron is connected to approximately 10000 other neurons mostly through dendritic connections [4]. Adults have an average of 10^4 neurons per cubic mm and 5 x 10^{14} synapses [4]. The activity of the brain is manly related to the currents transferred through these synapses [4]. When, for some reason, an exchange of ions across the neuron membrane occurs, a temporary change in the membrane potential (action potential) happens and it is transmitted along the axon (see Fig. 1.2b). As consequence, postsynaptic potentials will occur in the following neuron.

EEG signal measured on the scalp mainly reflects summated, slow post-synaptic potentials of neurons in the cerebral cortex [5]. Large populations of active neurons with the same orientation and the same type of input (i.e. excitatory or inhibitory) are needed in order to generate enough potential to be recordable using the scalp electrodes [4]. The signal recorded by a single electrode provides estimates of synaptic sources averaged over tissue masses containing between roughly 100 million and 1 billion neurons [6]. Moreover, the layers of tissue that are between the cortex and the scalp (membranes, cerebral liquid and skull) and the scalp itself significantly attenuate the neural activity.

1.1.2 Acquisition

Typically, EEG is recorded with an non-invasive procedure that uses extra-cranial electrodes placed on the scalp. Invasive recording, the so-called intracranial EEG, can be also carried out by means of surgically implanted electrodes. Hereafter we will refer to the EEG recorded by using the non-invasive procedure; in Fig. 1.2 a subject undergoing this acquisition is shown.

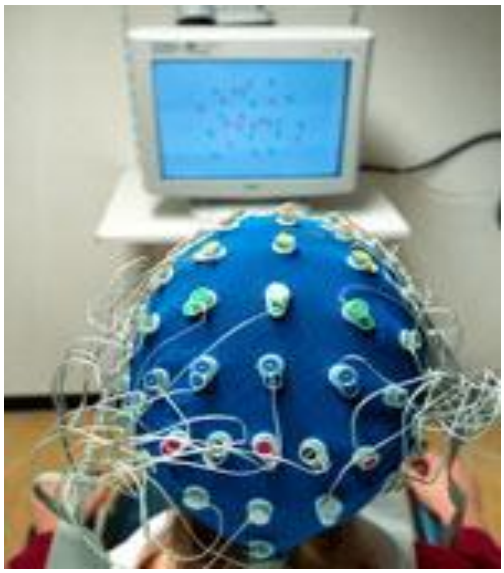

Figure 1.2. Example of a subject undergoing a non-invasive EEG acquisition.

Nowadays, EEG acquisition is typically carried out by using digital electroencephalographs. Multichannel recordings are the routine and electrode caps are often used (see Fig. 1.2). Commonly used scalp electrodes consist of Ag/AgCl disks, less than 3 mm in diameter; they are usually placed on the scalp according the so called 10-20 system, recommended by the International Federation of Societies for Electroencephalography and Clinical Neurophysiology. Electrodes convert into electrical currents the changes of ionic concentrations on the scalp. These currents are then amplified in order to put in prominence the EEG signal and attenuate interferences given by the electrode presence and the

mains signal. Other important acquisition parameters are the sample rate, the gain, the highpass and lowpass filter characteristics, and the notch filter.

However, the activity recorded by the electrodes itself is subjected to artifacts, physiological or not, that are superimposed to the neural activity. The most common non physiological artifacts are mains noise, spurious electrical noise from other sources, artifacts due to body or electrode movement or brief electrode detachments. Physiological artifacts are due to changes of eye potential, muscular activity, electrocardiogram intrusion, sweat [7]. Some artifacts can be corrected for example by using spatial filtering, such as Independent Component Analysis [8], or ARX filtering [9]; for other artifacts, however, this is not possible and the corresponding portion of data is usually excluded from further analysis.

1.1.3 General properties

EEG signal is characterized by a high temporal resolution (few milliseconds) and so it is able to track the temporal dynamics of the neural activities, better than the other neuro-imaging techniques. Although the spatial resolution is limited, EEG signal provides an overall vision of the neural activity of brain, that is very significant in many cases. Traditionally, EEG has been studied in frequency domain. It has been decomposed in five major brain waves distinguished by their different frequency ranges. These rhythms, four of which are represented in Fig. 1.3, are called alpha (α), theta (ϑ), beta (β), delta (δ), and gamma (γ) and cover the frequencies between 0.5 and 70 Hz, even if a considerable amount of the EEG energy signal is located in low frequencies, i.e., between 0.5 and 30 Hz [10]. Delta rhythm lies within the range of 0.5–4 Hz. These waves are primarily associated with deep sleep and may be present in the waking state [4] or in cerebral anomalies [10]. Theta waves (4 – 8 Hz) are present in infancy and childhood; in adult age, they have been related to the level of arousal, meditation, deep. Moreover, various pathological problems are related to theta rhythms [4]. The alpha wave comprises the frequency between 8 and 13 Hz, it

indicates relaxed awareness without any attention or concentration [4]. It is the most prominent EEG rhythm (see Fig. 1.1b where a four-second EEG epoch and its corresponding power spectrum are shown) and it is the typical rhythm visible when a subject closes his eyes. A beta wave is the usual waking rhythm of the brain associated with active thinking, active attention, focus on the outside world [4]. Finally, gamma waves cover the frequency above 30 Hz and they appear during intense mental activity [10].

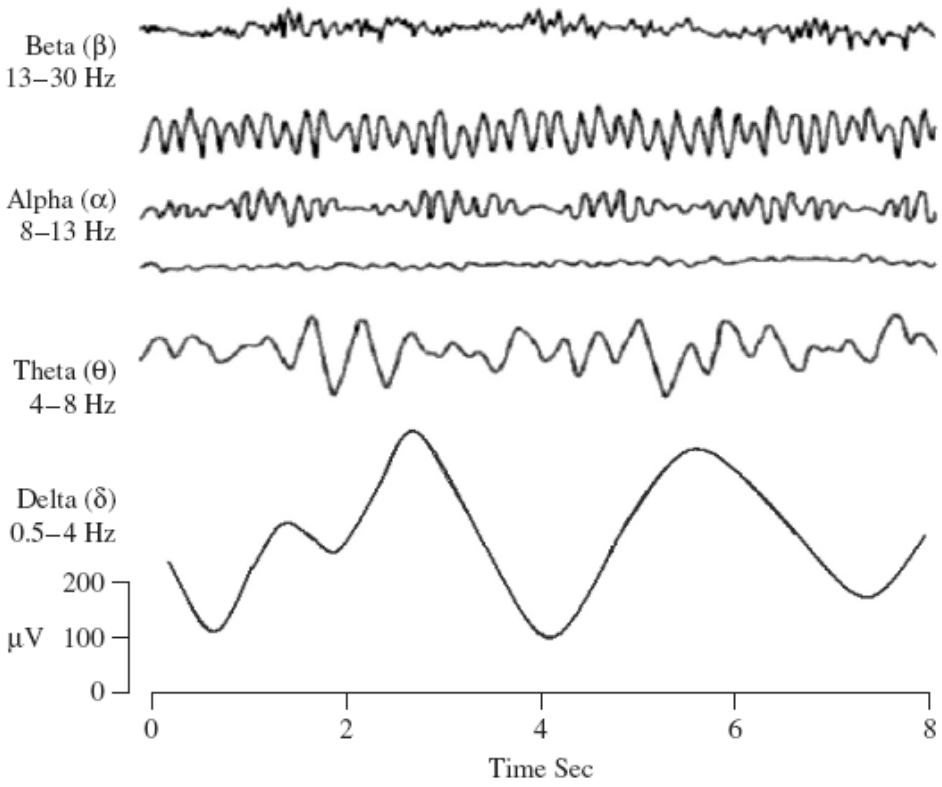

Figure 1.3. From [4]. The main EEG rhythms from high to low frequencies.

For its own nature, EEG signal is greatly variable. As described above, each of EEG rhythms is associated to specific physiological or pathological states; moreover, EEG characteristics change in the resting state too and stationarity of the signal can be assumed only on brief time intervals [4]. A great variability of the EEG characteristics can be also found among different subjects [11]. In order to deal with such a complex, signal advanced analysis techniques have been

proposed, we refer the reader to [10,12] for some recent reviews of these techniques.

1.1.4 Applications

Although EEG signal is so variable and sometimes too difficult to analyze, it is one of the most common techniques for extracting information from the human brain for research and clinical purposes, also thanks to its non-invasive recording procedure and to the relative cheapness of the instrumentation. In this context, signal processing methodologies represent a very useful tool to describe, in a quantitative way, the characteristics of the EEG signal in time, frequency and time-frequency domain. In this way it is possible both to associate EEG patterns to physiological states and to valuate the modifications due to pathological causes. Some applications regard the investigation of the sleep physiology, the monitoring of the cognitive engagement, the study of the development of the brain, the monitoring during anaesthesia [4]. The study of the EEG signal can be very useful also for the investigation of many neurological and psychological disorders and other abnormalities. It has been used for monitoring alertness, coma, brain death; locating areas of damage following head injury, stroke, and tumor; investigating epilepsy and locating seizure origin; testing epilepsy drug effects; investigating mental disorders; investigating sleep disorders [4]. Other applications regard the use of EEG to control brain-computer interfaces and to study depression characteristics [10]. Finally, an important field concerns cognitive neuroscience, the study of the most complex brain functions such as perception, language, emotion, memory, and consciousness. In order to explore these complex human behaviors, experimental tasks are used to raise specific changes in the EEG activity due to the response of specific brain networks hypothesized to be involved in these functions [2]. Among these changes, an important class is represented by the event-related potentials.

1.2 Event-related potentials

1.2.1 Origin and general properties

Sensory, motor and cognitive events cause changes in the EEG ongoing activity in the form of event-related synchronization and desynchronization (ERS/ERD), event-related phase resetting (ERPR) and event-related brain potentials (ERPs) [13]. ERS/ERD are transient increases/decreases of power, in a well-defined EEG frequency band, caused by a synchronization/desynchronization of the activity of a population of neurons. ERPR consists in transient reorganization (or 'resetting') of the phase of ongoing EEG oscillations [13].

ERPs reflect synchronous changes of slow postsynaptic potentials occurring within a large number of similarly oriented cortical neurons of a compact area of the cortex [5]. They appear as sequences of brief monophasic deflections embedded in the background EEG [13]. These deflections are called peaks, waves or components and they are characterized by polarity, latency, amplitude and scalp distribution. Fig. 1.4 shows typical examples of ERPs.

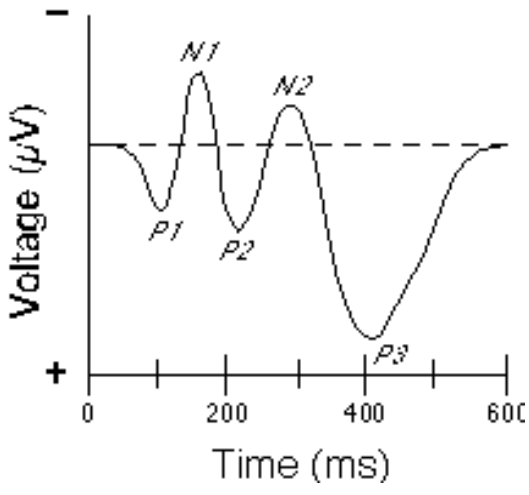

Figure 1.4. Example of ERP waveform. Note the typical positive (P) and negative (N) deflections.

Traditionally, ERP component are indicated by using a letter P/N which means positive/negative-going peak, and a number that represents the peak's position within the waveform [14]. The sequence of ERP peaks reflects the flow of information through the brain [14].

Each component has functional meaning and a specific scalp distribution related to the cortical region where it has been generated. Among the many ERP components we will concentrate on the P300 (or P300) component, one of the most addressed waves in experimental and clinical studies. It appears as a positive peak at about 300 ms after the stimulus onset. This component can be detected in an ERP waveform if the stimulus is task-relevant and/or if it is infrequent but there is no clear consensus about what neural or cognitive process the P300 wave reflects [14]. Some researchers have hypothesized that P300 amplitude was a measure of resource allocation [14] while the P300 latency was considered to be a measure of stimulus classification speed [15].

1.2.2 Applications

A big variety of experimental tests, in which cognitive, sensory and motor functions are involved, are used to elicit ERPs. Each task is associated with a group of distinct psychological operations such as detection and recognition of stimuli, updating working memory, initiation of action and action suppression, monitoring the results of actions and so on [16]. Each of these psychological operations involves neurons in a certain brain area and is related to a particular ERP component. So, ERPs are very useful tool in cognitive neuroscience to study memory processes, attention, spatial processes, language. In particular, attention is addressed to quantitative evaluation of ERPs components (e.g., latency and amplitude of the principal peaks and valleys).

ERP can be also used in several clinical applications e.g. [15,17,18]. For example, for diagnosis and treatment of central nervous system diseases and in clinical studies of sensory pathways. Also multiple sclerosis and surgical monitoring often involve ERPs.

1.2.3 ERP extraction: the Conventional Averaging technique

The main problem associated to the study of the ERPs is the difficult extraction procedure. ERPs are generally recorded during suitable experimental tasks, in which a sequence of stimuli is delivered to a subject. Each stimulus will elicit an ERP that can be thought as superimposed on the EEG background activity. So, ERPs can be obtained by somehow reducing the contribute of the background EEG that is seen as noise. This is the critical point in the ERP estimation context. The EEG background activity appears as a signal with a much high amplitude than the ERP responses and it often totally obscures the useful signal. Moreover, the spectral content of the background EEG covers frequencies that are in the typical range of the ERP signals, so a pass-band filtering procedure cannot be utilized. In the following, we will denote with $\boldsymbol{y}^i$ the i-th sweep ($i = 1, \dots, N$) recorded as response to a stimulus. We assume that $\boldsymbol{y}^i$ is composed by the ERP signal, denotes as $\boldsymbol{u}^i$, and a noise component denotes as $\boldsymbol{v}^i$.

The first technique proposed in order to extract the ERPs is the Conventional Averaging (CA), introduced by Dawson [19]. The idea of using an averaging procedure to estimate at least a "mean" ERP from a series of responses, evoked by a sequence of stimuli, relies upon the consideration that the ERP signal occurs after a interval related to the time of stimulus presentation whereas the background EEG activity and non-neural noise should occur in a more random fashion. In particular, CA technique is based on a simple signal model in which the i–th sweep $\boldsymbol{y}^i$ ($i = 1, \dots, N$) is assumed to be composed by a deterministic, evoked component $\overline{\boldsymbol{u}}$ and a random noise $\boldsymbol{v}^i$ asynchronous to the stimulus

$$\boldsymbol{y}^i = \overline{\boldsymbol{u}} + \boldsymbol{v}^i \qquad (1.1).$$

The noise $\boldsymbol{v}^i$ is assumed to derive from the ongoing process which, in this model, is a stationary process with zero-mean and variance σ_v^2, uncorrelated from sweep to sweep [20].

The estimate given by the CA technique is given by the coherent averaging of the N sweeps collected after N identical stimuli

$$\widehat{\overline{\boldsymbol{u}}} = \frac{1}{N}\sum_{i=1}^{N} \boldsymbol{y}^i = \overline{\boldsymbol{u}} + \frac{1}{N}\sum_{i=1}^{N} \boldsymbol{v}^i \tag{1.2}.$$

Under the above-discussed assumptions the CA estimator in Eq. (1.2) has important statistical properties. Since the noise is a zero-mean process, the mean value of $\widehat{\overline{\boldsymbol{u}}}$ is equal to the $\overline{\boldsymbol{u}}$

$$E[\widehat{\overline{\boldsymbol{u}}}] = \overline{\boldsymbol{u}} + E\left[\frac{1}{N}\sum_{i=1}^{N} \boldsymbol{v}^i\right] = \overline{\boldsymbol{u}} \tag{1.3}$$

so the CA estimator is unbiased. Moreover, it is also consistent because its variance tends to zero with an increasing value of N

$$Var[\widehat{\overline{\boldsymbol{u}}}] = E[(\widehat{\overline{\boldsymbol{u}}} - E[\widehat{\overline{\boldsymbol{u}}}])^2] = E\left[\left(\frac{1}{N}\sum_{i=1}^{N} \boldsymbol{v}^i\right)^2\right] = \frac{\sigma_v^2}{N} \tag{1.4}$$

this is because the noise is assumed to be uncorrelated from sweep to sweep.

Although this technique is still the most commonly used for its simplicity, it presents some limitations due to the poor reasonableness of the hypotheses on

which it bases. In particular, the most critical assumptions regard the ERP invariance and the stationarity of the noise among trials. The assumption that the ERP is invariant among trials results inadequate in several applications, for example, in intra-operative monitoring [20] o when late potentials, characterized by a higher variability, are considered. Moreover, various factors, such as subject expectation and habituation or environmental activity, may introduce variations of the ERPs among trials [20]. Also the hypothesis of the stationarity of EEG noise among trials is quite critical. In fact the stationarity of the signal can be assumed only on brief time intervals [4]. Finally, often a rather large number N of sweeps is often required to obtain an acceptable estimate of the ERP; this number can range from some tens to some thousands, depending on the kind of ERP and on the single-sweep signal-to-noise ratio (SNR). However, large values of N imply too long experimental times and make difficult performing neuropsychological studies involving attention, above all on children and patients who do not tolerate long-lasting experiments.

Because of these limitations of the CA technique, until now many techniques have been developed in order to extract the ERPs from the EEG background activity. On the one hand, one research branch has focused on the estimation of an “average” ERP, in particular on the improvement of the estimate given by the CA technique and on the reduction of the number of necessary sweeps. On the other hand, the variability of the evoked responses during the recording has stimulated the setting up of methods able to provide the ERPs estimation at single-trial level.

1.3 Aim of the thesis and outline

In this thesis, Bayesian approach is proposed for the improved estimation of the average ERP and for the single-trial ERP estimation. In particular, two methods, with different degree of sophistication, are implemented. The first method is based on a two-stage procedure. In the first stage each raw sweep is processed

by an individual optimal filter by exploiting a 2nd order *a priori* statistical information on the background EEG and on the unknown ERP, then, an average ERP is estimated as weighted averaging of the N filtered sweeps. In the second stage, single-sweep estimation is dealt with within the same framework, by using the average ERP estimated in the previous stage as *a priori* expected response. The second method is based on a one-stage multi task learning Bayesian procedure. Differently from the most estimation approaches, the method provides the estimation of the average and the single-trial responses by processing just once all the N sweeps simultaneously. The method assumes that the generic sweep can be modeled as the sum of three independent stochastic processes: an average curve of population that is common to all the sweeps, an individual shift that differentiates each sweep from the others, a background EEG noise component varying sweep by sweep. As in the first method, *a priori* information available on the unknown signals and on the noise is exploited.

The present thesis is organized as follows.

After this brief introduction, a review of the methods presented in literature, both those aimed to improve the estimate of the average response and those finalized to the single-trial estimation, is given in the second chapter.

The third and the fourth chapters are focused on the presentation of the two proposed techniques. The description of the procedures is carried by separately treating the estimation of the average ERP and the single-trial responses.

In the fifth chapter the assessment of the techniques on simulated data is presented. The capability of the two methods in estimating the average profile with a reduced number of sweeps and in tracking the variability of the simulated ERPs, in particular with respect to the estimation of the P300 component, is tested.

The results of the application of the procedures to real data recorded during a cognitive task are described in the sixth chapter.

Finally, conclusive remarks are discussed.

2 MEASUREMENT OF ERP: STATE OF THE ART

A synthetic review of the state of the art is the topic of this chapter. An exhaustive and detailed analysis of all the published techniques would be beyond the intent of the present work, therefore we refer the reader to some recent reviews [4,13,20,21]. However, since the proposed methodologies provide an improved estimate of the average ERP and the single-trial estimation at same time, in this chapter the most representative methods both for the average ERP estimation and for the single-trial one will briefly described, in order to give an idea of the variety of the proposed methods. Indeed, because of the increasing interest of engineers, mathematicians, physicists and computer scientists in neuroscience, the ERP estimation is a many-sided and rapidly developing area. The methodologies aimed to estimate the average ERP are dealt with in section 2.1, while section 2.2 is devoted to single-trial estimation techniques.

In the following, we will denote with $\boldsymbol{y}^i$ the i-th sweep ($i = 1, \dots, N$) recorded as response to a stimulus. We assume that $\boldsymbol{y}^i$ is composed by the ERP signal, denoted as $\boldsymbol{u}^i$, and a noise component denoted as $\boldsymbol{v}^i$. With $\overline{\boldsymbol{u}}$ we indicate the "mean" average ERP, namely the signal that represents the average response to the sequence of stimuli.

2.1 Techniques for the average ERP estimation

The most representative methods aimed to improve the estimation of the average ERP with respect to the CA technique are presented in this section.

2.1.1 Averaging using an artifact criterion

Averaging using an artifact criterion [21] is a simple way to eliminate high components of noise. According to this approach, the epochs with a peak-to-peak voltage larger than a certain threshold value are excluded from the

average. This technique has been largely used above all in order to eliminate epochs corrupted by high amplitude artifacts such as eye-blink or non physiological artifacts due to abrupt variations of electrode impedance. Nowadays, more sophisticated methods for the correction of different types of artifacts are used, which allow to considerably reduce the number of eliminated epochs, for example the Independent Component Analysis (ICA) [8].

2.1.2 Weighted averaging

The *weighted averaging* technique introduced by Hoke et al. [22] is the first and most important method that takes into account the non-stationarity of the EEG noise among the different sweeps. The estimate of the mean ERP is obtained by averaging, with sweep-dependent weights, the set of epochs

$$\hat{\boldsymbol{u}} = \frac{\sum_{i=1}^{N} w^i \boldsymbol{y}^i}{\sum_{i=1}^{N} w^i} \tag{2.1}$$

The quantity w^i to be assigned to the i-th sweep is defined as follows:

$$w^i = \frac{1}{P^i} \tag{2.2}$$

where P^i is the power of the noise in the i-th sweep. In particular, it is assumed that each sweep consists mainly in noise and that the useful signal gives a negligible contribute to the power computation, so P^i is approximated computed as the power of the i-th sweep. As the weighted averaging was proved to improve that SNR of the average ERP, it was used in several works [23-25] and many techniques arose out of it. One of these techniques is the *iterative averaging*.

2.1.3 Iterative averaging

The *iterative averaging* was introduced by Riedel et al. [21] in order to improve the computation of the weights of Eq. (2.2). As discussed in [26], the computation of P^i as the power of the measured epoch instead of the sole noise leads to an underestimation of the magnitude of the useful signal. Within *iterative averaging* the estimation of the noise of each sweep is updated at each iteration. At first, the noise in a single epoch is defined to be the epoch itself. In this case, the computation of the weights corresponds to that provided by the weighted averaging. Then, the weighted averaging is repeated improving the estimate of the noise by subtracting from each epoch the average computed in the previous iteration.

2.1.4 Sorted averaging

The *sorted averaging* method was introduced by Mühler and von Specht [27] and employed e.g. for the estimation of auditory event-related responses [28]. The available sweeps are sorted according to the level of noise estimated from the power of each epoch. This allows to separate accepted and rejected epochs by setting a critical noise value. This critical value is automatically determined by minimizing the power of the mean cumulative normalized noise.

2.1.5 Latency-dependent averaging

This methodology is focused on the variability of ERP latency and amplitude among sweeps. It assumes that a temporal synchronization of trials before the averaging can improve the quality of the estimate. One of the first techniques was proposed by Woody [29]. According to this method the ERPs are assumed to have the same waveform among trials but different latencies

$$\boldsymbol{y}^i(t) = \overline{\boldsymbol{u}}\left(t + \tau^i\right) + \boldsymbol{v}^i(t) \qquad (2.3).$$

The latency τ^i is estimated, using a matched filter, as the time in which the maximum of the cross-correlation between the i-th single trial and a template constructed by CA occurs. Subsequently, the trials are shifted according to the estimated latency and then averaged.

On the basis of the same model, Pham et al. [30] proposed to determine the latency variations by using a maximum likelihood approach. Successively other authors proposed to take into account also variations in amplitude in order to give a description at a single-trial level of the ERPs. These issues will be discussed in section 2.2. Finally, among the methods that compute the average ERP by using a corrected-in-latency averaging procedure, let us mention Gupta et al. [31] in which a non linear ERP latency distortion among the trials is introduced.

2.1.6 Median averaging and trimmed estimators

Other authors proposed estimators different from the mean. Borda and Forst [32] introduced the median averaging, successively drawn on by Yabe et al. [33]. It is similar to the conventional averaging with the difference that median is used instead of mean. In [34], in particular, the technique has been slightly modified by employing baseline-corrected trials. This method has been found to be more appropriate than the averaging if the number of available trials is small, being less sensitive to the infrequent artifacts and the extreme variations (for example the lack of some signals). Moreover, it is less affected than the CA by the jitter in latency occurring trial by trial. Nonetheless, the median averaging has been strongly criticized because of its over-robustness and because it discards a large part of information present in the data. In [35] alternative techniques for averaging of ERPs have been proposed, such as the trimmed mean, the Winsorized mean, the trimmed L-mean and the new tanh mean. They are estimators of data location more robust than conventional mean but not as over-robust as median; they have been considered suitable estimators especially when a small number of sweeps is involved.

2.1.7 Filtering methods

A large group of methodologies aims to improve the estimate of the average ERP applying some filtering procedures to the CA-based average response or to the single trials before the actual averaging.

One of the first approaches within this category was introduced by Walter [36] and is based on a Wiener filtering of the average response. This approach has been employed by several works and proposed in many variants, because of the optimality of the Wiener filter in the mean square error (MSE) sense. However, it has been also strongly criticized because it requires the knowledge of the spectra of both signal and noise and it assumes the stationarity of the involved signals [37]. In order to overcome these limitations, both *adaptive filtering* procedures and techniques that employ *a priori* knowledge, without assuming the stationarity of the signals, have been introduced.

Adaptive filtering involves the utilization of a filter with variable coefficients and an adaptive algorithm which adjusts the filter coefficients by minimizing the MSE between a primary input and a reference input. An example of application of adaptive filtering for the ERP estimation is given by Thakor [38]: one sweep is used as primary input while the following one as reference input. An adaptive algorithm has also been used to estimate the Fourier coefficients used to model the evoked potentials [39]. Furthermore, Laguna et al. [40] employ an impulse that is time-locked to the stimulus onset as reference input.

Among the filtering techniques that employ *a priori* knowledge an important branch is represented by those methodologies that address the ERP extraction problem in a general mean square error estimation framework. In this context the statistical information of both the signal and the noise is needed. An optimal filter for application to averaged responses has been presented by Furst and Blau [41]. The auto-covariance functions of signal and noise are simultaneously estimated from the raw sweeps and used to determine the filter coefficients for which the MSE is minimized. The statistical information of the ERP and the noise

can be also obtained by employing *a priori* parametric models for the description of the signals. Several models and approaches have been proposed. In particular, in Sparacino et al. [37] the second order statistical information of the unknown signal is obtained sweep by sweep by using a multiple integration of a white noise process. The average response is obtained by weighted averaging of all thus filtered sweeps. One of the two approaches proposed in this thesis bases on the above-cited work.

2.2 Techniques for the single-trial ERP estimation

In this section some representative single-trial methods will be described with particular attention to the study of the variability of the P300 component.

2.2.1 Early stages

The particularly unfavorable SNR at a single-trial level makes the determination of the parameters of the ERP components extremely difficult without a sort of pre-processing of the recorded sweeps. Obviously, SNR is related to the amplitude of the ERP component. The P300 wave has greater amplitude than many other components, therefore some very simple approaches have been used that rely upon the visual inspection of the peak in the single-trial raw sweep, e.g. [42,43]. Clearly, this method is feasible if the SNR ratio is particular favorable, but estimated latencies and amplitudes will be inaccurate and biased [13]. Another pioneering method for P300 single-trial analysis is represented by the peak picking method [44], or MAX method, which consists in the detection of the largest positive peak in the P300 time interval in the low-pass pre-filtered sweep. Apart from these simple but rough methods, much more sophisticated methodologies have been developed in order to exploit the available *a priori* information on the evoked response.

2.2.2 Woody's method and related techniques

Woody's method [29], employed in several works [45,46], is a historic approach that takes into account the ERP variability among trials. Even if the aim of this technique is the improvement of CA estimate, the possibility of latency variation of the ERP gives the first single-trial description of the evoked responses. As already discussed in section 2.1, this method assumes that all the ERPs evoked by the sequence of stimuli have the same waveform but they can be shifted in latency. This model is described by Eq. (2.3). The latency τ^i is estimated, by using a matched filter, as the time in which the maximum of the cross-correlation between the i-th single trial and a template constructed by CA occurs. Once the latencies of all the ERPs have been estimated, the mean ERP $\overline{\boldsymbol{u}}$ is determined by using a corrected-in-latency averaging. Given $\overline{\boldsymbol{u}}$, the single-trial ERP can be determined by simply shifting the average ERP by a quantity given by the latency τ^i.

The modeling of the evoked response as a deterministic signal of fixed shape and variable latency and/or amplitude among trials has been adopted in many other works. Pham et al. [30] proposed a variant of Woody's method. They use a maximum likelihood approach to determine the latency variations, providing better estimates of the single-trial latencies of early ERP components. In particular, the estimation is performed in the frequency-domain and the ongoing activity is modeled, at different frequencies, as zero-mean Gaussian random variables with unknown variances. Successively other authors proposed to take into account also variations in amplitude in order to give a more complete description at a single-trial level of the ERPs.

Jaśkoswki and Verleger [47] proposed the following model

$$\boldsymbol{y}^i(t) = a^i \overline{\boldsymbol{u}}\left(t + \tau^i\right) + \boldsymbol{v}^i(t) \tag{2.4}$$

in which factor a^i expresses amplitude jitter. Such a model is surely more reasonable than that in Eq. (2.3) for late ERPs, for example the P300. For late ERPs, in fact, fluctuations in amplitudes cannot be neglected. Both latencies and amplitudes are estimated via maximum likelihood in the frequency domain, according to [30].

The above-described technique has been widely employed and extended. In Fjell et al. [48] for example, it was used to study the P300 parameters in function of age, as well as their relationship with the reaction times. Truccolo et al. [49] assume that the single trial ERP can be modeled as the linear combination of multiple components. Each component is assumed to have a trial-invariant waveform with trial dependent amplitude and latency:

$$\boldsymbol{y}^i(t) = \sum_{\boldsymbol{c=1}}^{\boldsymbol{C}} a^{ic}\boldsymbol{u}_c\left(t + \tau^{ic}\right) + \boldsymbol{v}^i(t) \tag{2.5}$$

where a^{ic} is the amplitude of the c-th ($c = 1, \dots, C$) component of the ERP waveform in the i-th sweep, τ^{ic} is its amplitude, while $\boldsymbol{u}_c$ is its waveform. The latencies, the amplitudes and the C waveforms are estimated by using an iterative procedure that provides a MAP (Maximum a Posteriori) solution.

Recently, Xu et al. [50] employed this model with multiple components by drawing on the idea of Pham at al. [30] of the estimation of the unknown parameters via Maximum Likelihood in the frequency domain. Moreover, an autoregressive model (AR) was adopted to describe the EEG ongoing activity.

2.2.3 Parametric time-series models

Several techniques employ parametric time-series models [51-54]. For example, in [53] an ARX (autoregressive with exogenous input) model has been used to derive the single-trial description of the evoked response. The i-th recorded

sweep, here denoted as $\boldsymbol{y}$ for the sake of simplicity, is assumed to be the sum of the single-trial ERP $\boldsymbol{u}$ and the background EEG $\boldsymbol{v}$. The ERP is modeled as a filtered version of a reference input $\boldsymbol{r}$ carrying the average information contained in each sweep while the background EEG is modeled as an AR process driven by a white noise

$$\boldsymbol{y}(k) = -\sum_{i=1}^{n} a_i \, \boldsymbol{y}(k-i) + \sum_{j=0}^{m+d-1} b_i \, \boldsymbol{r}(k-j) + \boldsymbol{e}(k) \qquad (2.6).$$

The parameters n and m are the orders of the autoregressive and moving average part, respectively; a_i's and b_i's are the model coefficients, $\boldsymbol{e}$ is a white noise process. A temporal delay d is introduced in order to take into account possible variations in the latency of single responses with respect to the reference signal. The traditional averaging of a sufficient number of sweeps is employed as reference input.

This technique has been extended in [54], in which the contribute of the EOG noise is also taken into account, and in [55], in which the reference signal is given by the running average of 20 consecutive sweeps. In Capitanio et al. [56], for the single-sweep extraction of movement-related brain macro-potentials, the reference signal has been obtained on the basis of the Current Source Density of the acquired sweeps. Other applications regard during neurosurgery, recovery assessment after photostress and the monitoring of patient sedation level [57,58].

2.2.4 Regularization approaches

Regularization methods have been successively applied to solve the ERP extraction problem [59,60]. These methods origin in the theory of the ill-posed inverse problems [61] and are directly connected with the Bayesian estimation.

In Karjalainen et al. [59] a subspace regularization method has been introduced. Assumptions about the evoked potentials and the background EEG can be easily implemented mathematically in the estimation procedure.

In particular, in a linear observation model, the single-trial evoked potential, here denoted $\boldsymbol{u}$ for the sake of simplicity, has been modeled as linear combination of Gaussian basis vectors that are the columns of the matrix $\boldsymbol{H}$

$$\boldsymbol{u} = \boldsymbol{H}\boldsymbol{\theta} \tag{2.7}.$$

The parameters $\boldsymbol{\theta}$ are estimated as solutions of the regularized least squares [62]

$$\boldsymbol{\theta}_\alpha = \underset{\boldsymbol{\theta}}{argmin}\{\|\boldsymbol{L}_1(\boldsymbol{y} - \boldsymbol{H}\boldsymbol{\theta})\|^2 + \alpha^2\|\boldsymbol{L}_2(\boldsymbol{\theta} - \boldsymbol{\theta}^*)\|^2\} \tag{2.8}$$

where $\boldsymbol{L}_1{}^T\boldsymbol{L}_1 = \boldsymbol{W}_1$ and $\boldsymbol{L}_2{}^T\boldsymbol{L}_2 = \boldsymbol{W}_2$ are positive definite weighting matrices and $\boldsymbol{\theta}^*$ incorporates *a priori* information about the unknown ERP. The first term in Eq. (2.8) is related to the data, while the second one to the *a priori* information about the unknown signal. The value α is the regularization parameter, since it weighs the second term of Eq. (2.8) in the objective function. So, in this approach, the *a priori* information about the unknown ERP is exploited, in addition to the data, in order to solve the ERP extraction problem. The matrices $\boldsymbol{W}_1$ and $\boldsymbol{W}_2$ can be related to the covariance matrices of the noise $\boldsymbol{v}$ and of the parameters $\boldsymbol{\theta}$, in this approach they are estimated from the data.

In Ranta-aho et al. [60] this method has been extended to multi-channel data, taking into account also spatial information.

2.2.5 Time-frequency methodologies

Many proposed methods employ time-frequency approaches such as wavelet decomposition and Gabor transform. For example, in Quian Quiroga and Garcia [63] a wavelet multi-resolution decomposition [64] with 5 levels was used. Quadratic bi-orthogonal B-Splines [65] were chosen as the basic wavelet functions due to their similarity with the event related responses. In particular, the wavelet denoising is performed as follows. First, the average ERP estimated by CA is decomposed by using the wavelet multi-resolution decomposition. The wavelet coefficients correlated with the ERPs are identified and the remaining ones are set to zero. Subsequently, a denoised average ERP is obtained by applying the inverse wavelet transform. Single-trial denoising is carried out with the same transform, eliminating those coefficients previously proved to be related to the noise. In several papers [63,66-69] time-frequency techniques, also associated with other approaches, have been successfully applied for single-trial estimation. In Effern et al. [68] the wavelet transform has been combined with techniques for the non-linear time series analysis that permit to exploit similarities in the state space. Time-frequency techniques have been used also to improve the estimate of the average ERP. In Turner et al. [70] a combination of wavelets and evolutionary algorithms is used to estimate an average ERP waveform with a small number of responses. An evolutionary algorithm is used to select, among 42 different wavelets, which wavelet to use and the coefficients of each level of decomposition. The algorithm minimizes the MSE between the filtered signal and a target waveform obtained by averaging 243 epochs. Finally, Hu et al. [69] wavelet analysis has been associated to ICA decomposition.

2.2.6 Spatial filtering techniques

Spatial filtering techniques such as Independent Component Analysis (ICA) and Principal Component Analysis (PCA) have been largely adopted for the ERP estimation. ICA technique has been employed in several works [8,71-74] for its capability to isolate different oscillatory activities and artifacts both on the

single-trial epochs and on the averaged response [8,71]. In Jung et al. [74], for example, ICA was demonstrated able to separate artifactual, stimulus-locked, response-locked, and non event related background EEG activities into separate components. In Zouridakis et al. [73], improved estimates of the ERP responses at single-trial level are associated to an improved estimate of the average ERP. The proposed technique, called iterative ICA, is inspired by Woody's method. At the i-th iteration a reference ERP is estimated by averaging the current estimates of the single-trial ERPs, then the independent components are obtained applying the ICA transform to all the single trials. In the successive step the correlation between each independent component and the reference ERP is computed and the independent components with absolute correlation less than a predefined threshold are set to zero. Finally, the remaining components are back-projected via inverse ICA transformation by providing updated single-trial waveforms and reference ERP. The procedure iterates until a convergence criterion is met. Similarly, PCA was used for single trial estimation [75,76]. In Rushby and Barry [75] the ERP components P1, N1, N2, P3a, P3b have been extracted by means of a PCA of the recorded sweeps. In particular, information about latency, amplitude and scalp topography has been used to identify the above-mentioned ERP components.

2.2.7 Radial basis function neural networks

The last class of techniques discussed in this review employs artificial neural networks. In particular, a detailed description of a methodology that uses a radial-basis function (RBF) neural network will be given in this section. This technique, presented in [77] for online extraction of somatosensory evoked potentials (SEPs) during scoliosis surgery, has been used in the present work as representative literature method with which the performance of the proposed techniques has been compared.

Radial-basis function neural networks are feed-forward neural network constituted of three layers:

- an input layer, consisting of an instant input $\boldsymbol{x}^{(p)}$ vector with p elements;
- a hidden layer with N neurons
- an output layer constituted by one neuron.

The activation function F_j of each neuron j has radial symmetry: it is characterized by a center vector $\boldsymbol{C}_j$ with p elements and a radius $\boldsymbol{d}_j$ that represents the Euclidean distance between the generic instant input $\boldsymbol{x}^{(p)}$ and the center vector $\boldsymbol{C}_j$. The output $\boldsymbol{u}$ of the network is given by the weighted sum of responses of the N neurons

$$\boldsymbol{u}(\boldsymbol{x}^{(p)}) = \sum_{j=1}^{N} w_j \; h_j(\boldsymbol{x}^{(\boldsymbol{p})}) \tag{2.9}$$

where $h_j(\boldsymbol{x}^{(p)})$ is the response of the j-th hidden neuron while w_j is the weight between the j-th hidden neuron and the output neuron. These weights are learnt in a supervised way which consists in minimizing the difference between the network output and a reference signal; the input weights, instead, are generally set to 1.

For the specific application to single-sweep detection of SEPs, the following configuration characterizes the network. First of all, a Gaussian function has been considered as radial-basis function

$$\boldsymbol{F}(\boldsymbol{x}^{(p)}, \boldsymbol{C_j}) = e^{-\left(|\boldsymbol{x}^{(p)} - \boldsymbol{C_j}|/\sigma_j\right)^2} \tag{2.10}$$

where σ_j is the spread and $\boldsymbol{C}_j$ is the mean.

A scalar value has been used as instant input instead of a vector. This scalar is the ordinal number of the current sample in the sweep, so the centers of the N Gaussian functions are distributed over the discrete time axis from 1 to M, where M is the total number of samples of each sweep.

The k-th sample of the detected SEP for the i-th sweep is

$$\boldsymbol{u}^i(k) = \sum_{j=1}^{N} w_j^i \, h_j(k) = \sum_{j=1}^{N} w_j^i \, e^{-\left(|k - C_j{}^i|/\sigma_j\right)^2} \tag{2.11}$$

where w_j^i is the current weight between the j-th node and the output unit and $C_j{}^i$ is the scalar center of the j-th neuron for that sweep.

In order to speed up the computation for online applications the number of neurons and the spread of the Gaussian functions have been experimentally determined and kept unchanged. The weights and the centers of the Gaussian functions are, instead, learnt sweep-by-sweep by a supervised algorithm that minimizes the MSE between the current recording and the network output. As described in [77], at the beginning the centers of the Gaussian functions are uniformly distributed over the discrete time axis; then, at each adaptation step, they are shifted by one sample if the current MSE is smaller of the previous one.

3 A TWO-STAGE APPROACH FOR THE EXTRACTION OF ERPS

3.1 Introduction

In Chapters 3 and 4, two new methodologies for ERPs extraction are presented in detail. They are both conceived to estimate an average ERP and the N single-trial ERPs. Both the techniques use a Bayesian approach: the involved signals are considered as stochastic processes and some *a priori* information available about them is exploited for their estimation. The first method exploits a two-stage procedure, in which the estimation of the average ERP is done before single-trial estimation and then exploited to perform it. The second technique is based on a one-stage multi-task learning approach where the average ERP and the N single-trial ERPs are simultaneously estimated.

The first technique, described in [78] is based on a two-stage procedure. It is a development of an approach originally presented in [37,79] for improving the quality of CA. In the first stage, all the available sweeps are processed in a Bayesian context in order to obtain an estimate of an average ERP. The purpose of the this first step is also to provide a reference signal to be used in the single-trial estimation step. In the second stage, in fact, each sweep is processed a second time by using the average ERP, estimated in the first step, as *a priori* expected value.

3.2 Model of the data

The method is based on the following additive measurement model

$$\boldsymbol{y} = \boldsymbol{u} + \boldsymbol{v} \tag{3.1}$$

where $\boldsymbol{y}$ is the n-size vector containing the n samples of the recorded raw sweep, $\boldsymbol{u}$ is the n-size vector containing the samples of the ERP generated as response to the stimulus and $\boldsymbol{v}$ is the zero-mean n-size vector of the samples of the noise that corrupts the useful signal. As the major component of the vector $\boldsymbol{v}$ is the background EEG, other sources of noise and artifacts have been considered negligible. Moreover, vectors $\boldsymbol{u}$ and $\boldsymbol{v}$ are assumed to be independent of each other. This is an acceptable assumption if the event-related response is considered to be not generated by modifications of the background activity.

The signals $\boldsymbol{u}$ and $\boldsymbol{v}$ are seen as realizations of stochastic processes. In order to account for *a priori* information, suitable models are used to describe them. This allows to embed the estimation procedure within a Bayesian context by minimizing the mean square error. In particular, a multi-integrated white noise model can be used in order to describe the ERP smoothness, while an autoregressive (AR) model can be adopted for the EEG noise.

3.3 Stage 1: average ERP estimation

The mean ERP $\overline{\boldsymbol{u}}$ is estimated by averaging, with suitable weights, the N available sweeps previously filtered in a Bayesian embedding. For each recorded sweep the additive measurement model described by Eq. (3.1) is assumed to be valid. According to the Bayesian approach, the optimal estimate of $\boldsymbol{u}$, in terms of minimizing the mean square error (MMSE), see [80] for details, is the mean of the posterior probability density function (PDF) $p(\boldsymbol{u}|\boldsymbol{y})$:

$$\widehat{\boldsymbol{u}} = E[\boldsymbol{u}|\boldsymbol{y}] \tag{3.2}$$

The function $p(\boldsymbol{u}|\boldsymbol{y})$ represents the PDF of $\boldsymbol{u}$ after the data $\boldsymbol{y}$ have been observed. As known, in general it is difficult to obtain an expression of the estimator in closed form unless the assumption of jointly Gaussian variables is

made. If Gaussian assumptions do not hold, a frequently used approach consists in finding the best linear estimator which, in general, is suboptimal.
The MMSE estimator has the following expression:

$$\widehat{\boldsymbol{u}} = E[\boldsymbol{u}|\boldsymbol{y}] = E[\boldsymbol{u}] + \boldsymbol{\Sigma_{uy}}\boldsymbol{\Sigma_{yy}}^{-1}(\boldsymbol{y} - E[\boldsymbol{y}]) \tag{3.3}$$

where $E[\boldsymbol{u}]$ and $E[\boldsymbol{y}]$ are the *a priori* expected values of $\boldsymbol{u}$ and $\boldsymbol{y}$, respectively, $\boldsymbol{\Sigma_{uy}}$ is the cross-covariance matrix of $\boldsymbol{u}$ and $\boldsymbol{y}$, $\boldsymbol{\Sigma_{yy}}$ is the covariance matrix of $\boldsymbol{y}$. By assuming that the vector $\boldsymbol{v}$ has zero mean and it is independent of $\boldsymbol{u}$, the estimator becomes:

$$\widehat{\boldsymbol{u}} = \boldsymbol{E}[\boldsymbol{u}] + \boldsymbol{\Sigma_{uu}}(\boldsymbol{\Sigma_{uu}} + \boldsymbol{\Sigma_{vv}})^{-1}(\boldsymbol{y} - \boldsymbol{E}[\boldsymbol{y}]) \tag{3.4}$$

where $\boldsymbol{\Sigma_{uu}}$ and $\boldsymbol{\Sigma_{vv}}$ are the covariance matrices of $\boldsymbol{u}$ and $\boldsymbol{y}$ respectively.
The performance of the estimator can be measured by the error

$$\boldsymbol{e} = \boldsymbol{u} - \widehat{\boldsymbol{u}} \tag{3.5}$$

whose mean is zero and whose covariance matrix is

$$\boldsymbol{\Sigma_{ee}} = \left(\boldsymbol{\Sigma_{uu}}^{-1} + \boldsymbol{\Sigma_{vv}}^{-1}\right)^{-1} \tag{3.6}.$$

As stated above, all the available N sweeps are filtered in this Bayesian context before to participate in the estimation of the average ERP. So, for each sweep i ($i = 1, \dots, N$) the covariance matrices of the signal $\boldsymbol{u}$ and of the noise $\boldsymbol{v}$ are needed. From now on, we indicate with a subscript i all the parameters that characterize the i-th sweep. By using the above-mentioned models to describe the signal $\boldsymbol{u}$ and the noise $\boldsymbol{v}$, it is possible to derive the expressions of the two covariance matrices $\boldsymbol{\Sigma_{uu}}^{i}$ and $\boldsymbol{\Sigma_{vv}}^{i}$ associated to the i-th sweep.

3.3.1 ERP model

A model of the unknown ERP can be obtained by exploiting its *a priori* known smoothness. In this way, no strong assumptions on the shape of the unknown ERP are made and so it is also possible to describe different ERP morphologies. A simple but versatile way to give an a *priori* probabilistic description of a smooth signal is to assume that it is the realization of a stochastic process obtained by the cascade of d integrators driven by a zero-mean white noise process $\{\eta_k^i\}$ with variance $(\lambda^i)^2$. This is a standard model used to describe a smooth signal, see for example [81,82]. Under this assumption, the covariance matrix of $\boldsymbol{u}^i$ can be computed as

$$\boldsymbol{\Sigma_{uu}}^i = (\lambda^i)^2 (\boldsymbol{F}^T \boldsymbol{F})^{-1} \tag{3.7}$$

where $\boldsymbol{F} = \boldsymbol{\Delta}^d$, with $\boldsymbol{\Delta}$ being the square n-dimension lower-triangular Toeplitz matrix the first column of which is $[1, -1, 0, \cdots, 0]^T$.

Typical values for d are between 1 and 6. For instance, for $d = 1$ the unknown signal is described by a random-walk model, which, in a Gaussian setting, tells us that, given u_{k-1}^i, then u_k^i will be with probability 99.7% in the range $u_{k-1}^i \pm 3\lambda^i$, i.e., the lower λ^i, the smoother $\{u_k^i\}$. The choice of the integer d is left to the user, but it can be easily handled by trials through a preliminary study on a small subset of data, as discussed for instance in Remark 1 and 2 of Sparacino et al. (2002). In particular, given the connection between d and the continuity properties of the estimate, one may expect *a priori* that relatively high values of d (e.g. $d = 4$) should be associated to spiky ERP waveforms (e.g. early potentials), while smaller values (e.g. $d = 1$) should result more suited to slow ERP profiles.

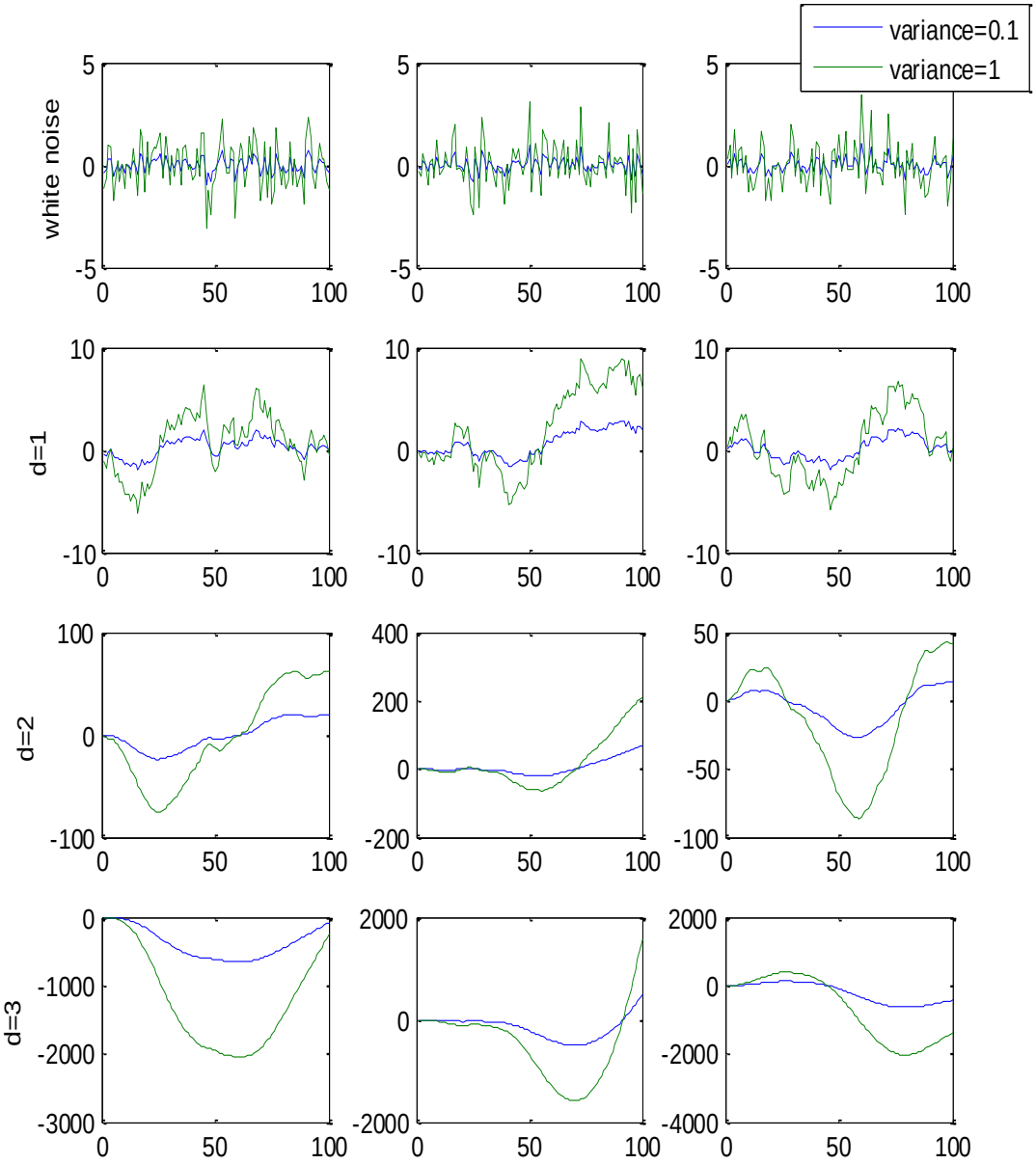

Figure 3.1. Different realizations of multi-integrated white noise processes. Top panels: three different realization of white noise, blue lines represent noises with variance equal to 0.1, green lines noises with variance equal to 1. Central rows: corresponding integrated processes with d=1 and d=2, respectively. Bottom panels: corresponding integrated processes with d=3.

In Fig. 3.1 some examples of realizations of multi-integrated white noise processes are reported. On the three top panels three different realizations of white noise processes are shown. Blue lines represent white noises with variance

equal to 0.1 while green lines represent white noises with variance equal to 1. In the two central rows of the figure the corresponding integrated processes, cases with $d = 1$ and $d = 2$ integrators respectively, are shown; in the bottom panels the case with $d = 3$. It is clear as lower values of the white noise variance correspond to smoother signals. Moreover, it is also evident that high values of d are associated to spiky waveforms.

3.3.2 EEG model

For the background EEG an AR model can be adopted. The AR modeling is commonly accepted and widespread used in EEG signal processing, see for example [53,59,83-85]. In particular, the parameters of the model are estimated, sweep by sweep, by using pre-stimulus samples. Before the stimulus onset, in fact, the unknown ERP is absent and only background EEG is present. By invoking the stationarity of the EEG noise on brief intervals [4], it is possible to exploit the statistical behavior of the noise, derived from the pre-stimulus, and extend it to the post-stimulus interval. In particular, by assuming that pre-stimulus can be described by an AR model, the *a priori* covariance matrix of $\boldsymbol{v}^i$ was computed as

$$\boldsymbol{\Sigma_{vv}}^i = \left(\sigma^i\right)^2 \left(\boldsymbol{A}^{i^T}\boldsymbol{A}^i\right)^{-1} \tag{3.8}$$

where $\boldsymbol{A}^i$ is the square n-dimensional Toeplitz matrix, whose first column $\left[1, a_1^i, \cdots, a_p^i, 0, \ldots, 0\right]^T$ comprises the coefficients of the pre-stimulus AR model $\left\{a_p^i\right\}$, $k = 1, \ldots, p^i$, and $\left(\sigma^i\right)^2$ is the variance of the white noise process which drives it.

According to the Eq. (3.4), the optimally filtered sweep is thus

$$\widehat{\boldsymbol{u}}^i = \left(\boldsymbol{A}^{i^T}\boldsymbol{A}^i + \gamma^i \boldsymbol{F}^T\boldsymbol{F}\right)^{-1} \boldsymbol{A}^{i^T}\boldsymbol{A}^i\boldsymbol{y}^i \tag{3.9}$$

where $\gamma^i = \left(\sigma^i/\lambda^i\right)^2$ is called regularization parameter or smoothing parameter. The role of γ^i can be easily understood by considering that $\widehat{\boldsymbol{u}}^i$ in Eq. (3.9) is the solution of

$$\underset{\boldsymbol{u}^i}{\operatorname{argmin}} \left\{ \left(\boldsymbol{y}^i - \boldsymbol{u}^i\right)^T \boldsymbol{A}^T \boldsymbol{A} \left(\boldsymbol{y}^i - \boldsymbol{u}^i\right) + \gamma^i \boldsymbol{u}^{i^T} \boldsymbol{F}^T \boldsymbol{F} \boldsymbol{u}^i \right\} \tag{3.10}.$$

It determines the compromise between the posterior information given by the data $\boldsymbol{y}^i$ and the *a priori* information contained in the matrix $\boldsymbol{F}$. Large values of γ^i are associated in very smooth estimates that do not match the data. In fact, if $\gamma^i \to \infty$ in Eq. (3.9) and Eq. (3.10), $\widehat{\boldsymbol{u}}^i \to 0$. On the other hand, if $\gamma^i \to 0$, $\widehat{\boldsymbol{u}}^i \to \boldsymbol{y}^i$, so $\widehat{\boldsymbol{u}}^i$ will accurately fit the data. The expression of Eq. (3.10) recalls the regularized mean squares described in section 2.2.4 and shows as regularization and Bayesian approach are related. In this approach, the covariance matrices of the noise and the unknown signal are not estimated directly from the data, as in [59], but they are obtained thanks to the employment of the specific models above-described.

3.3.3 Estimation of γ

The smoothing parameter γ^i is unknown, since it depends on λ^i which is unknown. In order to choose γ^i, several smoothing criteria can be adopted, see [82] for a review. In this case, the discrepancy criterion introduced by Twomey [86] is adopted. This criterion suggests to choose γ^i iteratively until

$$\boldsymbol{r}^{i^T} \boldsymbol{r}^i \cong E[\boldsymbol{v}^{i^T} \boldsymbol{v}^i] \tag{3.11}$$

where $\boldsymbol{r}^i$ is the residual vector associated to the i-th sweep, defined as

$$\boldsymbol{r}^i = \boldsymbol{y}^i - \widehat{\boldsymbol{u}}^i \tag{3.12}.$$

This criterion is based on the observation that the residual vector can be thought as an estimation of the measurement error vector $\boldsymbol{v}^i$.

3.3.4 Determination of the average ERP

Once the filtered sweeps have been obtained, the estimate of the mean ERP $\overline{\boldsymbol{u}}$ was computed as weighted averaging

$$\widehat{\overline{\boldsymbol{u}}} = \frac{\sum_{i=1}^{N} w^i \widehat{\boldsymbol{u}}^i}{\sum_{i=1}^{N} w^i} \tag{3.13}$$

where each weight w^i is inversely proportional to the expected value of the squared norm of the filter error, given by the trace of the covariance matrix of the estimation error $\tilde{\boldsymbol{e}}^i$

$$cov(\tilde{\boldsymbol{e}}^i) = \left(\sigma^i\right)^2 \left(\boldsymbol{A}^{i\,T}\boldsymbol{A}^i + \gamma^i \boldsymbol{F}^T\boldsymbol{F}\right)^{-1} \tag{3.14}.$$

In such a way, each sweep participates to the average estimation in proportion to its estimation accuracy. Another possibility consists in separately weighting each sample of each sweep. This can be done by taking as weight the inverse of the variance of the estimation error associated with the specific sample.

3.4 Stage 2: single-trial ERPs estimation

The second stage of the estimation procedure consists in the single-trial estimation. A procedure similar to that discussed for the first stage is performed. In particular, the ”average” profile $\widehat{\overline{\boldsymbol{u}}}$**,** obtained by Eq. (3.13), is exploited as if it were an *a priori* available information on the expected ERP. By using this information, the estimate $\breve{\boldsymbol{u}}^i$ of the i-th single-trial ERP is given by the following equation:

$$\breve{\boldsymbol{u}}^i = \hat{\hat{\boldsymbol{u}}} + \left(\boldsymbol{A}^{i\,T} \boldsymbol{A}^i + \xi^i \boldsymbol{L}^T \boldsymbol{L} \right)^{-1} \boldsymbol{A}^{i\,T} \boldsymbol{A}^i (\boldsymbol{y}^i - \hat{\hat{\boldsymbol{u}}}) \qquad (3.15).$$

The matrix $\boldsymbol{A}^i$ coincides with that identified in stage 1 for the same sweep and comprises the coefficients of the AR model used to describe the EEG background activity. Matrix $\boldsymbol{L}$ reflects the *a priori* model adopted to describe the deviation of the single-epoch ERP $\breve{\boldsymbol{u}}^i$ from the *a priori* expected value $\hat{\hat{\boldsymbol{u}}}$. Similarly to stage 1, a natural choice is to describe such a deviation as the realization of a white noise process, of variance denoted by $\left(\kappa^i\right)^2$, passed through p discrete integrators. Therefore, matrix $\boldsymbol{L}$ is equal to $\boldsymbol{\Delta}^p$. Fig. 3.2 shows some examples of deviations from the *a priori* expected value $\hat{\hat{\boldsymbol{u}}}$, modeled as white noise processes integrated $p = 1$ and $p = 2$ times. The *a priori* expected value $\hat{\hat{\boldsymbol{u}}}$ is assumed to be, in this example, obtained as an integrated white noise process, i.e. as a random walk process.

In the top panels deviations modeled as integrated white noise processes are shown, green lines represent profiles obtained by adding to the original random walk processes, shown by blue lines, deviations with white noise variance equal to 0.1, while red lines represent profiles obtained by adding to the original random walk processes deviations with white noise variance equal to 1. In the bottom panels profiles obtained with deviations modeled as doubly integrated white noise are represented. In principle, the value of p (related to the smoothness of the deviation of the single-trial ERP from the average ERP) may be different to that employed in the first stage for d (connected to the smoothness of the ERP per se). In general, in the ERP context, one may expect that p does not assume too high values. Obviously this depends on various factors, such as the level of similarity between the single trial profiles and the *a priori* expected value $\hat{\hat{\boldsymbol{u}}}$ and the variance of the input white noise process. This is clear in Fig. 3.2. With $p = 2$, in fact, profiles too different from the *a priori* expected value are

obtained if the variance is high, while acceptable deviations, even if substantial, result if the white noise variance is lower. As suggested for d, also the value of p can be set by trials through a preliminary study.

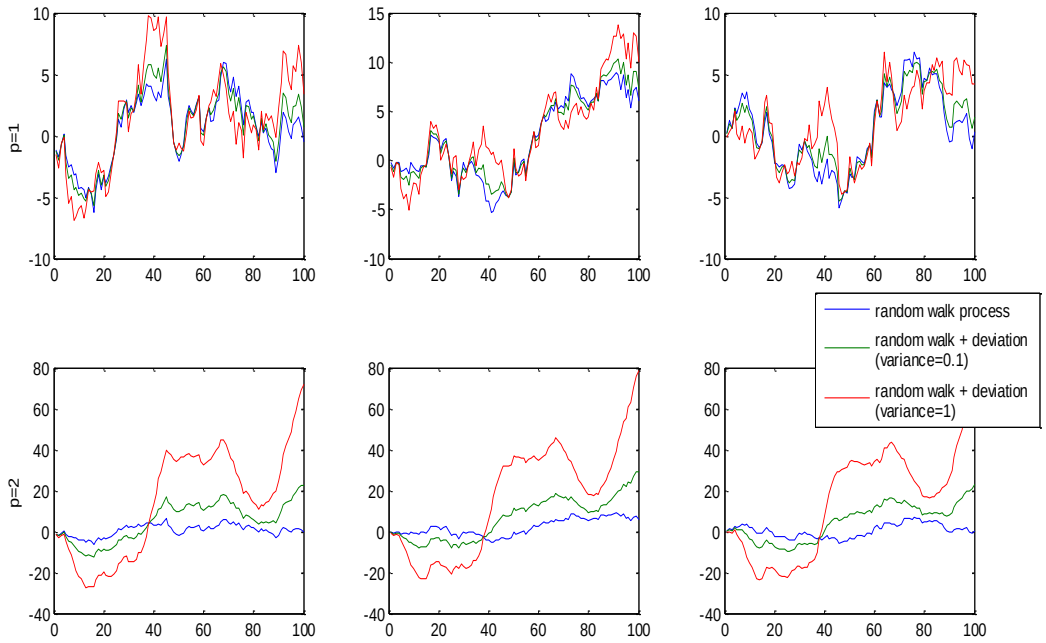

Figure 3.2. Different deviations from a random walk process. Top panels: three different realizations of random walk processes (blue lines), random walks plus deviations modeled as random walk with variance 0.1 (green lines), random walks plus deviations modeled as random walk with variance 1 (red lines). Bottom panels: as in the top panels but with deviations described by doubly integrated white noise models.

Finally, ξ^i represents, in this second stage, the ratio between $\left(\sigma^i\right)^2$ of Eq. (3.8) and the unknown variance $\left(\kappa^i\right)^2$ of the p-times integrated white noise process model which describes the deviation of the i-th ERP $\breve{\boldsymbol{u}}^i$ from the average response $\widehat{\boldsymbol{u}}$. As γ^i in stage 1, the unknown parameter ξ^i is estimated, independently sweep-by-sweep, by using the discrepancy smoothing criterion.

3.5 Numerical implementation

The estimate of the unknown ERP, as reported in Eq. (3.9) and (3.14), requires the inversion of a $n \times n$ matrix, and so $O(n^3)$ operations. This is very expensive from a computational point of view because of the regularization parameter has to be estimated by using an iterative procedure. For each iteration, the above-mentioned procedure implicates the computation of the estimate of the unknown vector and so the inversion of a $n \times n$ matrix, where n is the number of samples of a sweep. This procedure aimed to the determination of the regularization parameter is performed two times for each epoch, one time in the first stage and a second time in the second stage. In order to speed up this computation, two changes of coordinates have been carried out on the measurement model in order to whiten the noise and the unknown signal. In particular, an Singular Value Decomposition (SVD) strategy, extensively discussed in [87], can be used as described below.

Let's consider the measurement model of Eq. (3.1) that describes each recorded sweep as the sum of the unknown ERP and the EEG noise. For sake of simplicity, in this section the apex i used in the previous equations will be omitted. It is possible to obtain an analogous expression for the measurement model by subtracting to each member of Eq. (3.1) the *a priori* expected value of the average ERP as follows

$$\boldsymbol{y} - \overline{\boldsymbol{u}} = \boldsymbol{u}^* + \boldsymbol{v} \tag{3.16}$$

where $\boldsymbol{u}^* = \boldsymbol{u} - \overline{\boldsymbol{u}}$ and $\overline{\boldsymbol{u}}$ is the *a priori* expected value of the average ERP.

Thanks to a pre-multiplication by the Toeplitz matrix **A** (in the previous sections denoted with the apex i) that describes the EEG noise, it is possible to whiten the noise as follows

$$\boldsymbol{y}^* = \boldsymbol{A}\boldsymbol{u}^* + \boldsymbol{A}\boldsymbol{v} \tag{3.17}$$

where $\boldsymbol{y}^* = \boldsymbol{A}(\boldsymbol{y} - \bar{\boldsymbol{u}})$**.** In fact, in this way, the covariance matrix of the noise term $\boldsymbol{Av}$ in Eq. (3.17) is the diagonal matrix $\sigma^2 \boldsymbol{I}_n$.

Let's consider now the product $\boldsymbol{H} = \boldsymbol{AF}^{-1}$, where $\boldsymbol{F}$ indicates the matrix $\boldsymbol{F}^i$ of the first stage or the matrix $\boldsymbol{L}^i$ of the second stage. Three matrices $\boldsymbol{U}$, $\boldsymbol{Z}$, and $\boldsymbol{D}$ (with $\boldsymbol{U}$ and $\boldsymbol{Z}$ unitary and $\boldsymbol{D}$ diagonal) define the SVD decomposition of $\boldsymbol{H}$, shown in formula (3.18)

$$\boldsymbol{U}^T \boldsymbol{HZ} = \boldsymbol{D} \tag{3.18}.$$

By using these matrices it is possible to define the following change of coordinates that allows to make diagonal the covariance matrix of the unknown vector $\mathbf{u}^*$

$$\boldsymbol{\xi} = \boldsymbol{U}^T \boldsymbol{y}^* \tag{3.19}$$

$$\boldsymbol{\varepsilon} = \boldsymbol{U}^T \boldsymbol{Av} \tag{3.20}$$

$$\boldsymbol{\varepsilon} = \boldsymbol{Z}^T \boldsymbol{Fu}^* \tag{3.21}$$

By exploiting the (3.19), (3.20), and (3.21), the following expression can be obtained for the (3.17)

$$\boldsymbol{\xi} = \boldsymbol{D\eta} + \boldsymbol{\varepsilon} \tag{3.22}.$$

In this system of coordinates the covariance matrices of the vectors $\boldsymbol{\eta}$ and $\boldsymbol{\varepsilon}$ are diagonal and the estimate of $\boldsymbol{\eta}$ can be easily obtained as follows

$$\hat{\boldsymbol{\eta}} = (\boldsymbol{D}^T \boldsymbol{D} + \gamma \boldsymbol{I}_n)^{-1} \boldsymbol{D}^T \boldsymbol{\xi} \tag{3.23}$$

where γ is the regularization parameter that has to be estimated. Since the matrix $\boldsymbol{D}$ is diagonal, the estimate of the single sample η_k $(k = 1, \dots, n)$ can be expressed as

$$\hat{\eta}_k = \frac{d_k}{d_k^2 + \gamma} \xi_\kappa \tag{3.24}$$

where d_k is the k-th element of the diagonal of the matrix $\boldsymbol{D}$. So, thanks to this strategy, the unknown vector is estimated, for each iteration with γ changing, in $O(n)$ operations.

The computation of the weighted sum of the squared residuals, useful for the determination of the optimum value of the parameter γ according to the discrepancy criterion, is obtained in a similar way.

The use of this optimization scheme considerably reduces the computational time. Even if the entire procedure requires $O(n^3)$ operations, because of the presence of the SVD decomposition, the advantage is that this SVD decomposition is computed just one time for sweep.

3.6 Conclusions

The two-stage methodology above-described allows to obtain the estimates of the average ERP and of the single-trial ERPs in a simple and versatile way. Each sweep is characterized by its own parameters that describe the background EEG noise and the unknown ERP. While the parameters associated to the EEG noise present in the i-th sweep are estimated by exploiting the corresponding pre-stimulus data, the variance of the white noise process which drives the model that describes the *a priori* smoothness of the unknown ERP can be easily estimated from post-stimulus samples by using a smoothing criterion. So, in this approach, no strong assumptions on the shape of the unknown ERP signals are done. This makes the method very flexible and applicable to different ERP

morphologies, by tuning the number of integrators employed in the first and in the second stage. The number of integrators of the first stage describes the smoothness of the ERP per se, while that of the second stage models the smoothness of the deviation of the single-trial ERP from the average ERP. So, in this approach each single-trial ERP can be obtained by adding to the average ERP the above-mentioned deviation. This concept could be formalized in a more sophisticated way in a population analysis context. In fact, the ERPs generated during an experimental task present some similarities and the exploitation of this characteristic could be useful in the estimation procedure. The deviations of the single-trial ERPs from the average ERP can be seen as realizations of the same stochastic process whose parameters have to be estimated by utilizing all the data from all the available sweeps, similarly to the estimation of the average ERP. In the above-described two-stage approach, instead, the parameters associated to each sweep are estimated by utilizing only the data relative to the same sweep. A technique that uses a population approach will be described in the following chapter. It assumes that each sweep can be modeled as the sum of three components: an average ERP common to all the sweeps, an individual shift that characterizes the current sweep, and a noise component variable from sweep to sweep. In this approach, all the data of all the sweeps are used to simultaneously determine the average ERP and the single-trial responses.

4 A ONE STAGE MULTI-TASK LEARNING APPROACH FOR THE EXTRACTION OF ERPS

4.1 Introduction

The one stage technique here adopted is based on a method originally presented in Neve et al. [88] and Pillonetto et al. [89], where it was employed to estimate xenobiotics and glucose concentration, respectively. By using this technique, here revised and adapted, the ERPs extraction problem is treated in a new context where the average response and single-trial ERPs are simultaneously estimated.

As known, even if identical stimuli are delivered to a subject, the ERPs evoked during an experimental task will be very similar among them but not exactly alike. They have probably the same pattern, i.e. the same expected peaks, but latencies and amplitudes of these peaks will change trial by trial. In the light of this, the evoked responses could be considered as the elements of a "population". As "population", they will have common characteristics condensed in a curve called "population average component". Each of them, as "individual", will have its own features that differentiate it from the other individuals and that are described in the so-called "individual shift". So, each ERP, denoted as "individual component", will contain both the "average component" and the "individual shift". Since the ERPs are seen as members of a population, all the available information on one of them can be useful for estimating the others and vice versa, in an context in which all the sweeps are simultaneously used. As estimation results, the "average component" will represent effectively the average behavior of the ERPs, while the individual components will give information on the ERPs at single-trial level.

Remark. It is worth pointing out that this kind of approach is not new in biomedical applications. In fact, the so-called population analysis is largely used in the metabolism and pharmacokinetics areas, above all in cases in which few and noisy samples are available for each individual, see for example [90-93] and also in other contexts, such as medical imaging [94] and genomics [95]. A large number of individuals and their data often make up for the lack of samples available for each subject. In a more general framework, this problem can be seen as that of estimating several similar function from a finite number of noisy samples. It has been shown that, in this situation, the standard learning of a function at a time is often outperformed by the multi-task learning approach that simultaneously utilizes all the available information. Other fields of applications of this approach are, for example, economics and finance [96-98].

4.2 Model of the data

The method is based on the additive measurement model of Eq. (3.1) with the further assumption that the unknown ERP is given by the sum of two continuous-time functions: the average component $\bar{u}(t)$ and the individual shift $\tilde{u}(t)$. For the i-th ($i = 1, \dots, N$) sweep and the time instant t_k ($k = 1, \dots, n$) the noisy sample y_k^i is available

$$y_k^i = \bar{u}(t_k) + \tilde{u}^i(t_k) + v^i(t_k) \qquad (4.1).$$

The stochastic processes $\bar{u}(t)$, $\tilde{u}(t)$ and $v^i(t)$, are assumed independent of each other.

Simultaneously considering all the data of the N sweeps, the model can be written in a vector notation as

$$\boldsymbol{y} = \overline{\boldsymbol{u}} + \widetilde{\boldsymbol{u}} + \boldsymbol{v} \tag{4.2}$$

where

$$\boldsymbol{y} := [y_1^1 \ \ldots y_n^1 \ y_1^2 \ \ldots y_n^2 \ldots y_1^N \ \ldots y_n^N] \tag{4.3}$$

$$\overline{\boldsymbol{u}} := [\,\overline{u}\,(t_1) \ \ldots \overline{u}\,(t_n)\,\overline{u}\,(t_1) \ \ldots \overline{u}\,(t_n) \ldots \overline{u}\,(t_1) \ \ldots \overline{u}\,(t_n)] \tag{4.4}$$

$$\widetilde{\boldsymbol{u}} := [\,\widetilde{u}^{\,1}(t_1) \ \ldots \widetilde{u}^{\,1}(t_n)\,\widetilde{u}^{\,2}(t_1) \ \ldots \widetilde{u}^{\,2}(t_n) \ldots \widetilde{u}^{\,N}(t_1) \ \ldots \widetilde{u}^{\,N}(t_n)] \tag{4.5}$$

$$\boldsymbol{v} := [\,v^1(t_1) \ \ldots v^1(t_n)\,v^2(t_1) \ \ldots v^2(t_n) \ldots v^N(t_1) \ \ldots v^N(t_n)] \tag{4.6}.$$

Note that in this model, the involved vectors have a dimension equal to $n_{TOT} = N \times n$.

4.3 Derivation of the estimator of average and single-trial ERPs

4.3.1 The average ERP estimator

Consider the measurement model of Eq. (4.2). In a Bayesian embedding, the MMSE of the vector $\overline{\boldsymbol{u}}$ is the mean of the posterior PDF $p(\overline{\boldsymbol{u}}|\boldsymbol{y})$. As already pointed out in section 3.3, this estimator can be expressed in a closed form if the involved processes are jointly Gaussian. Alternatively, a linearity constraint on the estimator can be assumed.

The Bayesian estimate of $\overline{\boldsymbol{u}}$, in terms of minimizing the MMSE is obtained as

$$\widehat{\overline{\boldsymbol{u}}} = E[\overline{\boldsymbol{u}}|\boldsymbol{y}] = \boldsymbol{\Sigma}_{\overline{\boldsymbol{u}}}\left(\boldsymbol{\Sigma}_{\boldsymbol{y}}\right)^{-1}\boldsymbol{y} = \boldsymbol{\Sigma}_{\overline{\boldsymbol{u}}}(\boldsymbol{\Sigma}_{\overline{\boldsymbol{u}}} + \boldsymbol{\Sigma}_{\widetilde{\boldsymbol{u}}} + \boldsymbol{\Sigma}_{\boldsymbol{v}})^{-1}\boldsymbol{y} \tag{4.7}$$

where $\boldsymbol{\Sigma}_{\bar{\boldsymbol{u}}}$, $\boldsymbol{\Sigma}_{\tilde{\boldsymbol{u}}}$ and $\boldsymbol{\Sigma}_{\boldsymbol{v}}$ are the covariance matrices of the vectors $\bar{\boldsymbol{u}}$, $\tilde{\boldsymbol{u}}$, and $\boldsymbol{v}$, respectively. In order to build $\boldsymbol{\Sigma}_{\bar{\boldsymbol{u}}}$, $\boldsymbol{\Sigma}_{\tilde{\boldsymbol{u}}}$ and $\boldsymbol{\Sigma}_{\boldsymbol{v}}$, let us recall how these three vectors have been constructed: as evident from Eq. (4.4), Eq. (4.5) and Eq. (4.6), the first n values of the vectors $\bar{\boldsymbol{u}}$, $\tilde{\boldsymbol{u}}$, and $\boldsymbol{v}$ are the n samples referred to the first sweep, the subsequent n samples are referred to the second sweep, and so on. In order to obtain the expressions of the covariance matrices of these vectors, the covariance functions of the average curve $\bar{u}(t)$, of the individual shifts $\tilde{u}^i(t)$ (with i varying from 1 to N) and of the noise vectors must be computed.

As regards the unknown signals, we denote with $\bar{R}(t,\tau)$ and $\tilde{R}(t,\tau)$ these matrices

$$\bar{R}(t,\tau) := Cov[\bar{u}(t),\bar{u}(\tau)] \tag{4.8}$$

$$\tilde{R}(t,\tau) := Cov\left[\tilde{u}^i(t),\tilde{u}^i(\tau)\right] \tag{4.9}.$$

Suitable models for the description of the unknown signals are needed in order to compute $\bar{R}(t,\tau)$ and $\tilde{R}(t,\tau)$.

4.3.1.1 ERP model

According to the scheme proposed in [88] integrated Wiener processes are employed in order to give a description of the smoothness of the average curve and of the individual shifts. An integrated Wiener process can be described by the following state-space model

$$\begin{aligned} \dot{x}(t) &= \boldsymbol{A}x(t) + \boldsymbol{B}w(t) \\ z(t) &= \boldsymbol{C}x(t) \end{aligned} \tag{4.10}$$

where $x(0) \sim N(0, \boldsymbol{X}_0)$, $w(t) \sim WGN(0, \lambda^2)$ independent of $x(0)$ and

$$\boldsymbol{A} = \begin{bmatrix} 0 & 1 \\ 0 & 0 \end{bmatrix}; \boldsymbol{B} = \begin{bmatrix} 0 \\ 1 \end{bmatrix}; \boldsymbol{C} = [1 \quad 0].$$

The parameter λ^2 is the variance of the white Gaussian noise process $w(t)$ that drives the model and it is related to the regularity of the realizations; in fact smaller values correspond to smoother signals. In particular, the elements of the average ERP $\bar{u}(t)$ are assumed to be extracted from a zero mean integrated Wiener process driven by a white noise process with unknown variance $\bar{\lambda}^2$. The elements of the individual shift vectors $\tilde{u}^i(t)$ are modeled in the same way, but with the unknown variance of the white noise process equal to $\tilde{\lambda}^2$. A such continuous-time population model has been introduced in [88] in order to deal with the problem, typical in pharmacokinetics, of samples not uniformly spaced in time. As proved in the above-cited work, in case of signals whose initial conditions can be assumed deterministically known (and this is the case of our signals that are assumed to be zero at the time zero), the auto-covariance functions of the processes assume the following expressions

$$\bar{R}(t,\tau) = \bar{\lambda}^2 \begin{cases} \frac{t^2}{2}(\tau - \frac{t}{3}), & t \leq \tau \\ \frac{\tau^2}{2}(t - \frac{\tau}{3}), & t > \tau \end{cases} \tag{4.11}$$

$$\tilde{R}(t,\tau) = \tilde{\lambda}^2 \begin{cases} \frac{t^2}{2}(\tau - \frac{t}{3}), & t \leq \tau \\ \frac{\tau^2}{2}(t - \frac{\tau}{3}), & t > \tau \end{cases} \tag{4.12}.$$

where the parameters $\bar{\lambda}^2$ and $\bar{\lambda}^2$ represent the unknown variances of the white noise processes. By assuming valid this model for the description of the unknown signals the following expressions are obtained for the covariance matrices $\boldsymbol{\Sigma}_{\bar{\boldsymbol{u}}}$ and $\boldsymbol{\Sigma}_{\tilde{\boldsymbol{u}}}$

$$\boldsymbol{\Sigma}_{\bar{\boldsymbol{u}}} = \begin{bmatrix} \bar{\boldsymbol{R}} & \cdots & \bar{\boldsymbol{R}} \\ \vdots & \ddots & \vdots \\ \bar{\boldsymbol{R}} & \cdots & \bar{\boldsymbol{R}} \end{bmatrix} \tag{4.13}$$

where

$$\bar{\boldsymbol{R}} = \begin{bmatrix} \bar{R}(t_1, t_1) & \cdots & \bar{R}(t_1, t_n) \\ \vdots & \ddots & \vdots \\ \bar{R}(t_n, t_1) & \cdots & \bar{R}(t_n, t_n) \end{bmatrix} \tag{4.14}$$

$$\boldsymbol{\Sigma}_{\tilde{\boldsymbol{u}}} = blockdiag\{\tilde{\boldsymbol{R}}, \dots, \tilde{\boldsymbol{R}}\} \tag{4.15}$$

where

$$\tilde{\boldsymbol{R}} = \begin{bmatrix} \tilde{R}(t_1, t_1) & \cdots & \tilde{R}(t_1, t_n) \\ \vdots & \ddots & \vdots \\ \tilde{R}(t_n, t_1) & \cdots & \tilde{R}(t_n, t_n) \end{bmatrix} \tag{4.16}.$$

Note that $\boldsymbol{\Sigma}_{\tilde{\boldsymbol{u}}}$ is a block diagonal matrix, this is because the individual shifts are assumed to be independent of each other among the different sweeps.

4.3.1.2 EEG model

As regards the noise, a specific model able to describe the characteristics of the background EEG has been employed. As in the previous method, the evidence that the background EEG can be described, on segments of brief duration, by an autoregressive model can been exploited. Order and parameters of this model are estimated the pre-stimulus signal of each sweep, as done previously. Before the stimulus onset, in fact, the unknown ERP is absent and only background EEG is present. By invoking the stationarity of the EEG noise on brief intervals, it is possible to exploit the statistical behavior of the noise, derived from the pre-stimulus, and extend it to the post-stimulus interval. For the i-th sweep the covariance matrix of $\boldsymbol{v}^{\boldsymbol{i}}$ is

$$\boldsymbol{\Sigma}_{\boldsymbol{v}}^{i} = (\sigma^{i})^{2}(\boldsymbol{A}^{i^{T}}\boldsymbol{A}^{i})^{-1} \tag{4.17}$$

where $\boldsymbol{A}^{i}$ is the square n-dimensional Toeplitz matrix, whose first column $\left[1, a_1^i, \cdots, a_{p^i}^i, 0, \ldots, 0\right]^T$ comprises the coefficients of the pre-stimulus AR model $\left\{a_k^i\right\}$, $k = 1, \ldots, p^i$, and $\left(\sigma^i\right)^2$ is the variance of the white noise process which drives it.

By adopting this model for the EEG noise and by remembering the independence of the noise vectors among the different sweeps, the following expression can be derived for $\boldsymbol{\Sigma}_{\boldsymbol{v}}$

$$\boldsymbol{\Sigma}_{\boldsymbol{v}} = blockdiag\{\boldsymbol{\Sigma}_{\boldsymbol{v}}{}^{1}, \ldots, \boldsymbol{\Sigma}_{\boldsymbol{v}}{}^{N}\} \tag{4.18}.$$

4.3.1.3 Estimation of the hyper-parameters

As evident from Eq. (4.7), the estimate of the average ERP is dependent only from the parameters $\bar{\lambda}^2$and $\tilde{\lambda}^2$. Since *a priori* knowledge about these parameters is often not available, they have been estimated from the data via Maximum Likelihood (ML). So, the hyper-parameters are such that

$$\left[\bar{\lambda}^2, \tilde{\lambda}^2\right] = argmin\left(\log\left[det\left(\boldsymbol{\Sigma}_{\boldsymbol{y}}\right)\right] + \boldsymbol{y}^T\boldsymbol{\Sigma}_{\mathbf{y}}{}^{-1}\boldsymbol{y}\right) \tag{4.19}.$$

4.3.2 The single-trial ERP estimator

The estimation of the single-trial ERPs is performed similarly to the estimation of the average ERP. The linear additive model of Eq. (4.2) is assumed to be valid. So, the individual shifts to be added to the average ERP have to be estimated. Under

the same assumption discussed in the previous section the mean of the posterior PDF $p(\widetilde{\boldsymbol{u}}|\boldsymbol{y})$ is computed as follows

$$\widehat{\widetilde{\boldsymbol{u}}} = E[\widetilde{\boldsymbol{u}}|\boldsymbol{y}] = \boldsymbol{\Sigma}_{\widetilde{\mathbf{u}}}\left(\boldsymbol{\Sigma}_{\mathbf{y}}\right)^{-1}\mathbf{y} = \boldsymbol{\Sigma}_{\widetilde{\mathbf{u}}}(\boldsymbol{\Sigma}_{\overline{\mathbf{u}}} + \boldsymbol{\Sigma}_{\widetilde{\mathbf{u}}} + \boldsymbol{\Sigma}_{\mathbf{v}})^{-1}\mathbf{y} \quad (4.20).$$

where $\boldsymbol{\Sigma}_{\overline{\boldsymbol{u}}}$, $\boldsymbol{\Sigma}_{\widetilde{\boldsymbol{u}}}$ and $\boldsymbol{\Sigma}_{\boldsymbol{v}}$ are the covariance matrices of the vectors $\overline{\boldsymbol{u}}$, $\widetilde{\boldsymbol{u}}$, and $\boldsymbol{v}$, respectively.

These covariance matrices are the same obtained in the previous section and, as already discussed, they depend only from the parameters $\bar{\lambda}^2$ and $\tilde{\lambda}^2$. These parameters are the same estimated from Eq. (4.19). Note that only one parameter, i.e. $\tilde{\lambda}^2$, is used to describe the individual shifts that are considered as realizations of the same stochastic process. Another possibility consists in assuming a different $\tilde{\lambda}^2$ for each sweep and in estimating $N + 1$ parameters via ML.

Once the individual shifts have been computed for the i-th ($i = 1, \dots, N$) sweep and the time instant t_k ($k = 1, \dots, n$) the i-th single-trial ERP at t_k is given by

$$u^i(t_k) = \overline{u}(t_k) + \tilde{u}^i(t_k) \quad (4.21).$$

Note that the average ERP and the individual shift are simultaneously estimated by employing all the available data. First, the hyper-parameters are computed by minimizing a function that depends from all the data of all the sweeps contained in the vector $\boldsymbol{y}$ and from the covariance matrix $\boldsymbol{\Sigma}_{\boldsymbol{y}}$. Once the hyper-parameters have been determined, the estimates of the average ERP and the individual shifts are directly computed from the (4.7) and (4.20), in which all the available data are again utilized.

4.4 Numerical implementation

In order to obtain the estimates of the unknown vectors, the inverse of the matrix $\boldsymbol{\Sigma_y}$ has to be computed. Moreover, the hyper-parameters have to be evaluated via likelihood maximization and this requires the computation of the inverse and the determinant of the matrix $\boldsymbol{\Sigma_y}$. Since in the vector $\boldsymbol{y}$ all the data of all the sweeps are contained, the computational time needed for these operations is a cubic function of n_{TOT}, that is the total number of samples. In case of EEG signals this number can be very high.

The computational effort can be reduced by using efficient computational strategies, described in detail in [89]. These strategies allow to obtain the estimate of the unknown signals by using an algorithm whose complexity scales with the cube of the number of samples of each sweeps. Since the number and the location of the sampling instants are the same for all the available sweeps, the determinant of the covariance matrix $\boldsymbol{\Sigma_y}$ and the product $\boldsymbol{\Sigma_y}^{-1}\boldsymbol{y}$, present in the (4.7), (4.19) and (4.20), can be computed in $O(n^3)$ operations.

In fact, the matrix $\boldsymbol{\Sigma_y}$ has the following expression

$$\boldsymbol{\Sigma_y} = \begin{bmatrix} \overline{\boldsymbol{R}} & \cdots & \overline{\boldsymbol{R}} \\ \vdots & \ddots & \vdots \\ \overline{\boldsymbol{R}} & \cdots & \overline{\boldsymbol{R}} \end{bmatrix} + blockdiag(\widetilde{\boldsymbol{R}} + \boldsymbol{\Sigma_v^1}, \dots, \widetilde{\boldsymbol{R}} + \boldsymbol{\Sigma_v^N}) \tag{4.22}$$

where $\overline{\boldsymbol{R}}$ and $\widetilde{\boldsymbol{R}}$ are the matrices defined in Eq. (4.14) and (4.16).

In this condition, the covariance matrix can be handled more easily, see [89]. In particular, the computation of the determinant of $\boldsymbol{\Sigma_y}$ is carried out as follows

$$det(\boldsymbol{\Sigma_y}) = \left(\prod_{i=1}^{N} det(\boldsymbol{C}_{ii}) \right)^{\boldsymbol{2}} \tag{4.23}$$

where $\boldsymbol{C}_{ii}$ are $n \times n$ square matrices such that

$$\boldsymbol{C}_{ii} = chol[\boldsymbol{A}_{ii} - \boldsymbol{D}_i] \tag{4.24}$$

$$\boldsymbol{C}_{(i+1)i} = (\overline{\boldsymbol{R}} - \boldsymbol{D}_i)\left(\boldsymbol{C}_{ii}{}^{T}\right)^{-1} \tag{4.25}$$

$$\boldsymbol{C}_{ki} = \boldsymbol{C}_{(i+1)i} \qquad for\ k > i+1 \tag{4.26}$$

$$\boldsymbol{D}_{i+1} = \boldsymbol{D}_i + \boldsymbol{C}_{(i+1)i}\boldsymbol{C}_{(i+1)i}{}^{T} \tag{4.27}$$

where $\boldsymbol{A}_{ii} = \overline{\boldsymbol{R}} + \widetilde{\boldsymbol{R}} + \boldsymbol{\Sigma}_{\boldsymbol{v}}^{i}$ and $\boldsymbol{D}_i = \boldsymbol{0}$ is the initial position.

$chol[\boldsymbol{X}]$ indicates the Cholesky factorization of the symmetric and positive definite matrix $\boldsymbol{X}$, i.e. the lower triangular matrix $\boldsymbol{C}$ such that $\boldsymbol{C}\boldsymbol{C}^{T} = \boldsymbol{X}$.

The computation of the product $\boldsymbol{\Sigma}_{\boldsymbol{y}}{}^{-1}\boldsymbol{y}$ requires $O(n^3)$ operations too. This is thanks to the particular structure of the covariance matrix of $\boldsymbol{y}$ and to the application of the matrix inversion lemma; see [89] for a detailed explanation of the procedure.

Remark. Furthermore, it is interesting to note that, once the hyper-parameters are known, it is possible to obtain the estimate of the components also in a time instant for which the measurement is not available. This possibility can be exploited in order to reduce the dimension of the matrix by which the computational complexity mainly depends; in fact, the estimate on all the available samples can be obtained also by employing data of a subset of the sampling grid.

4.5 Discussion

In the present and in the previous chapters two estimation methodologies proposed for the extraction of the ERPs have been presented in detail.

These technique have several analogies. They both works in a Bayesian embedding in which the involved signals are assumed to be realizations of stochastic processes, about which some *a priori* knowledge is available. So, they differ from the techniques that hypothesize that the unknown ERP has a fixed waveform. Although they both assume the knowledge of some information about the unknown signals, they utilize non parametric models. The assumptions on the signals are reduced to a minimum and, in particular, only the knowledge about the smoothness is exploited. In the first technique, the ERP is modeled as the realization of a stochastic process obtained as the cascade of some integrators driven by a white noise sequence. In the second case, and in a more general context, a continuous stochastic model is adopted and the unknown signals are modeled as integrated Wiener processes. The main difference between the two approaches lies in the procedure used to estimate the average and the single-trial ERPs. Both the techniques assume that the ERP is given by the sum of an average component and of an individual one. The first technique computes the average ERP as weighted averaging (with suitable values) of all the sweeps. These sweeps are employed after a filtering in a Bayesian embedding. In the subsequent stage it is assumed that the average component is present in all the sweeps and the difference between this component and the average ERP is estimated in the same context. This estimation is carried out for each sweep by using only its data and by estimating a parameter that is related to the smoothness of the particular sweep. In the second technique the average component is directly computed in a different way by using all the available sweeps, under the hypothesis that this component is common to all the sweeps. The individual components are directly estimated by exploiting all the data of all the sweeps. They are considered as different realization of a stochastic process whose hyper-parameter has been estimated from the data.

In the next chapter the performance of the proposed approaches will be assessed on a simulated dataset, also in comparison with literature methods.

5 ASSESSMENT ON SIMULATED DATA

This chapter is focused on the results obtained on simulated datasets. The capability of the two techniques in estimating the average profile and in extracting single-trial ERPs is tested at different levels of SNR by valuating suitable performance indexes. The first two sections deals with the procedure used to construct simulated data and with the description of the adopted performance indexes. In the three successive sections, the estimation results are presented and discussed.

5.1 Database description

In this section the procedure used to create simulated datasets with different levels of SNR will be described. Each simulated sweep has been constructed by adding to a simulate single-trial ERP a simulated EEG noise realization, according to the additive model of Eq. (3.1). Single-trial ERPs and EEG noise sequences have been created as follows. First, a reference ERP was obtained by fitting a sum of five Gaussian functions against a real ERP. This ERP was estimated through CA technique from an EEG signal recorded in one of the young normal subjects performing the task later described in section 6.1. Fig. 5.1 and Table 5.1 shows the reference ERP and the parameters of the five Gaussian functions.

Amplitudes and occurrences of the peaks of the Gaussian functions shown in Table 5.1 can be associated to latencies and amplitudes of some of ERP components. For example, the first function has a negative peak with amplitude of -4 μV occurring at a time of 110 ms. It could be identified with the N1 component shown in Fig. 1.4. The other four functions obtained by the fitting procedure have, instead, positive peaks. Particular attention will be paid on the fourth Gaussian function, shown on shaded background in Table 5.1. It presents

a latency of 390 ms and an amplitude of 13 μV, typical characteristics of the P300 wave.

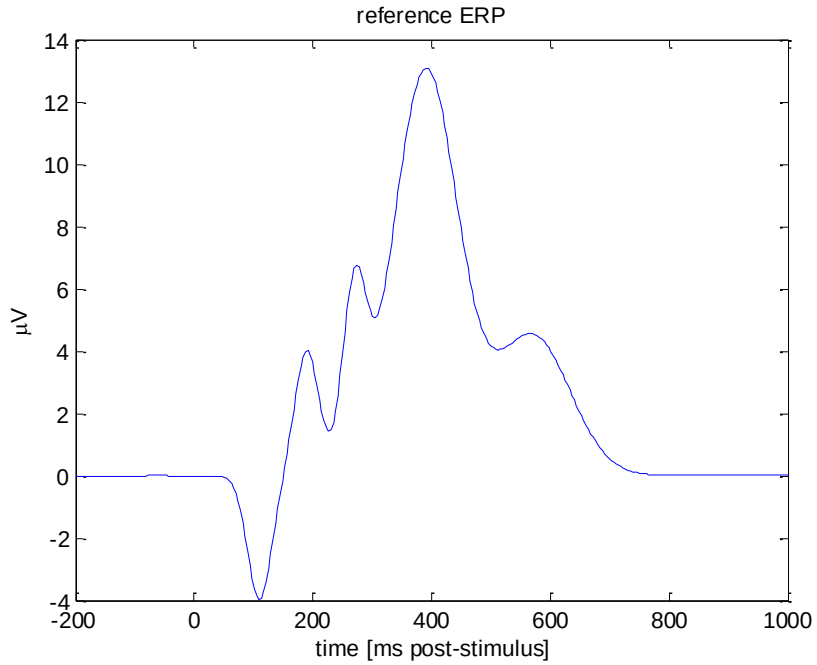

Figure 5.1. Reference ERP obtained by fitting a sum of five Gaussian functions against a real ERP estimated from real data.

Gaussian function	Peak amplitude [in μV]	Peak occurrence [in ms]	Standard deviation [in ms]
1	-4	110	28.3
2	4	190	28.3
3	5.5	270	28.3
4	13	390	75.5
5	4.5	570	89.4

Table 5.1. Peak amplitude, peak latency and standard deviation of the five Gaussian functions used to simulate the reference ERP.

Once the reference ERP has been constructed as sum of the five Gaussian functions, synthetic single-trial ERPs have been obtained by perturbing, according to Gaussian distributions, amplitudes and occurrences of the peaks of the five functions. The standard deviations of the Gaussian functions, related to the width of "bells", have not been modified. Expected values and standard deviations of Gaussian distributions according to which amplitudes and occurrences of the peaks of the five functions have been perturbed are reported in Table 5.2.

Gaussian function	**Mean of amplitudes [in μV]**	**Standard deviation of amplitudes [in μV]**	**Mean of latencies [in ms]**	**Standard deviation of latencies [in ms]**
1	-4	0.5	110	6
2	4	0	190	12
3	5.5	0	270	18
4	13	1	390	25
5	4.5	0	570	15

Table 5.2. Expected values and standard deviations of the Gaussian distribution from which amplitudes and latencies of the peaks reproducing the ERP components have been drawn.

For each of the five Gaussian functions, two Gaussian distributions have been defined: the first distribution describes the amplitude variability, while the second one describes the latency variability. The peak amplitude of the corresponding function in the reference ERP has been chosen as mean value of the Gaussian distribution that describes the amplitude variability. The time of peak occurrence of the corresponding function in the reference ERP has been

chosen as mean of the Gaussian distribution that describes the latency variability. With regard to the standard deviations of the distributions, special attention has been paid to the fourth function reproducing the P300 component, whose corresponding parameters are shown on shaded background in Table 5.2. For the P300 amplitude, a standard deviation of 1 μV was used. This means that about 68% of the generated P300 amplitudes are within the range [12 – 14] μV, about 95% lie in the range [11 – 15] μV, and about 97% fall in the range [10 – 16] μV. For the P300 latency, a standard deviation of 25 ms was used. This means that about 68% of the generated P300 latencies are within the range [365 – 415] ms, about 95% lie in the range [340 – 440] ms, and about 97% fall in the range [315 – 465] ms. As regards the latencies of the other components, a high enough standard deviation has been chosen for late potentials while a low standard deviation for the early ones. As far as the amplitudes of the other components are concerned, only the amplitude of the first component has been allowed to vary with a standard deviation equal to 0.5 μV. For simplicity, the other components have been considered to have a fixed amplitude. In Fig. 5.2, 15 representative simulated ERPs are shown.

According to the additive model of Eq. (3.1), EEG noise sequences have to be added to the so-obtained ERPs. These EEG noise sequences have been created by simulating AR models driven by white noise. The parameters of the used AR models were obtained by fitting the pre-stimulus data of pre-processed EEG signals (see section 6.1). In particular, with a sampling frequency of 256 Hz, 500 ms long pre-stimuli have been employed and parameters of the AR model have been determined according to the Yule-Walker approach. The optimum order has been chosen in the range [2-14] by evaluating the improvement of the variance of the prediction error. In particular, the order p has been selected if the difference between the variance of the prediction error at order p and that at order p+1 was inferior to the 5 % of the variance of the prediction error at the order p. Unstable AR models, or AR models that did not pass the Anderson test on the whiteness of the prediction error have not been considered.

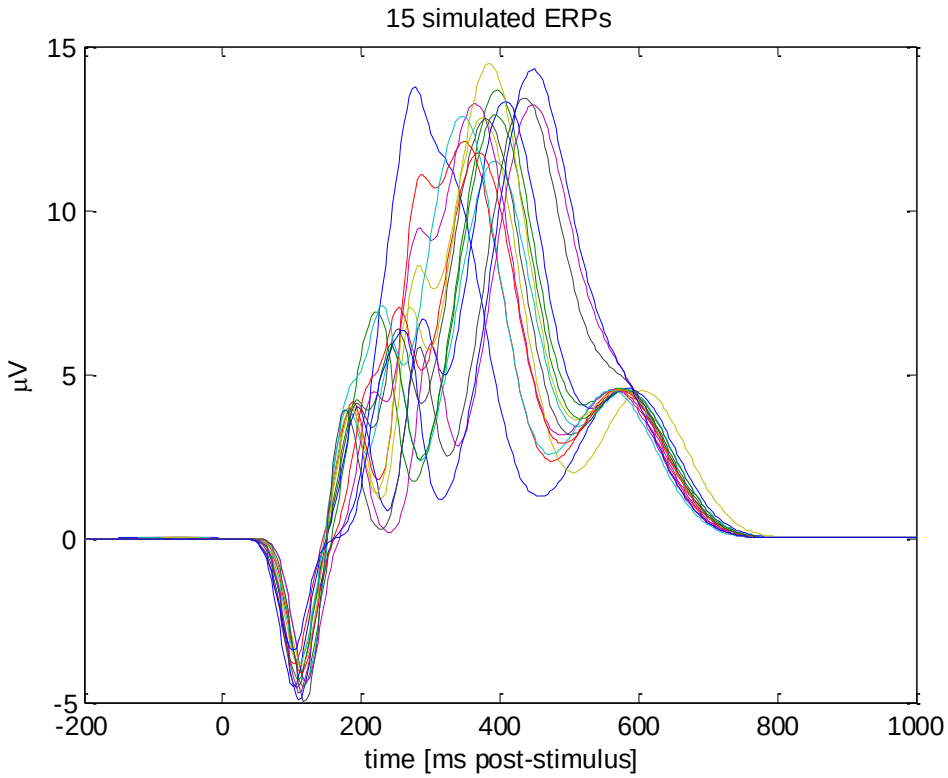

Figure 5.2. 15 simulated ERPs.

In order to obtain different simulated datasets with different levels of SNR, these synthetic EEG epochs were multiplied by an suitable scale factor. For each sweep, the SNR was defined as the ratio between the average power of the true signal and the average power of the noise. To simulate different SNR conditions, five groups of 2000 synthetic sweeps were generated. Each group comprised sweeps having a SNR uniformly distributed in one of five non overlapping 0.2 width bins (0.2-0.4, 0.4-0.6, 0.6-0.8, 0.8-1,1-1.2), as shown in Table 5.3; a similar procedure can be found in several works, e.g. [72,73] .

group	1	2	3	4	5
SNR range	0.2 – 0.4	0.4 – 0.6	0.6 – 0.8	0.8 - 1	1 – 1.2

Table 5.3. The 5 groups and the corresponding SNR ranges.

In order to give an idea of the variability of the simulated sweeps at different levels of SNR, Fig. 5.3 shows, for three SNR levels, 5 sweeps obtained by adding to the 5 simulated ERPs the simulated EEG noise multiplied by the appropriate scale factor. As visible from the figure, in the first group (worst case) the underlying ERPs, represented by thick lines, are totally hidden by the noise that has a very large amplitude; in the last group, instead, the ERPs are more easily recognizable.

In order to evaluate the effectiveness of the methods as the number of the employed sweeps and the SNR conditions change, for each SNR level 100 groups of N sweeps (with N varying from 2 to 20) were obtained by drawing, for 100 times, N different signals from the 2000 sweeps simulated with the corresponding SNR. The values of N have been chosen intentionally small in order to test the performance of the ERP estimation techniques when few sweeps are available. As discussed in section 1.2.3, in fact, the reduction of the number of sweeps traditionally required for the estimation of the average profile is one of the main problems in this context. Obviously, the number of sweeps required to obtain an acceptable average ERP waveform is variable and it can range from some tens to some thousands, depending on the kind of ERP and on the SNR.

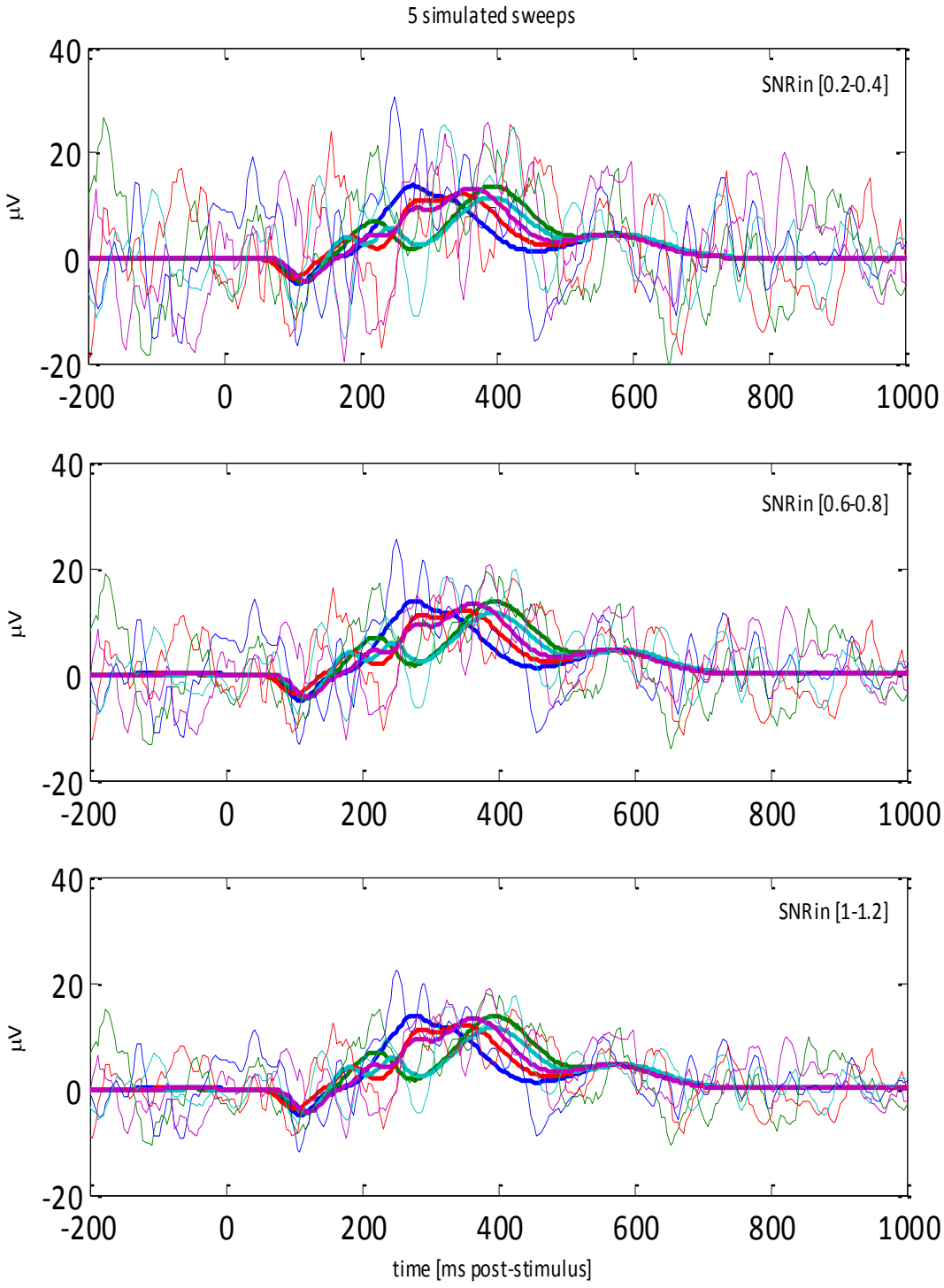

Figure 5.3. Simulated sweeps at different SNR levels. Top panel: 5 simulated sweeps with SNR in the range [0.2-0.4], the underlying simulated ERPs are represented by thick lines. Central panel: the same simulated ERPs of the top panel with SNR in the range [0.6-0.8]. Bottom panel: the same simulated ERPs of the top panel with SNR in the range [1-1.2].

5.2 Indexes for performance evaluation

This section is focused on the indexes used to evaluate the performance of the two techniques.

In order to evaluate the capability in estimating the average ERP, the percentage error E_{ave}, concerning the estimation of the average profile $\overline{\boldsymbol{u}}$, was calculated for each group j (j=1, …, 100) of N sweeps (with N varying from 2 to 20) as

$$E_{ave} = \frac{\left\|\widehat{\overline{\boldsymbol{u}}} - \overline{\boldsymbol{u}}\right\|^2}{\|\overline{\boldsymbol{u}}\|^2} \times 100 \qquad (5.1).$$

These values, averaged over the 100 groups, were used to evaluate the performance of the methods with N varying from 2 to 20.

As regards the estimation of the single-trial profiles, the index E_{ind} was calculated as follows. Once the number N of sweeps has been fixed, the percentage error concerning the estimation of the individual single-trial profile $\boldsymbol{u}^i$ was calculated for each sweep i (i=1, …, N) belonging to each group j. For each group j, these values were then averaged over the N sweeps obtaining the error index E_{ind}

$$E_{ind} = \frac{1}{N}\sum_{i=1}^{N} \frac{\left\|\widehat{\boldsymbol{u}}^i - \boldsymbol{u}^i\right\|^2}{\|\boldsymbol{u}^i\|^2} \times 100 \qquad (5.2).$$

In addition to these measures of the overall morphology adherence of the estimated signals to the true ones, other four error indexes have been considered in order to evaluate the performance of the proposed techniques in the estimation of the single-trial P300 amplitude and latency. P300 amplitude and latency were determined, for each estimated sweep, by simply identifying the maximum of the estimated profile in the interval 250-600 ms. E_a and E_l denote the average percentage error in determining amplitudes and latencies, respectively, while AE_a and AE_l the correspondent quantities in absolute value. E_a and AE_a have been calculated as follows. For each sweep i ($i=1, \dots, N$), belonging to each group j, the difference between the estimated and the true P300 amplitude, $\widehat{A_i}$ and A_i, was calculated. These values were averaged over the N sweeps belonging to each group, both with sign, obtaining E_a, and in absolute value, obtaining AE_a

$$E_a = \frac{1}{N}\sum_{i=1}^{N} \widehat{A_i} - A_i \tag{5.3}$$

$$AE_a = \frac{1}{N}\sum_{i=1}^{N} \left|\widehat{A_i} - A_i\right| \tag{5.4}.$$

In the same way E_l and AE_l can be obtained by substituting A_i and $\widehat{A_i}$ with the true and estimated latencies L_i and $\widehat{L_i}$

$$E_l = \frac{1}{N}\sum_{i=1}^{N} \widehat{L_i} - L_i \tag{5.5}$$

$$AE_l = \frac{1}{N}\sum_{i=1}^{N}\left|\widehat{L_i} - L_i\right| \quad (5.6).$$

5.3 Results: estimation of the average ERP profile

This section is focused on the results regarding the estimation of the average profile. The performance of the two proposed techniques is tested by evaluating the index E_{ave}, defined in section 5.2, which measures the adherence of the estimated average profile to the true one. Moreover, the results obtained by using the proposed approaches have been compared with those provided by the CA, the method commonly used to estimate the average response.

5.3.1 Performance evaluation

As discussed in section 1.2.3, the main problem in estimating the mean ERP lies in the high number of sweeps necessary to obtain a stable waveform that can be used to correctly evaluate latency and amplitudes of the principal ERP components. Naturally, the number of needed sweeps is related to the level of noise that obscures the useful signal. As described in section 5.1, for each SNR level 100 groups of N sweeps (with N varying from 2 to 20) have been drawing from all the available simulated sweeps. In this way, 100 values of the index E_{ave} are available to evaluate the performance of the three estimation methods at a given number of sweeps and at a given SNR. In Fig. 5.4 the mean values of the 100 E_{ave} indexes are shown as function of the number of available sweeps. For the sake of simplicity, the results regarding only three SNR levels are shown: in the top panel the case with SNR in the range [0.2 – 0.4], in the middle panel the case with SNR in the range [0.6 - 0.8], in the bottom panel the case with SNR in the range [1 – 1.2]. Red points represent the values obtained by estimating the average ERP with the two-stage methodology described in Chapter 3, from now on called 'TS' method. Blue plus signs are referred to the one-stage technique presented in section 5.2, from now on called 'MTL' method. Lastly, the values

computed by considering the estimates given by the CA technique are represented by a cyan triangles.

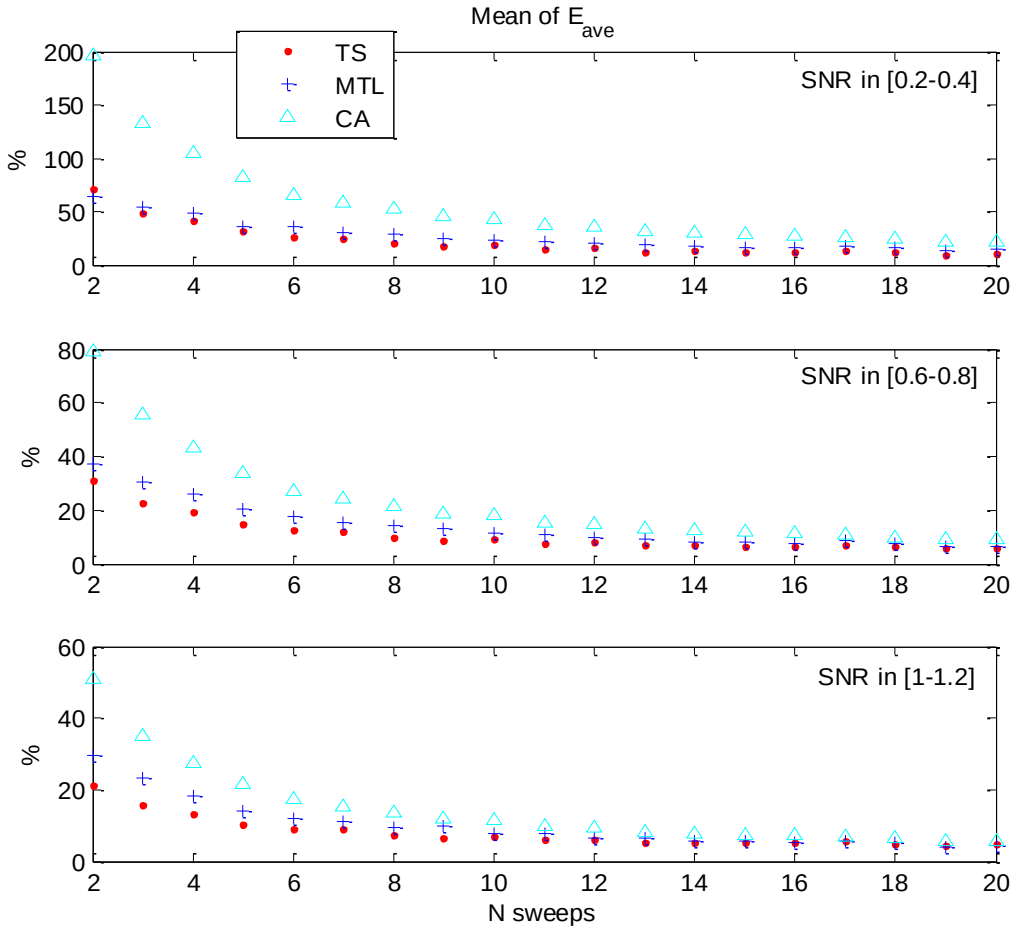

Figure 5.4. Mean values of E_{ave} over the 100 groups as function of the number of available sweeps. Red points: values provided by the two-stages method (TS); blue plus signs: values provided by the multi-task learning method (MTL); cyan triangles: values provided by the CA technique. Top Panel: SNR level in the range [0.2- 0.4]. Central Panel: SNR level in the range [0.6- 0.8]. Bottom panel: SNR level in the range [1- 1.2].

As evident from the figure, for all the three methods the mean value of E_{ave} decreases as the number of available sweeps increases. The estimation of the average profile, as expected, improves if a greater number of sweeps is utilized. Moreover, by observing the range of values covered by the mean values of E_{ave} in the three different panels it is also evident that the errors in estimating the

average profile decreases if the SNR increases and that this happens for all the three methods. From Fig. 5.4 it is possible to easily compare the performance of the three techniques at a given number of sweeps and at a given SNR. In particular, for the two Bayesian techniques the mean values of the error index are always lower than those obtained by using the CA technique; this improvement is evident for each SNR level. In the light of this, it is clear that by using these Bayesian methods less sweeps are needed with respect to the CA technique in order to obtain the same error. For clarity, in Table 5.4 the mean values of E_{ave} obtained by employing 8, 12, and 20 sweeps are reported.

	Mean of E_{ave} over the 100 groups for TS (%)			**Mean of E_{ave} over the 100 groups for MTL (%)**			**Mean of E_{ave} over the 100 groups for CA (%)**		
	SNR in 0.2-0.4	**SNR in 0.6-0.8**	**SNR in 1-1.2**	**SNR in 0.2-0.4**	**SNR in 0.6-0.8**	**SNR in 1-1.2**	**SNR in 0.2-0.4**	**SNR in 0.6-0.8**	**SNR in 1-1.2**
8 sweeps	20.17	10.00	7.36	28.82	14.14	9.65	52.49	21.66	13.77
12 sweeps	15.57	8.02	6.07	19.94	9.53	6.50	36.61	15.03	9.52
20 sweeps	10.90	6.03	4.74	14.36	6.71	4.50	21.64	9.08	5.76

Table 5.4. Mean values of E_{ave} calculated for the three methods by using 8, 12, and 20 sweeps at three different SNR levels ([0.2-0-4], [0.6-0.8], [1-1.2]).

For example, the value obtained by using 20 sweeps in case of SNR in [0.2-0.4] is equal to 21.64 for the CA technique. Note that this value is greater than the value provided by the TS method by using only 8 sweeps and than that provided by the MTL method with 12 sweeps. Although less disparity between the methods characterizes the cases with high SNR, analogous considerations can be done. Moreover, some differences can be found between the two proposed approaches. Although their performances in estimating the average profile are

very similar, the method TS seems to work better. Moreover, one can notice from Table 5.4 that this difference seems to become negligible as the SNR and the number of available sweeps increase.

In addition to the coarse information given by the mean values of E_{ave} over the 100 groups, more complete characterization of the capability of the three methods in estimating the average profile can be given by analyzing the distribution of E_{ave} over the 100 groups, once the number N of available sweeps and the SNR level have been fixed. Some box plots of the distribution of E_{ave} obtained for the three methods are shown in Fig. 5.5 and in Fig. 5.6. For the sake of simplicity, only the results obtained by using 8 (Fig. 5.5) and 20 sweeps (Fig. 5.6) are shown. As in the previous figure, the cases with SNR in range [0.2-0.4], [0.6-0.8], [1–1.2] are shown in the top, the middle and the bottom panels respectively.

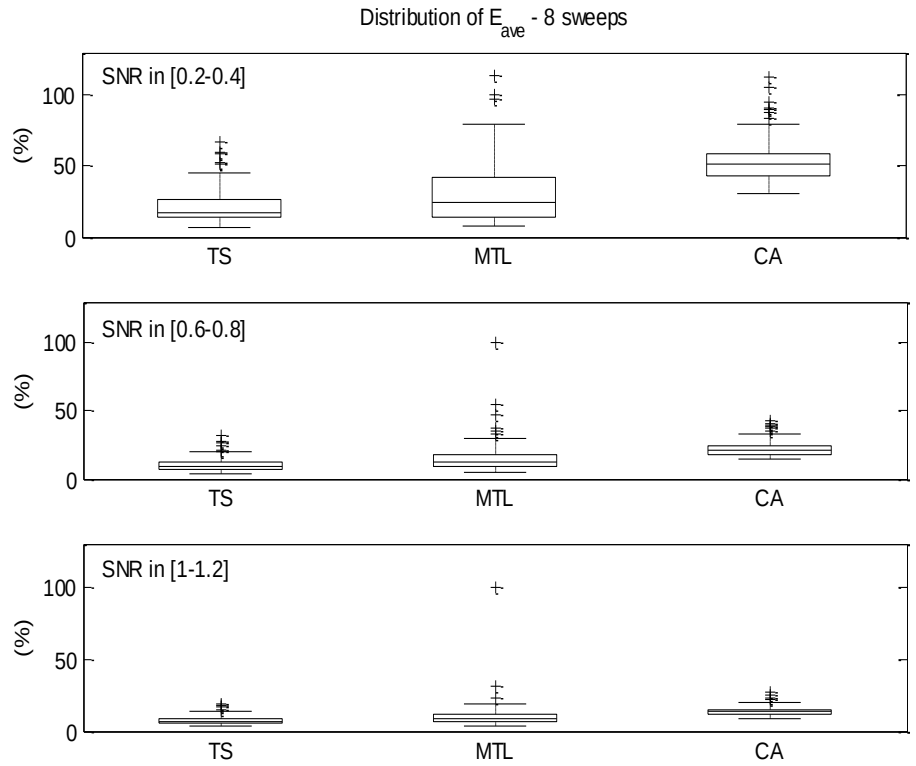

Figure 5.5. Distribution of E_{ave} over the 100 groups of 8 sweeps for the three methods. Top Panels: SNR level in the range [0.2-0.4]. Central Panels: SNR level in the range [0.6-0.8]. Bottom panels: SNR level in the range [1-1.2].

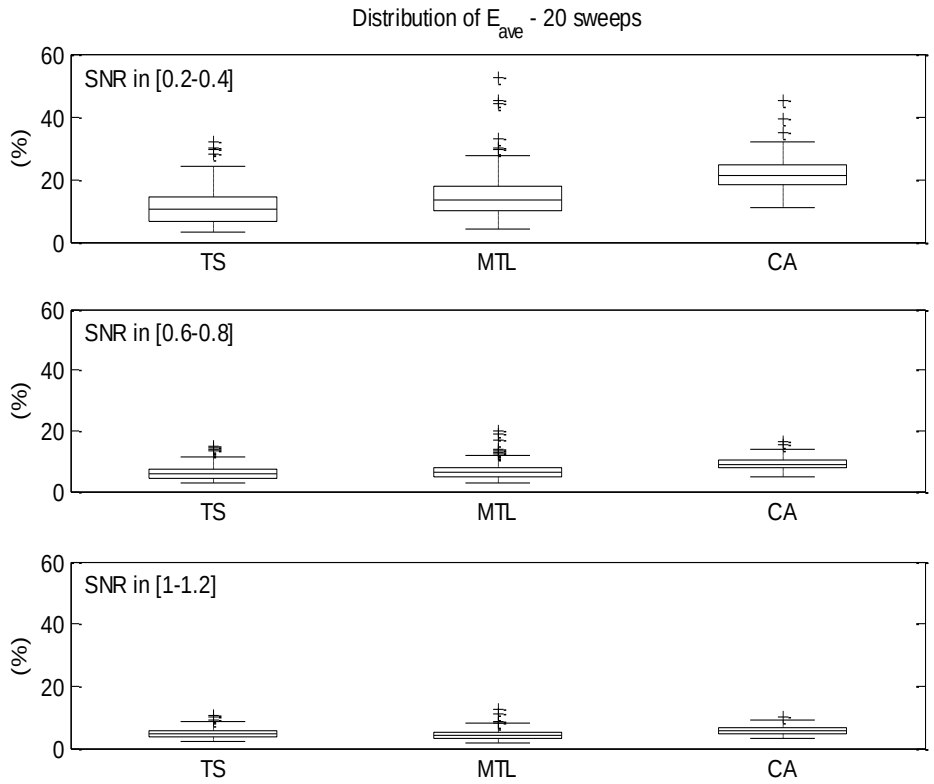

Figure 5.6. Distribution of E_{ave} over the 100 groups of 20 sweeps for the three methods. Top Panels: SNR level in the range [0.2-0.4]. Central Panels: SNR level in the range [0.6-0.8]. Bottom panels: SNR level in the range [1-1.2].

The distribution of E_{ave} over the 100 groups confirm the observations previously carried out. In fact, it is evident from the figures that the values of the error index provided with the CA technique are in general greater than those provided by the two Bayesian techniques. Between TS and MTL, the first method works slightly better.

In order to test for statistical significance, the values of E_{ave} over the 100 groups, provided by the three methods for each SNR level, have been compared by using a Kruskal-Wallis test. Such a non parametric statistical test has been chosen after having verified the non-normality of the E_{ave} values by using the Lilliefors test. Whenever a significance level $p \leq 0.05$ has been reached, post-hoc comparison have been performed by using the Tukey's criterion. Differences in the distribution of the E_{ave} values are highly significant for all SNR levels, both for 8

and 20 sweeps. In Fig. 5.7 the results of the post-hoc comparisons are shown, for the E_{ave} values obtained by using 8 (top panel) and 20 (bottom panel) sweeps, respectively. Significant differences are shown with brackets.

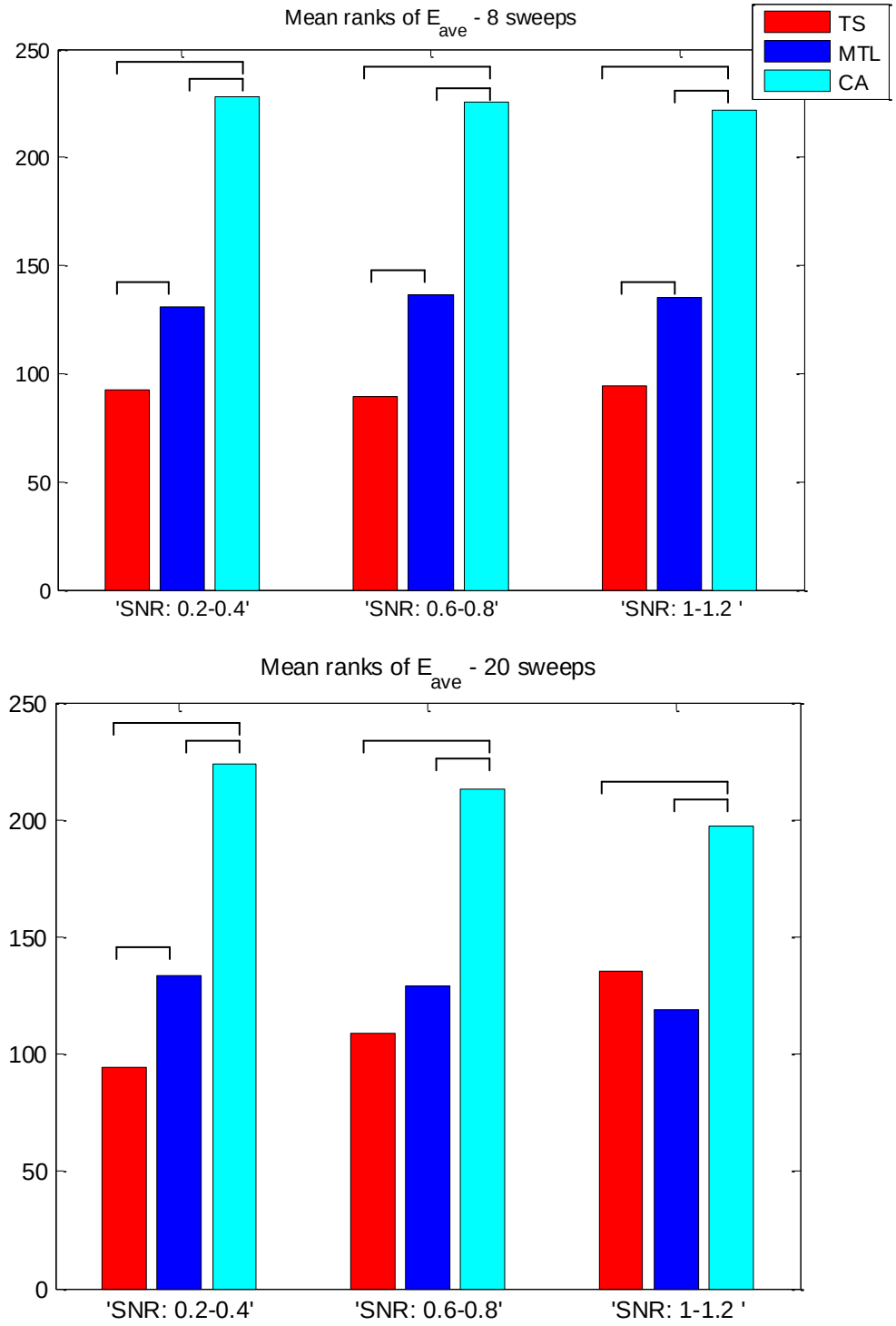

Figure 5.7. Mean ranks of E_{ave} obtained for the three techniques at SNR in (0.2-0.4), (0.6-0.8), (1-1.2). Significant differences are shown with brackets.

As evident from the figure, the two new approaches provide a reconstruction of the average ERP significantly better than that provided by the CA technique, for all SNR levels and both for 8 and 20 sweeps. Moreover, if few sweeps are available, the TS method gives results significantly better of the MTL method.

5.3.2 Estimated average ERP profiles

In order to visually evaluate the capability of the three techniques to estimate the average profiles, three groups have been chosen, as examples, among all the 100 groups of 8 and 20 sweeps. The results are shown in Fig. 5.8, 5.9, 5.10, 5.11, 5.12 and 5.13.

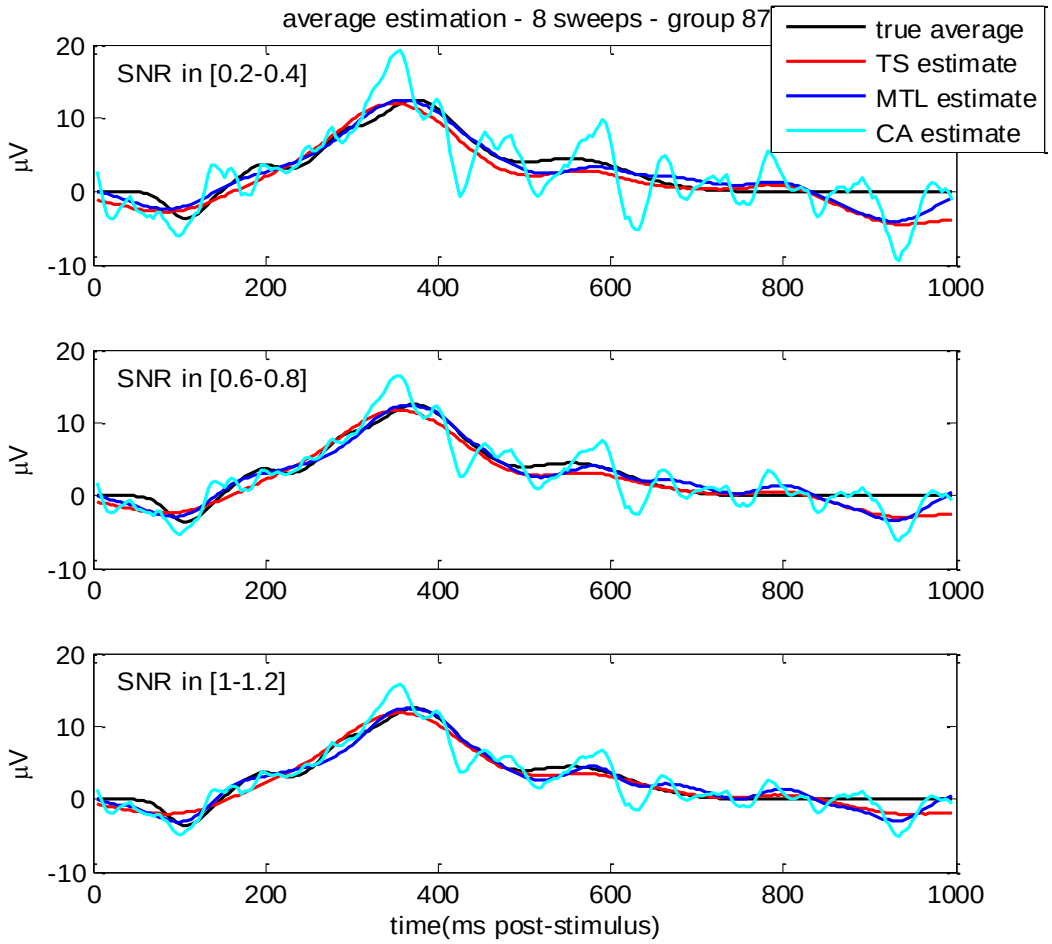

Figure 5.8. Average ERP estimation for the group 87 by using 8 sweeps. Top Panels: SNR level in the range [0.2-0.4]. Central Panels: SNR level in the range [0.6-0.8]. Bottom panels: SNR level in the range [1-1.2]. True average ERP (black dashed line), TS estimate (red dash-dot line), MTL estimate (blue thick line), CA estimate (cyan thin line).

For all the figures, the three SNR levels ([0.2-0.4],[0.6 - 0.8],[1-1.2]) are presented in the top, in the middle and in the bottom panels respectively. The true average profile and the estimates given by the three methods are plotted superimposed on the same panel. In particular, the true average profile is represented by a black line, the estimate given by the two-stage methodology (TS) by a red line, that provided by the one-stage methodology (MTL) by a blue line while a cyan line has been used to represent the CA estimate.

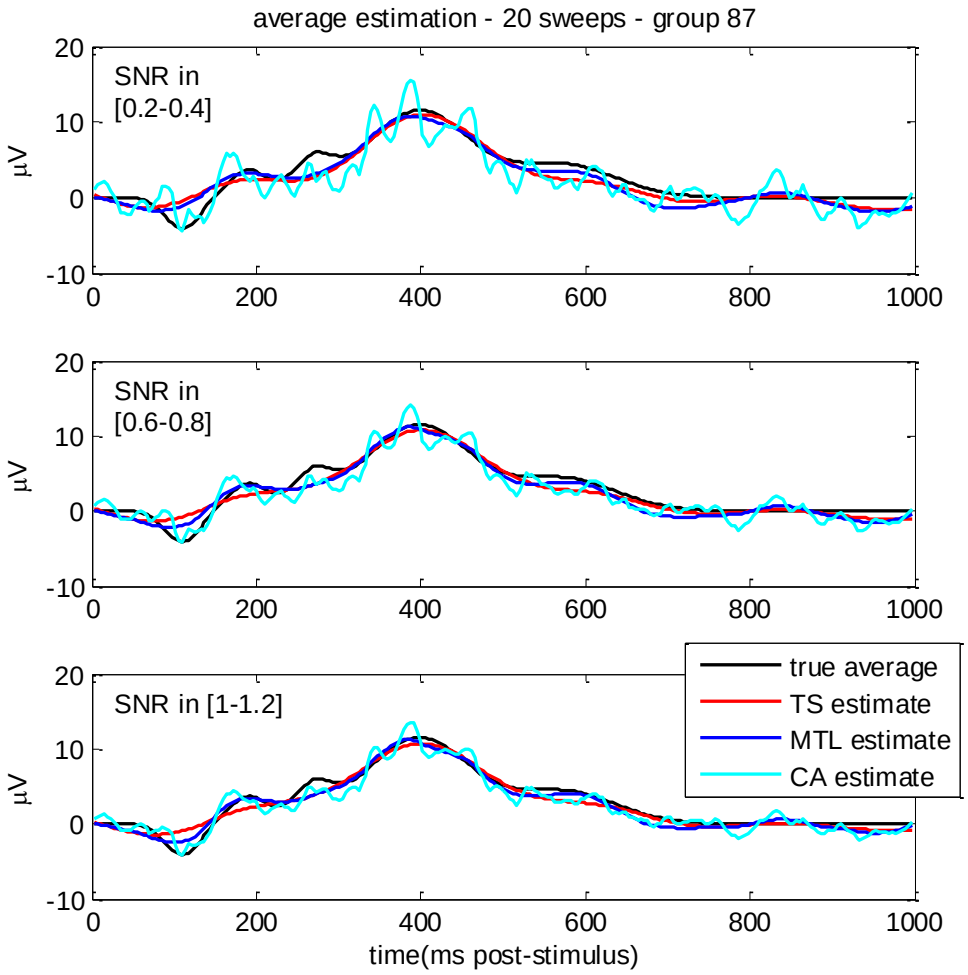

Figure 5.9. Average ERP estimation for the group 87 by using 20 sweeps. Top Panels: SNR level in the range [0.2-0.4]. Central Panels: SNR level in the range [0.6-0.8]. Bottom panels: SNR level in the range [1-1.2]. True average ERP (black dashed line), TS estimate (red dash-dot line), MTL estimate (blue thick line), CA estimate (cyan thin line).

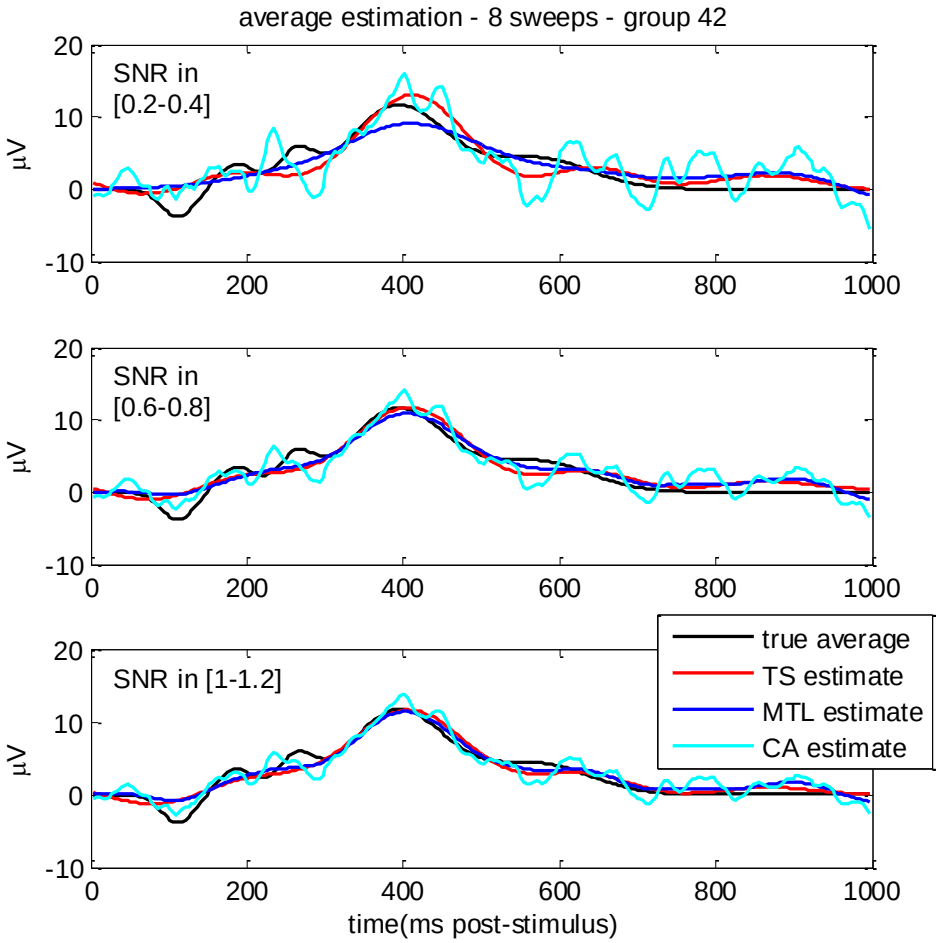

Figure 5.10. Average ERP estimation for the group 42 by using 8 sweeps. Top Panels: SNR level in the range [0.2-0.4]. Central Panels: SNR level in the range [0.6-0.8]. Bottom panels: SNR level in the range [1-1.2]. True average ERP (black dashed line), TS estimate (red dash-dot line), MTL estimate (blue thick line), CA estimate (cyan thin line).

Figures show as the two proposed approaches are able to provide an improved estimate of the average ERP with respect to the CA technique. See Fig. 5.8 and 5.9. The CA estimate is characterized, above all in case of low SNR, by pronounced oscillations that are not present in the true signal. At higher SNR levels these oscillations become less evident even if they can still be misleading in the determination of latency and amplitude of peaks, for example the P300 component, see the bottom panels of the two figures. On the other hand the two proposed approaches provides average ERP estimates much more similar to the true signals, also if few sweeps are used, see the top panel of Fig. 5.8. Fig.

5.10 and 5.11 shown the estimation results of the group 42. Also in this case the proposed approaches provide estimates that are closer to the true signals than the CA estimates even if at low SNR there is a higher error with respect to the previous case. Central panels shown the condition with SNR in [0-6-0.8] in which the performance of all the methods improves.

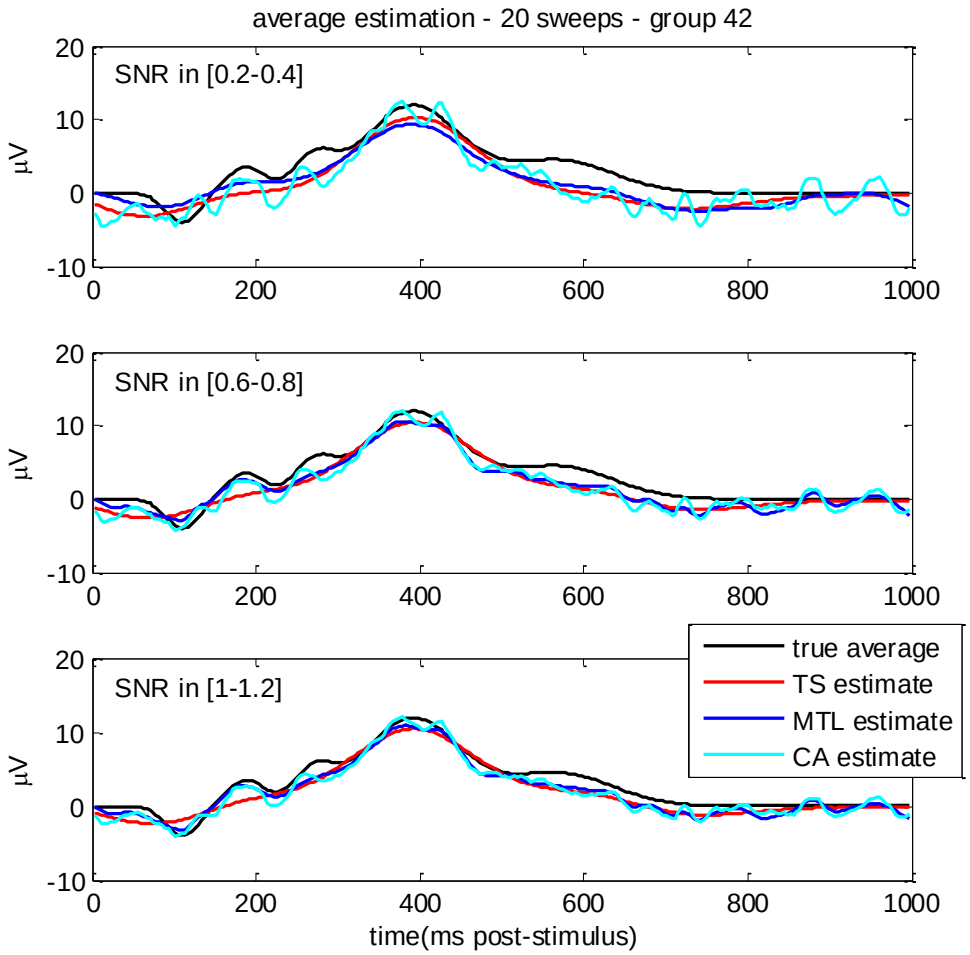

Figure 5.11. Average ERP estimation for the group 42 by using 20 sweeps. Top Panels: SNR level in the range [0.2-0.4]. Central Panels: SNR level in the range [0.6-0.8]. Bottom panels: SNR level in the range [1-1.2]. True average ERP (black dashed line), TS estimate (red dash-dot line), MTL estimate (blue thick line), CA estimate (cyan thin line).

Other critical cases are shown in Fig 5.12 and Fig. 5.13. Note the improvement of the estimates as the SNR and the number of available sweeps increase. It is worth to notice that the estimates given by the two Bayesian approaches are quite similar even if, in general, the estimates given by the MTL method is better in tracking the peaks, above all if less prominent, present in true signal, see for example the central panels of the Fig. 5.13 and that of Fig. 5.11.

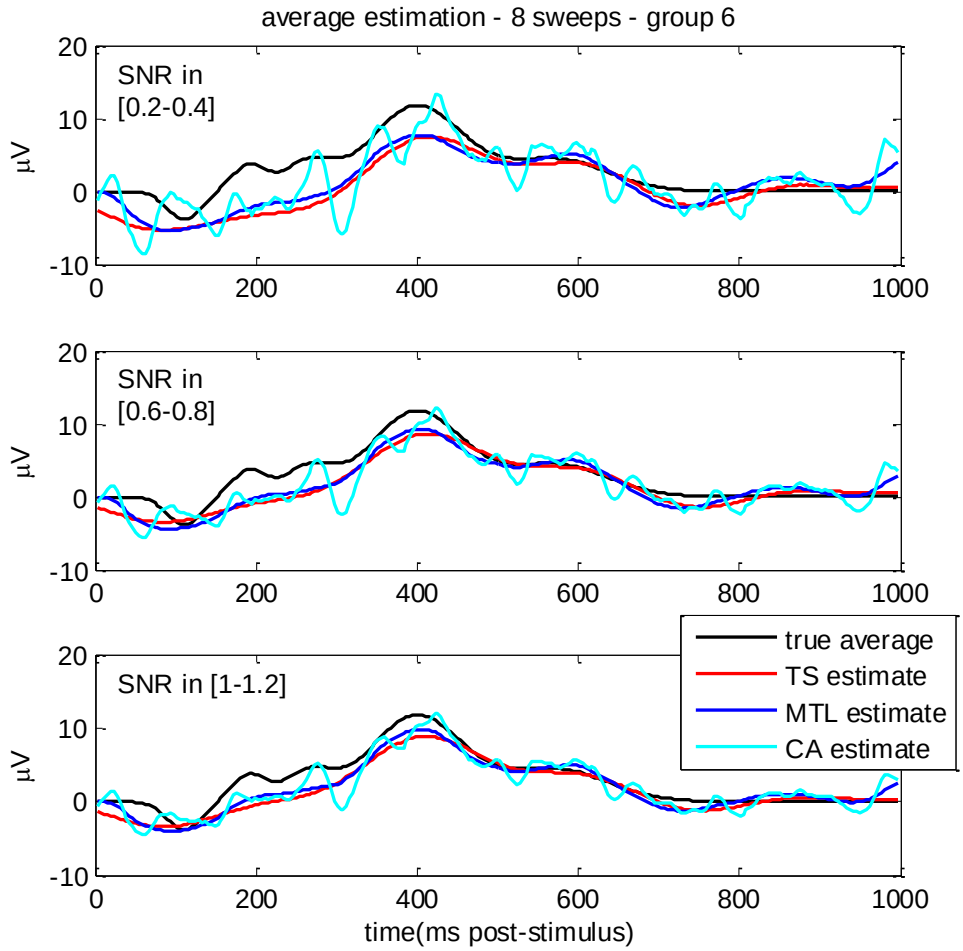

Figure 5.12. Average ERP estimation for the group 6 by using 8 sweeps. Top Panels: SNR level in the range [0.2-0.4]. Central Panels: SNR level in the range [0.6-0.8]. Bottom panels: SNR level in the range [1-1.2]. True average ERP (black dashed line), TS estimate (red dash-dot line), MTL estimate (blue thick line), CA estimate (cyan thin line).

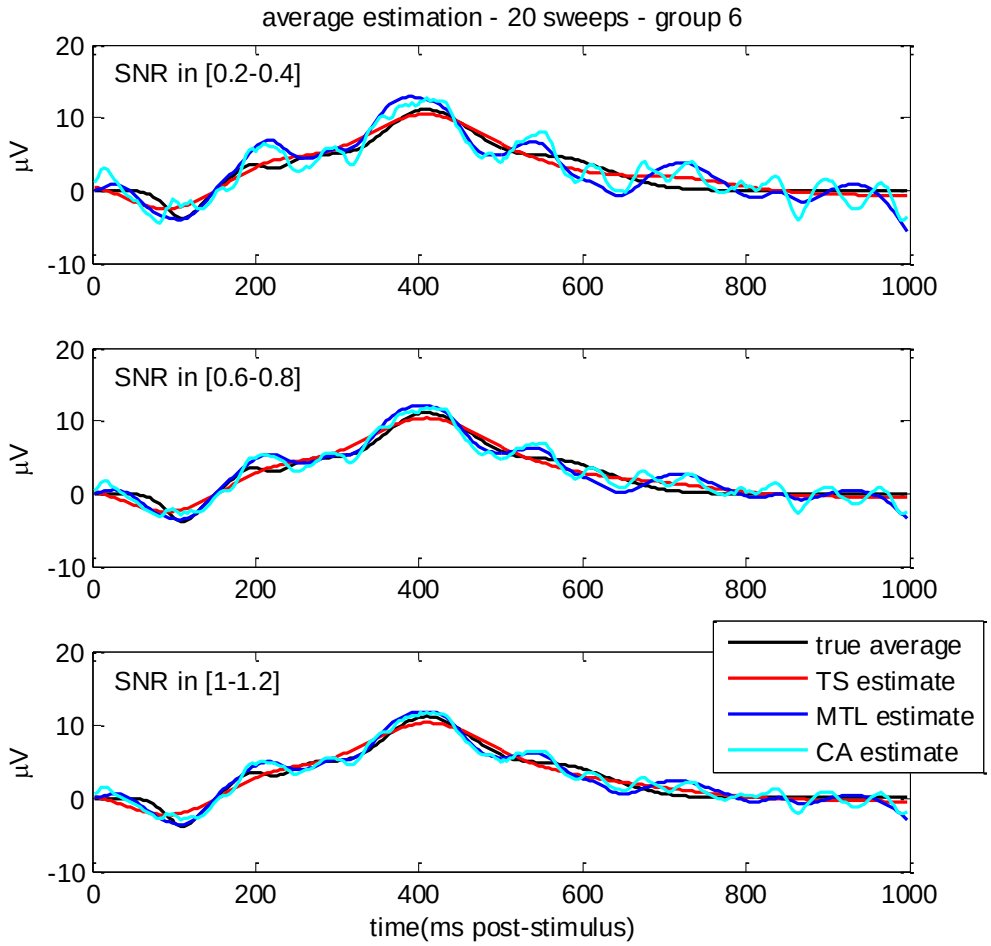

Figure 5.13. Average ERP estimation for the group 6 by using 20 sweeps. Top Panels: SNR level in the range [0.2-0.4]. Central Panels: SNR level in the range [0.6-0.8]. Bottom panels: SNR level in the range [1-1.2]. True average ERP (black dashed line), TS estimate (red dash-dot line), MTL estimate (blue thick line), CA estimate (cyan thin line).

At the same time it seems to be more sensitive to the oscillations of the CA estimate. In the same situations, the estimates given by the TS method are, instead, smoother. Very probably this difference is due to the different procedures used to estimate the average response and to the models used to describe it. Let us recall that for the TS method all the sweeps are previously filtered by assuming that the ERPs can be modeled as multi-integrated white noise processes (in particular, one integrator has been used). Then the mean ERP

is estimated by averaging the filtered sweeps with weights proportional to their estimation accuracy. The MTL method, instead, estimates the average ERP directly by assuming that it can be modeled by an integrated Wiener process. So, it is not strange that the estimates given by the MTL method are less smooth than those given by the TS method.

5.4 Results: estimation of single-trial ERPs

In the single-trial estimation, the two proposed techniques have been evaluated with regard to their capability both in estimating the single-trial profiles and in determining amplitude and latency of the P300 component. Moreover, the results obtained by using the proposed approaches have been compared with other two techniques, the classical maximum peak (MAX) method [44] and a recent single-trial approach presented in [77]. The first technique provides estimates of single-trial P300 latencies and amplitudes by simply detecting the maximum, in the typical P300 range, of a sweep profile obtained after a simple pre-processing (in this case, band-pass filtering between 0.7 and 30 Hz). The second approach is a sophisticated single-trial ERP estimation method based on a Radial Basis Function (RBF) neural network with Gaussian activation functions. The number of neurons, the spread factor and the convergence rate (see [77] for details) were previously selected by a preliminary study and set equal to 25, 1.5 and 0.0025, respectively. The weights of the network and the centers of the Gaussian functions are, instead, learnt by a supervised algorithm, as described in [77]. We refer the reader to section 2.2 for details on these techniques.

5.4.1 Performance evaluation

In order to give a measure of the adherence of the estimated single-trial ERPs to the true ones, the index E_{ind} has been introduced. As described in section 5.2, the above mentioned index represents the mean, over the N sweeps belonging to the same group, of the percentage square error in estimating a single-trial

ERP. So, 100 values of the index E_{ave} are available in order to evaluate the performance of the three estimation methods at a given SNR and at a given number of sweeps.

The single-trial estimates given by the two proposed techniques are affected, although in a different way, by the number N of available sweeps. In Fig. 5.14 the mean values of the 100 E_{ind} indexes are shown as function of the number of available sweeps.

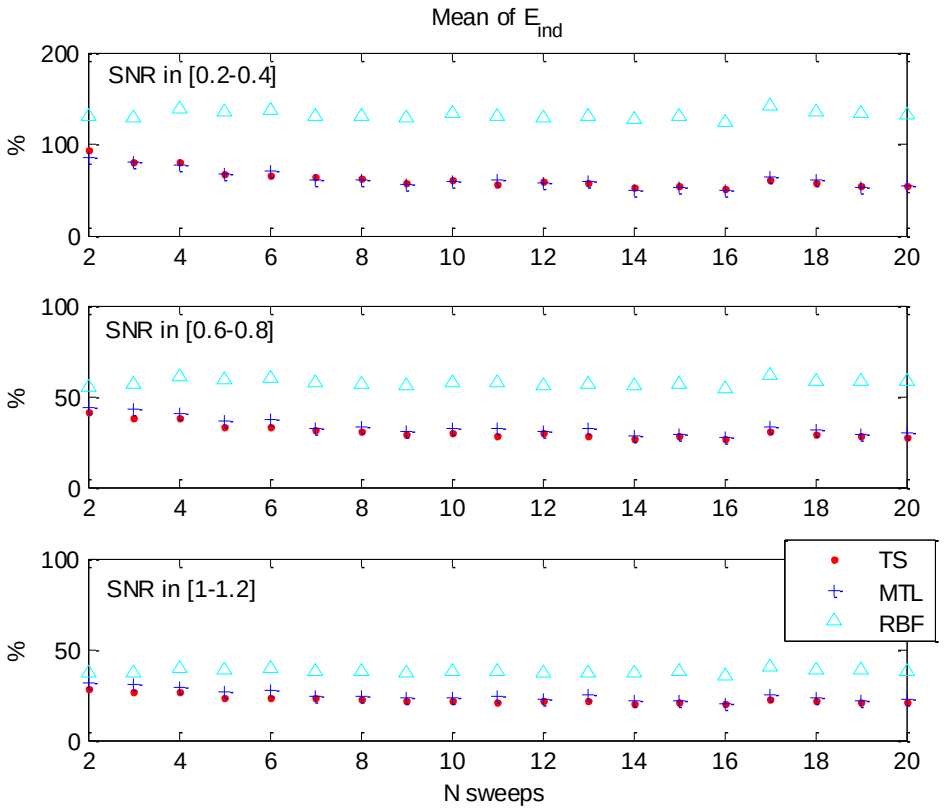

Figure 5.14. Mean values of E_{ind} over the 100 groups as function of the number of available sweeps. Red points: values provided by the TS method; blue plus signs: values provided by the MTL method; cyan triangles: values provided by the RBF technique. Top Panel: SNR level in the range [0.2-0.4]. Central Panel: SNR level in the range [0.6- 0.8]. Bottom panel: SNR level in the range [1-1.2].

As in the previous figures, the results regarding only three SNR levels are shown. In the top panel the case with SNR in the range [0.2-0.4], in the middle panel the case with SNR in the range [0.6-0.8], in the bottom panel the case with SNR in the range [1-1.2]. Red points represent the values obtained by estimating the average ERP with the TS method. Blue plus signs are referred to the MTL method. Lastly, the values computed by considering the estimates given by the RBF technique are represented by a cyan triangles. By analyzing the mean values of E_{ind} in the three different panels it is evident that the errors in estimating the single-trial profiles decrease if the SNR increases and that this happens for all the three methods. Different behaviors characterize the dependence of E_{ind} on the number of the available sweeps. The single-trial estimates provided by the two Bayesian technique are positively influenced by the increasing of the available sweeps. The TS method makes use of the estimated average ERP in order to obtain the single-trial profiles; the MTL method uses all the available data in a population analysis context. On the other hand, the RBF methodology, conceived for on-line applications, provides the single-trial estimate sweep by sweep and without exploiting any kind of information deriving from the other sweeps. This explains why the mean values of E_{ind} for this technique are more or less constant with the number of sweeps. With regard the comparison among the methods, it is clear that the two Bayesian approaches give the best performances with very similar results.

In addition to the coarse information given by the mean values of E_{ind} over the 100 groups, more complete characterization of the capability of the three methods in estimating the single trial profiles can be given by analyzing the distribution of E_{ind} over the 100 groups, once the number N of available sweeps and the SNR level have been fixed. For sake of simplicity, only the results concerning the groups with N equal to 12 will be shown in the following figures. Such a number of sweeps has been selected because it can be seen as a middle case with respect to the test values, varying from 2 to 20. Moreover, as visible in Fig. 5.4 and Fig. 5.14, for the proposed techniques the errors in estimating the

average profile and the single-trial ERP seem to become stable. Fig. 5.15 shows the box plots representing the distribution of E_{ind} for the three techniques at the three SNR levels [0.2–0.4], [0.6–0.8], [1–1.2], shown in the top, the middle and the bottom panels respectively.

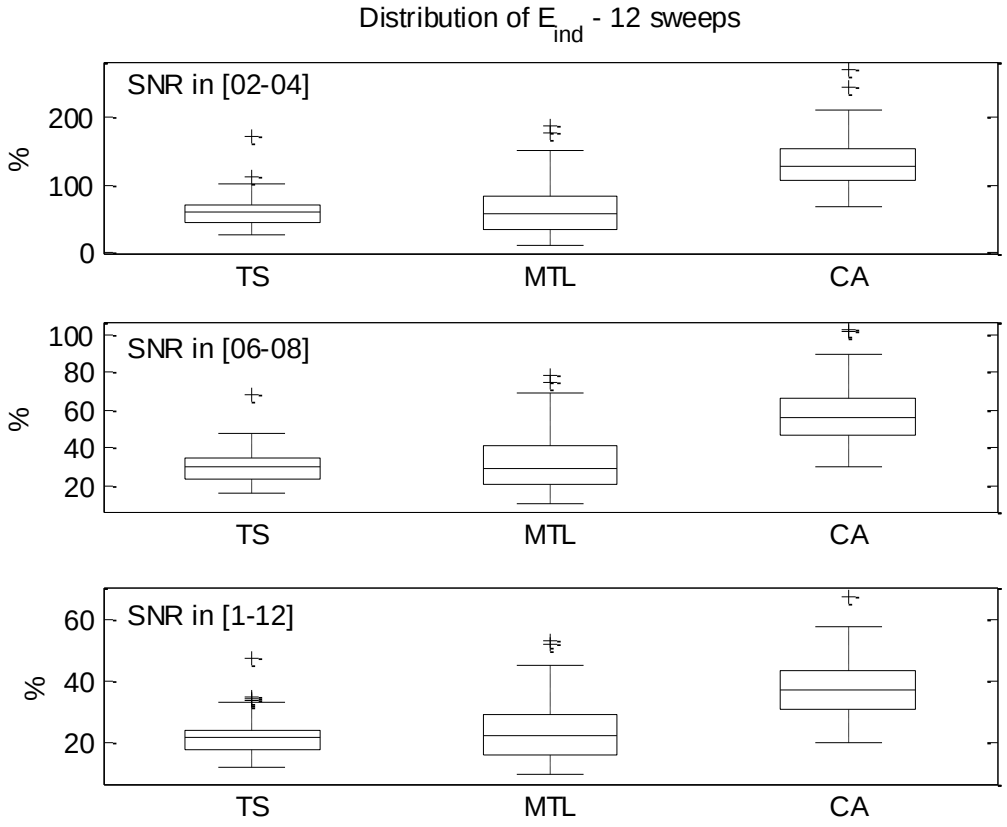

Figure 5.15. Distribution of E_{ind} over the 100 groups of 12 sweeps for the three methods. Top Panels: SNR level in the range [0.2-0.4]. Central Panels: SNR level in the range [0.6-0.8]. Bottom panels: SNR level in the range [1-1.2].

These distributions confirm the observations previously carried out. In fact, it is evident from the figure that the values of the error index provided with the RBF technique are in general greater than those provided by the two Bayesian techniques. The performance of the TS and MTL method are very similar.

In order to test for statistical significance, the values of E_{ind} over the 100 groups, provided by the three methods for each SNR level, have been compared by using a Kruskal-Wallis test. As in the case of E_{ave} a Lilliefors test has been used to

check the normality of the distribution. Whenever a significance level $p \leq 0.05$ has been reached, post-hoc comparison have been performed by using the Tukey's criterion. Differences in the distribution of the E_{ind} values are highly significant for all SNR levels. In Fig. 5.16 the results of the post-hoc comparisons are shown; significant differences are shown with brackets.

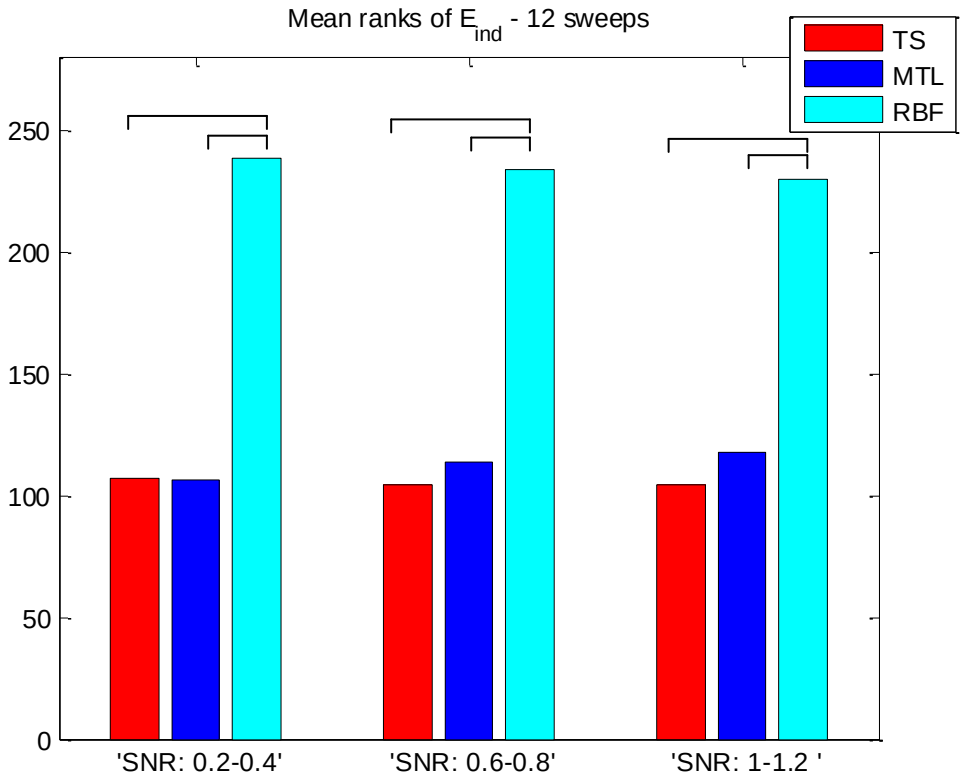

Figure 5.16. Mean ranks of E_{ind} obtained for the three techniques at SNR in (0.2-0.4), (0.6-0.8), (1-1.2). Significant differences are shown with brackets.

The two new approaches provide a reconstruction of the single-trial ERP profiles significantly better than that provided by the RBF technique for all SNR levels while no significant differences have been found between the two methods.

In addition to the evaluation of the techniques in estimating the ERP profile at single-trial level, specific performance indexes have been introduced in section 5.2 in order to evaluate the capability in detecting the P300 component. In

addition to the RBF methodology, also the maximum peak (MAX) method has been put in comparison with the two proposed techniques. Similarly to the index E_{ind}, 100 values of the indexes E_a, AE_a, $E_{l,}$ and AE_l are available to evaluate the performance of the four estimation methods at a given SNR and at a given number of sweeps. We will focus on the results given by using 12 sweeps. With regard to the estimation of P300 amplitude Fig. 5.17 and Fig. 5.18 show the distribution over the 100 groups of the indexes E_a and AE_a obtained for the four methods at three different SNR levels. As usual, the three SNR levels ([0.2-0.4], [0.6-0.8], [1-1.2]) are presented in the top, the middle and the bottom panels respectively.

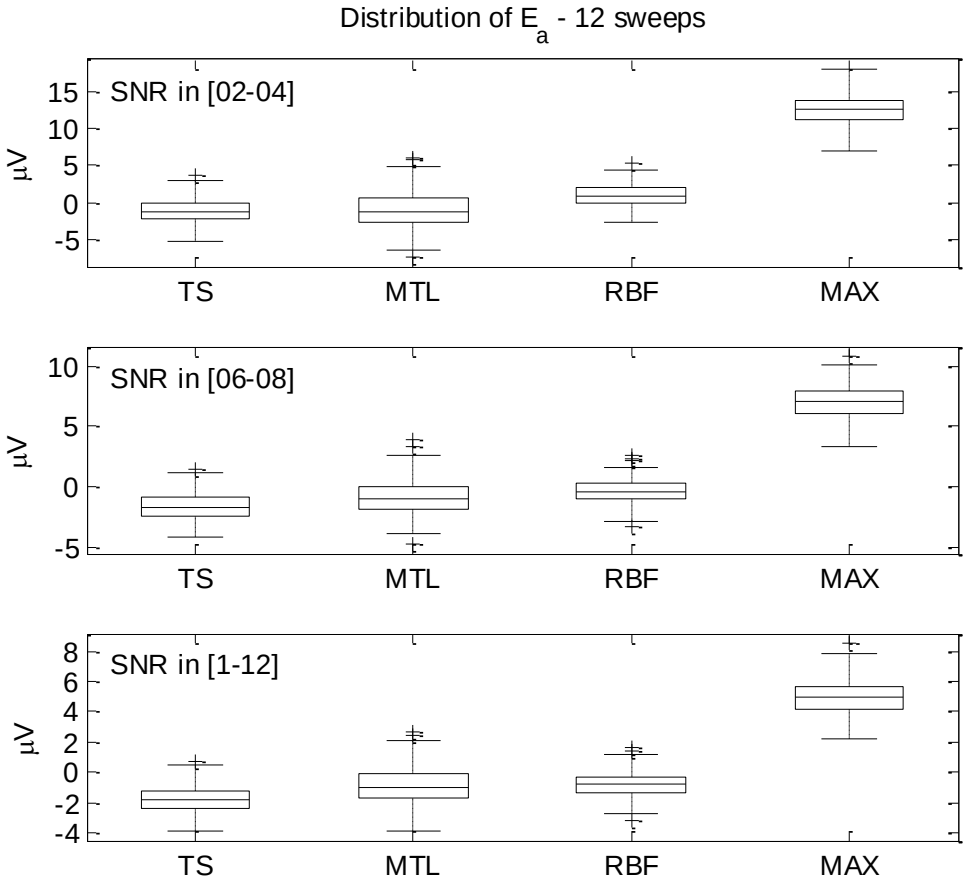

Figure 5.17. Distribution of E_a over the 100 groups of 12 sweeps for the four methods. Top Panels: SNR level in the range [0.2-0.4]. Central Panels: SNR level in the range [0.6-0.8]. Bottom panels: SNR level in the range [1-1.2].

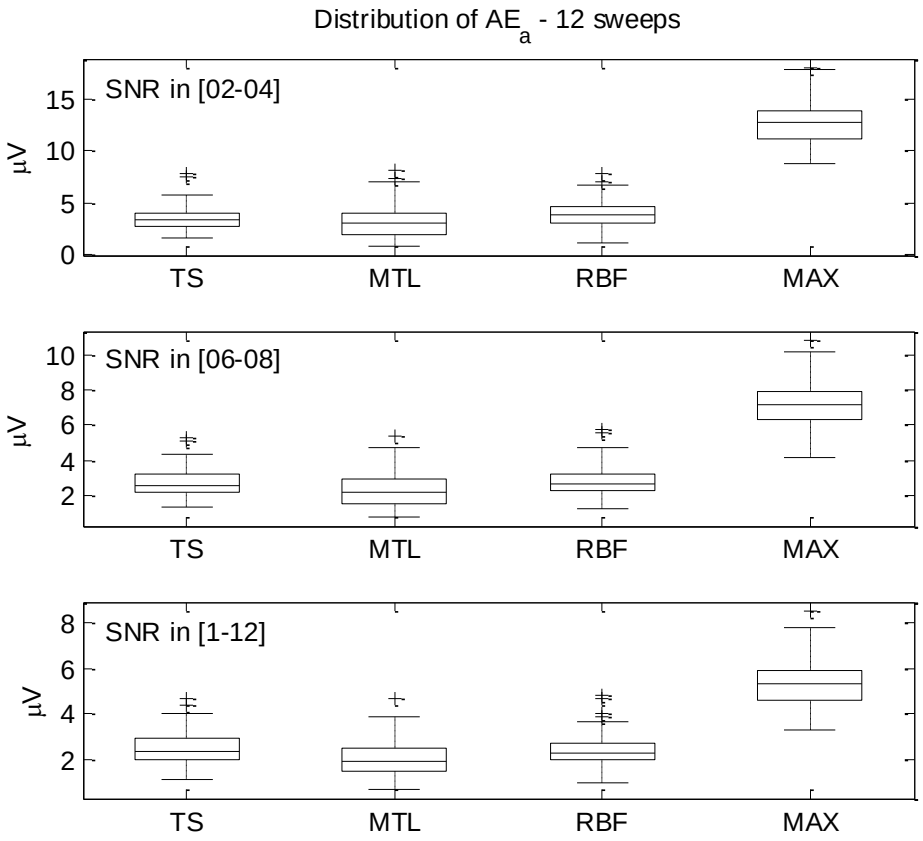

Figure 5.18. Distribution of AE_a over the 100 groups of 12 sweeps for the four methods. Top Panels: SNR level in the range [0.2-0.4]. Central Panels: SNR level in the range [0.6-0.8]. Bottom panels: SNR level in the range [1-1.2].

From the figure 5.17 it is evident that the two proposed techniques and the RBF approach give similar results. In particular, in all the three SNR cases the median of the E_a values obtained with the RBF method is the nearest to the zero value. The method TS results, instead, slightly negative biased. The worst performance is evidently given by the MAX method. It provides very positive biased estimates of the P300 amplitude. In case of low SNR the estimated amplitude can also be about the double of the true amplitude. As expected, the performances of all the methods improve if the level of EEG noise decreases. On the whole the same considerations hold for the absolute error in estimating the P300 amplitude.

In the same way, with regard the estimation of P300 latency Fig. 5.19 and Fig. 5.20 show the distribution over the 100 groups of the indexes $E_{l,}$ and AE_l obtained for the four methods at the three different SNR levels.

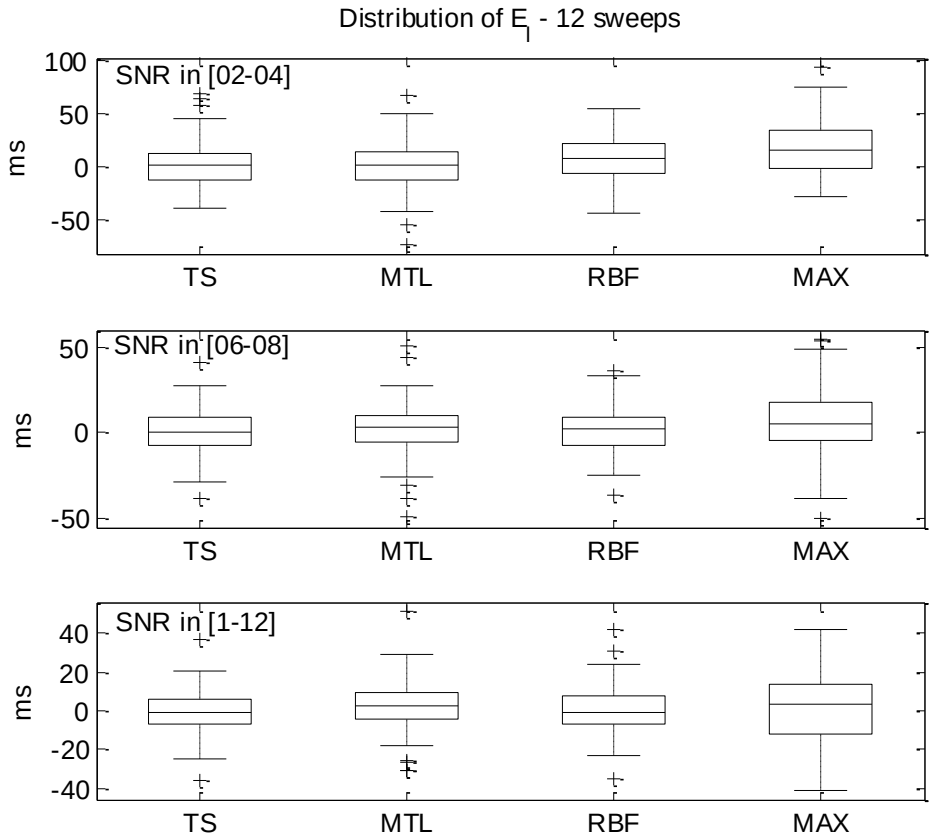

Figure 5.19. Distribution of E_l over the 100 groups of 12 sweeps for the four methods. Top Panels: SNR level in the range [0.2-0.4]. Central Panels: SNR level in the range [0.6-0.8]. Bottom panels: SNR level in the range [1-1.2].

As regards the index E_l all the techniques give comparable results. The median values, in fact, are of few milliseconds. So, we can say that none of the four techniques is biased in estimating the P300 latency.

The index AE_l gives, instead, an idea of the absolute error in estimating the P300 latency. From figure Fig. 5.20 it is clear that the two proposed techniques have

an advantage with respect to the RBF methodology and the MAX technique. The MAX method, in particular, has the worst performance.

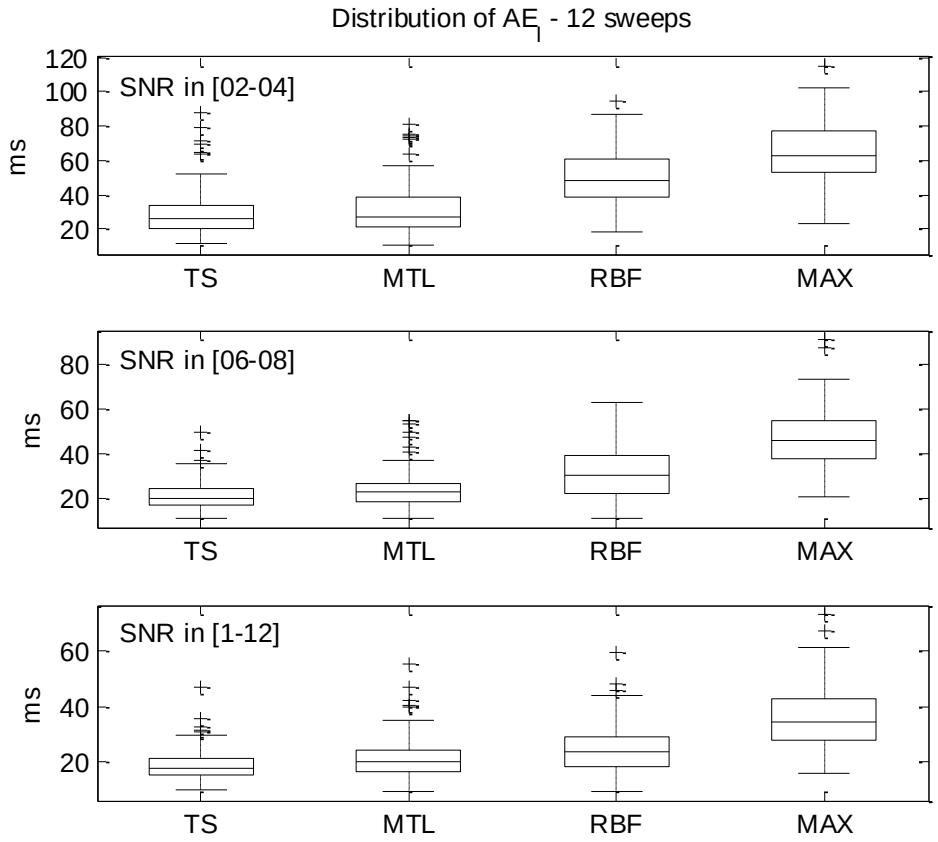

Figure 5.20. Distribution of AE_l over the 100 groups of 12 sweeps for the four methods. Top Panels: SNR level in the range [0.2-0.4]. Central Panels: SNR level in the range [0.6-0.8]. Bottom panels: SNR level in the range [1-1.2].

In order to test for statistical significance, the values E_a, AE_a, $E_{l,}$ and AE_l over the 100 groups, provided by the four methods for each SNR level, have been compared by using a Kruskal-Wallis test. Whenever a significance level $p \leq 0.05$ has been reached, post-hoc comparison have been performed by using the Tukey's criterion. In Fig. 5.21, 5.22, 5.22 and 5.23 the results of the post-hoc comparisons are shown; significant differences are shown with brackets.

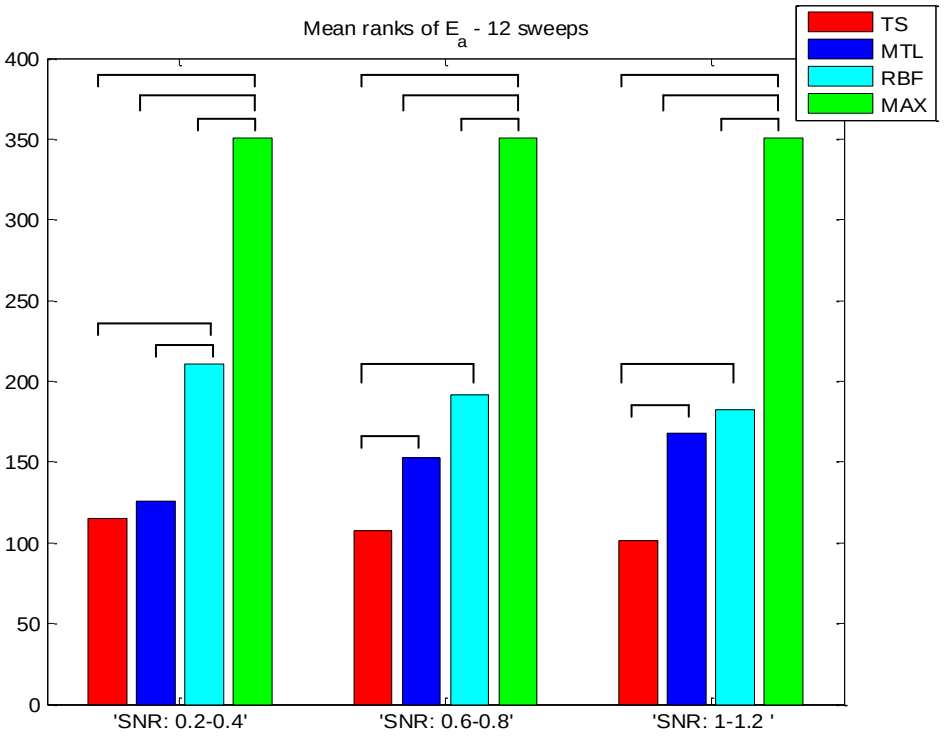

Figure 5.21. Mean ranks of E_a obtained for the three techniques at SNR in (0.2-0.4), (0.6-0.8), (1-1.2). Significant differences are shown with brackets.

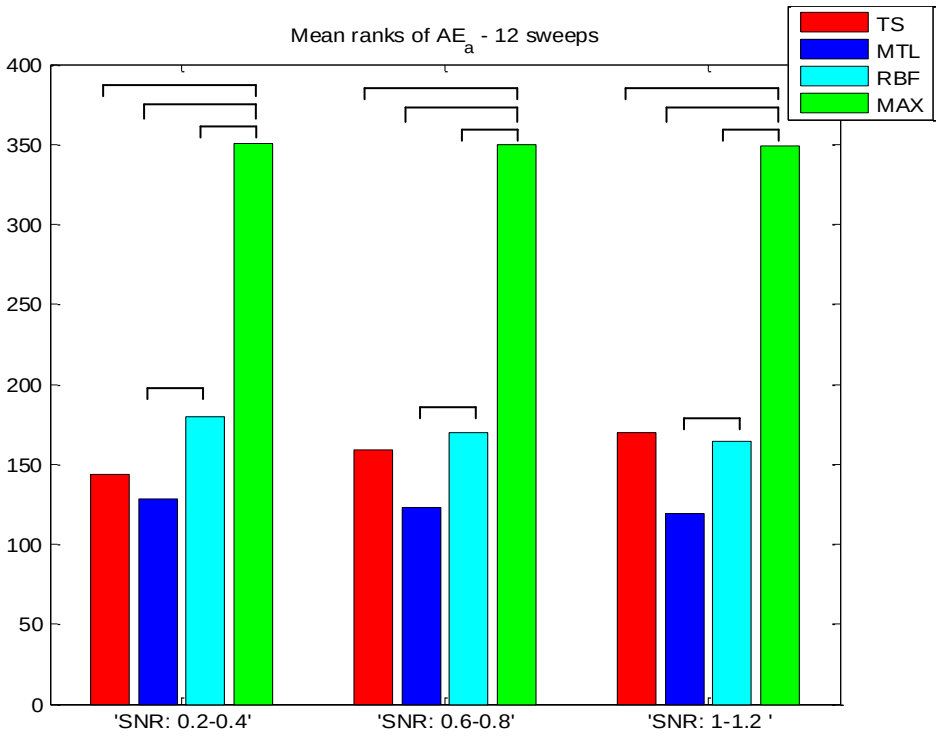

Figure 5.22. Mean ranks of AE_a obtained for the three techniques at SNR in (0.2-0.4), (0.6-0.8), (1-1.2). Significant differences are shown brackets.

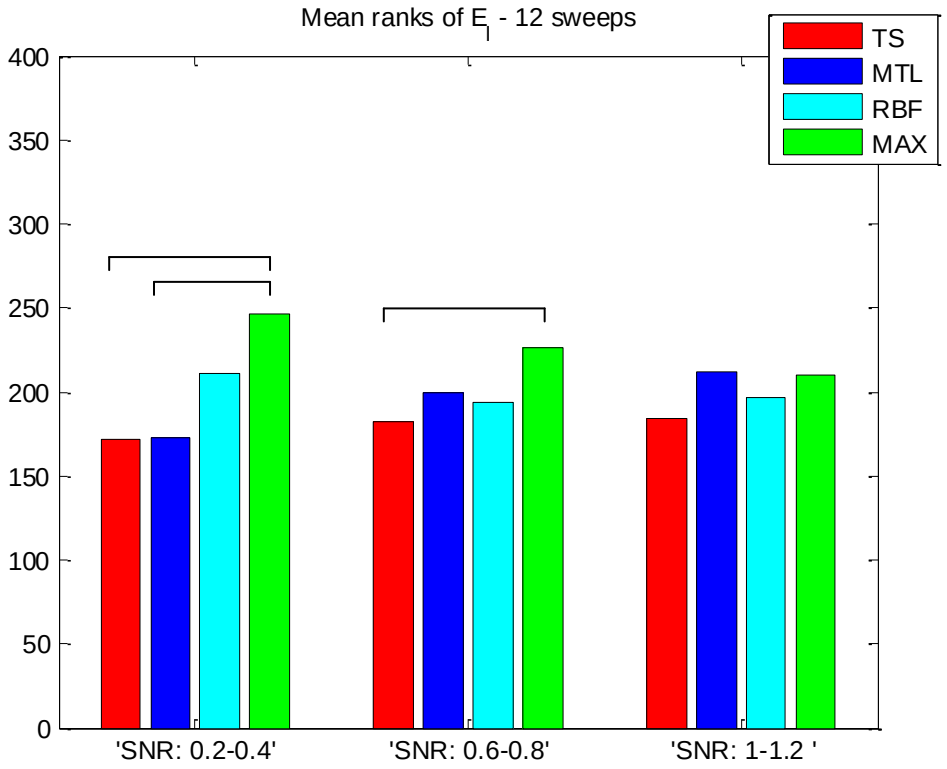

Figure 5.23. Mean ranks of E_I obtained for the three techniques at SNR in (0.2-0.4), (0.6-0.8), (1-1.2). Significant differences are shown brackets.

Results shown that the values of E_a provided by the MAX method are significantly larger than those provided by the other two approaches for each SNR level. Moreover, significant differences have been found between the RBF method and the two proposed approach at low SNR level. For higher SNR, instead, significant differences have been found between the MTL and the TS method while no significant difference between the MTL and the RBF method have been found. In fact, the box plots of Fig. 5.17 show as, at middle and high SNR, the performance of the MTL method becomes similar to that of the RBF approach, while the TS method seems to be positively biased. With regard to the AE_a index, the performance of the MAX method still results the worst while significant differences have been found between the RBF and the MTL method. The latter, in particular, gives the better estimates in terms of absolute errors in detecting the P300 amplitude. In the same way, with regard to the P300 latency, Fig. 5.23 and 5.24 show the results of the post-hoc comparisons.

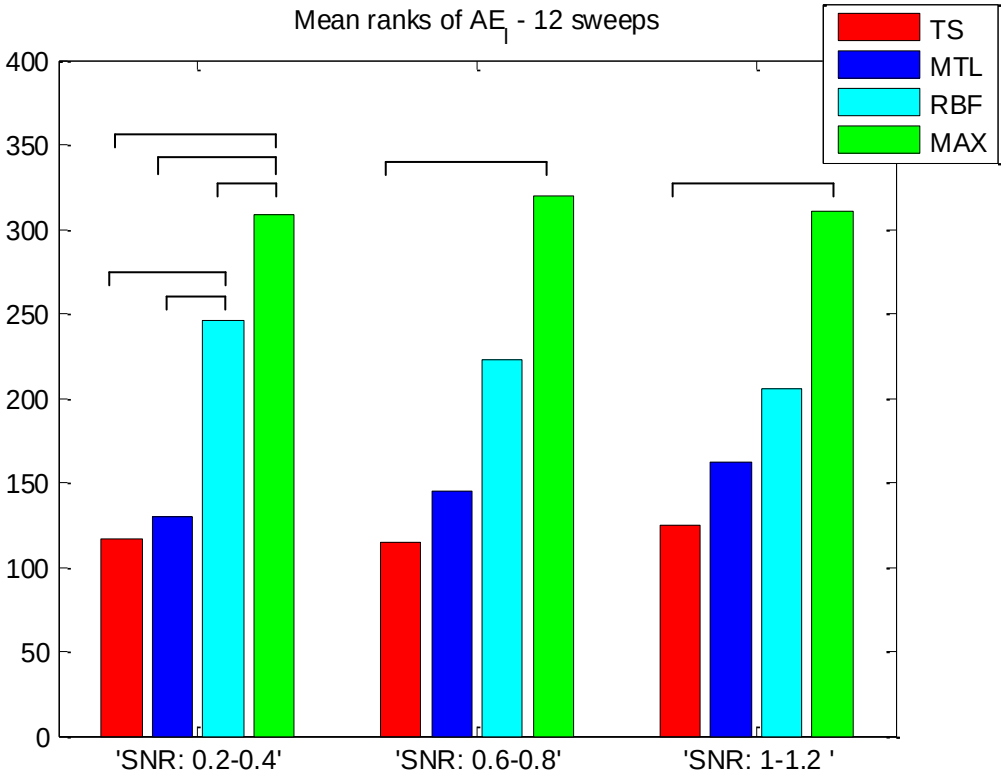

Figure 5.24. Mean ranks of AE_l obtained for the three techniques at SNR in (0.2-0.4), (0.6-0.8), (1-1.2). Significant differences are shown brackets.

In general, all the techniques give comparable results. Significant differences have been found only between the MAX method and the two proposed approaches, above with low SNR. A different trend characterizes the AE_l index. Fig. 5.28 clearly shows that at low SNR the two new approaches give results significantly better with respect to the other techniques while the MAX method gives the worst results. At higher levels of SNR, all the techniques seems to give similar results even if a significant difference has been found between the MAX technique and the TS approach, that gives the lowest values of AE_l.

5.4.2 Estimated single-trial ERP profiles

Among all the 100 groups of 12 sweeps, three groups have been chosen, as examples, in order to visually evaluate the capability of the three techniques (TS, MTL, and RBF) to estimate the single-trial profiles. Two representative sweeps have been chosen for each of the selected group. The corresponding results are

shown in figures 5.25, 5.26, 5.27, 5.28, 5.29 and 5.30. For all the figures, the three SNR levels ([0.2-0.4], [0.6-0.8], [1-1.2]) are presented in the top, the middle and the bottom panels respectively.

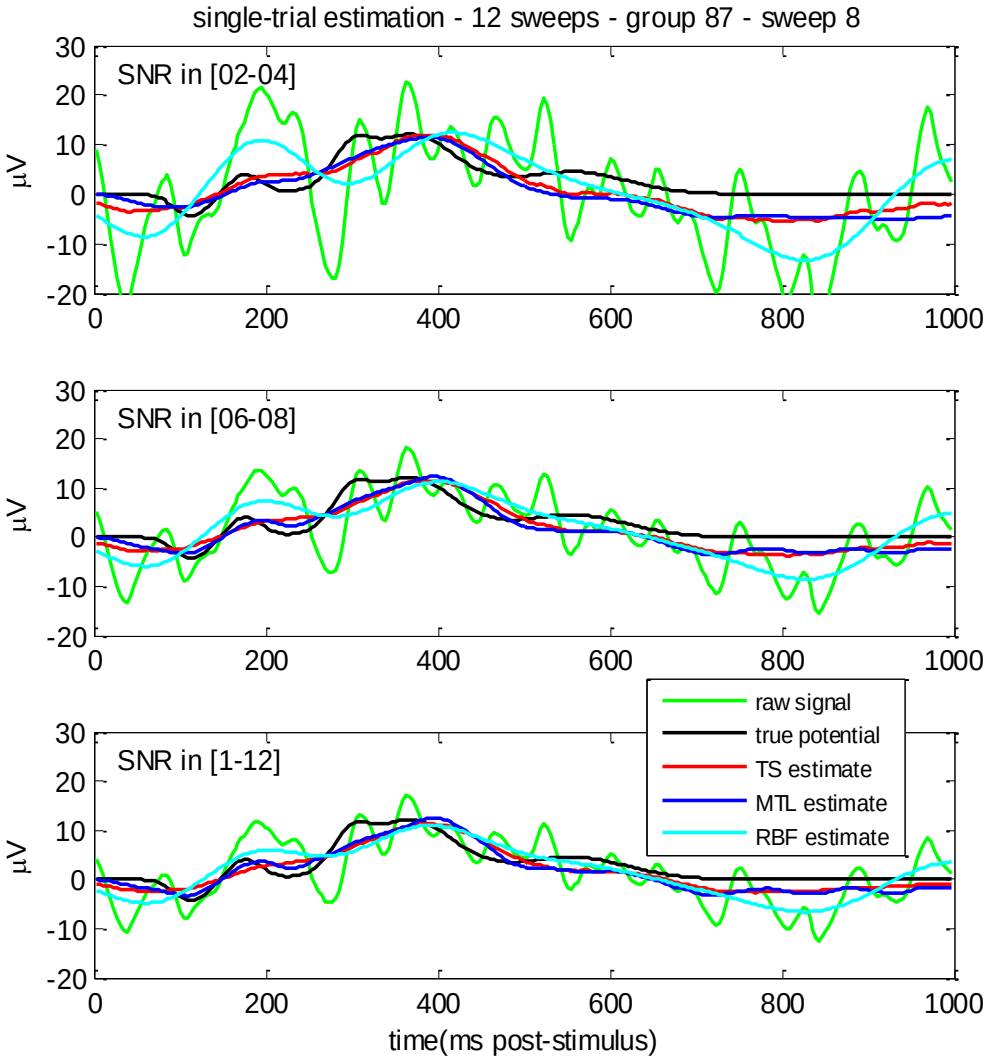

Figure 5.25. Single-trial ERP estimation for the sweep 8 of the group 87. Top Panels: SNR level in the range [0.2-0.4]. Central Panels: SNR level in the range [0.6-0.8]. Bottom panels: SNR level in the range [1-1.2]. Raw signal (green line), true single-trial ERP (black line), TS estimate (red line), MTL estimate (blue line), RBF estimate (cyan line).

The true ERP profile and the estimates given by the three methods are plotted superimposed on the same panel. In particular, the true ERP profile is represented by a black line, the estimate given by the TS method by a red line, that provided by MTL method by a blue line while a cyan line has been used to represent the RBF estimate. Fig. 5.25 and 5.26 show the results obtained for the group 87.

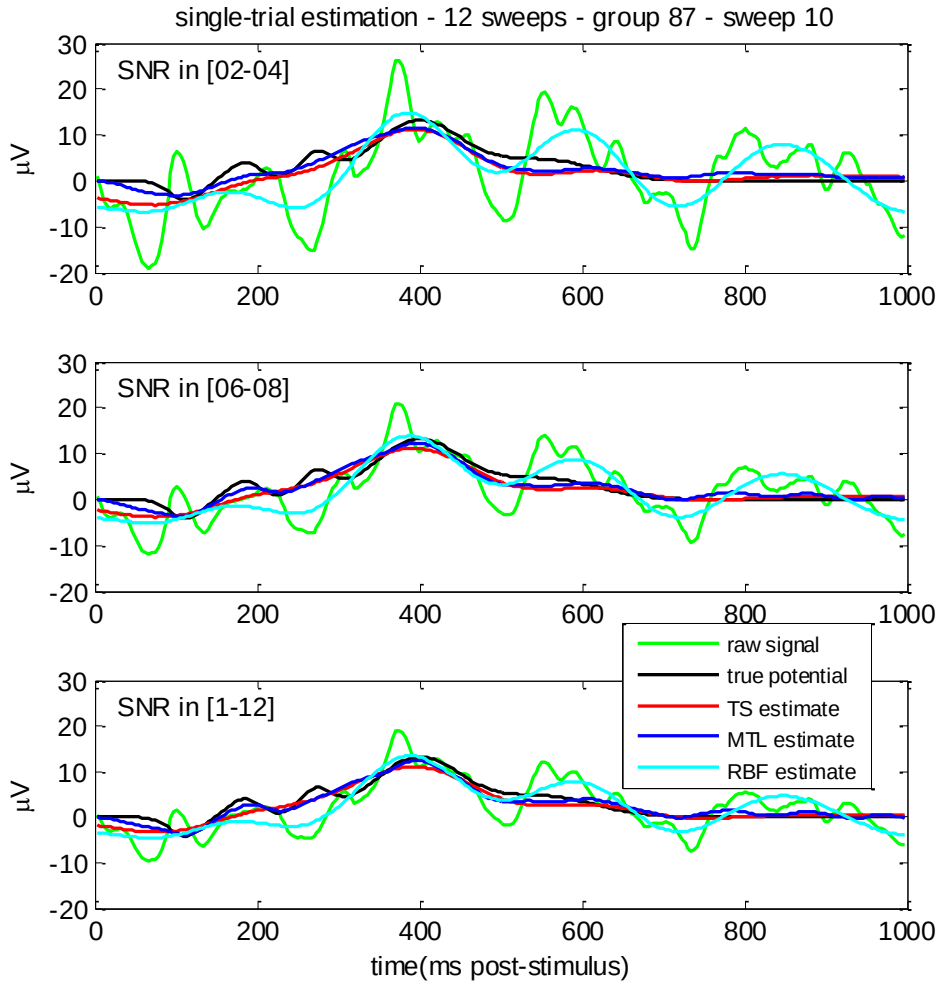

Figure 5.26. Single-trial ERP estimation for the sweep 10 of the group 87. Top Panels: SNR level in the range [0.2-0.4]. Central Panels: SNR level in the range [0.6-0.8]. Bottom panels: SNR level in the range [1-1.2]. Raw signal (green thin dashed line), true single-trial ERP (black dashed thick line), TS estimate (red dash-dot line), MTL estimate (blue thick line), RBF estimate (cyan thin line).

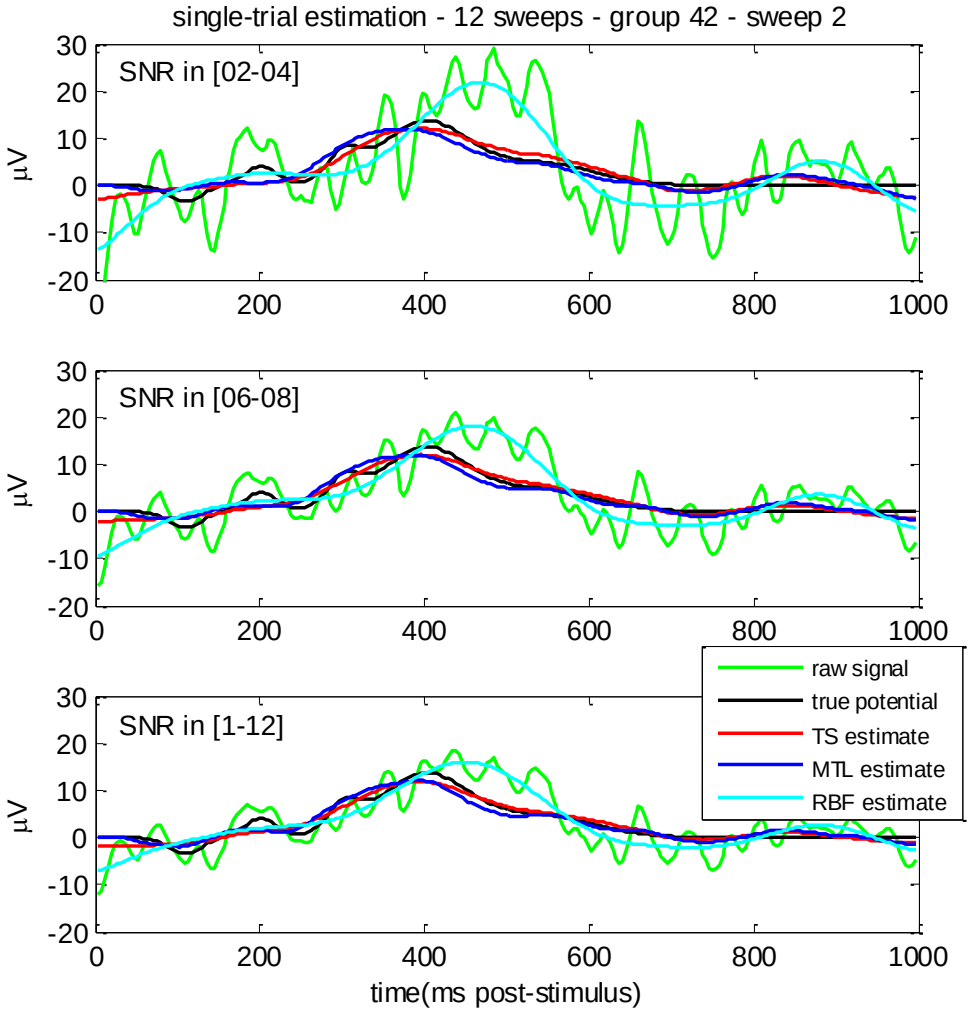

Figure 5.27. Single-trial ERP estimation for the sweep 2 of the group 42. Top Panels: SNR level in the range [0.2-0.4]. Central Panels: SNR level in the range [0.6-0.8]. Bottom panels: SNR level in the range [1-1.2]. Raw signal (green line), true single-trial ERP (black line), TS estimate (red line), MTL estimate (blue line), RBF estimate (cyan line).

In this case, the estimates given by the new Bayesian methods satisfactorily resemble the single ERPs embedded in the artificial sweep. For the sweep 8 in particular, the estimates are good in case of low SNR level too, see the top panel of the figure. Also the results given by the RBF methodology are satisfying. For the second sweep, for example, latency and amplitude of the P300 component seem to be well tracked.

The performance of the RBF method seems to be less good than the proposed techniques when the noise level is very large. See for example the top panel of Fig. 5.27 and note as the RBF estimate often follows the low-frequency oscillations present in the raw signal.

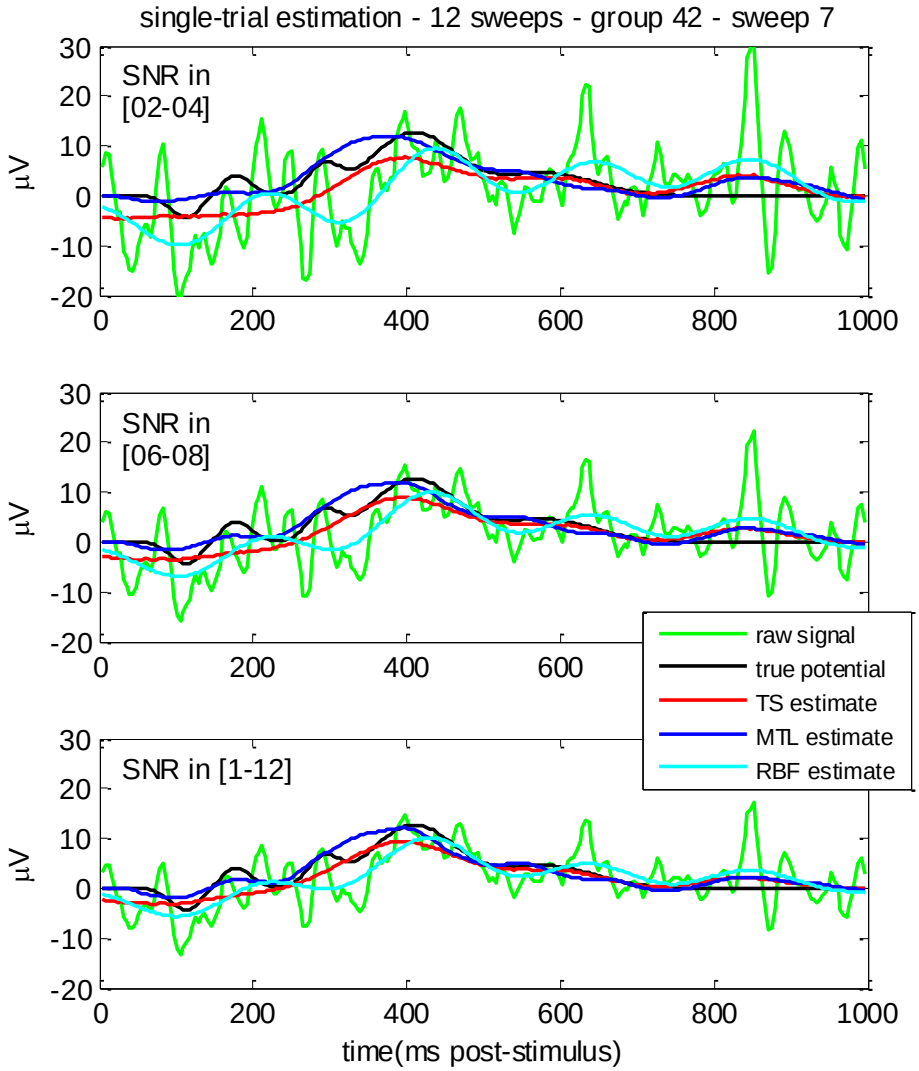

Figure 5.28. Single-trial ERP estimation for the sweep 7 of the group 42. Top Panels: SNR level in the range [0.2-0.4]. Central Panels: SNR level in the range [0.6-0.8]. Bottom panels: SNR level in the range [1-1.2]. Raw signal (green line), true single-trial ERP (black line), TS estimate (red line), MTL estimate (blue line), RBF estimate (cyan line).

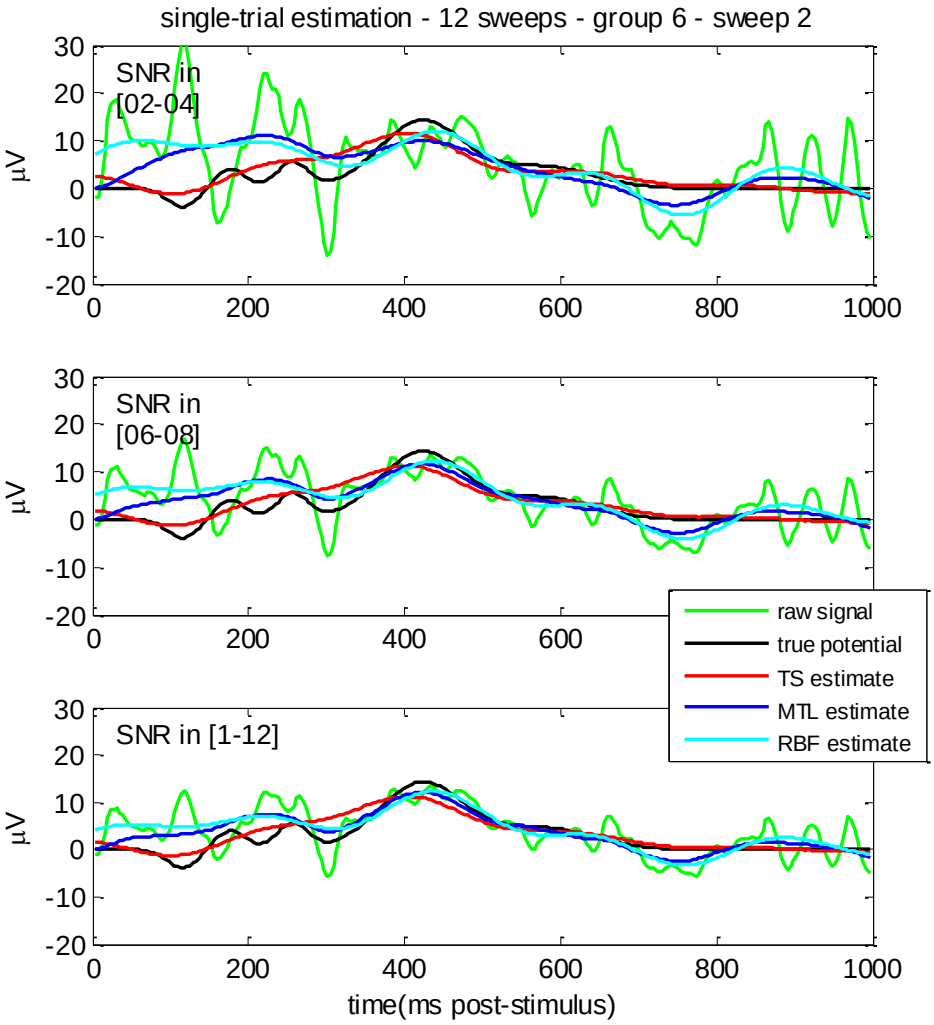

Figure 5.29. Single-trial ERP estimation for the sweep 2 of the group 6. Top Panels: SNR level in the range [0.2-0.4]. Central Panels: SNR level in the range [0.6-0.8]. Bottom panels: SNR level in the range [1-1.2]. Raw signal (green line), true single-trial ERP (black line), TS estimate (red line), MTL estimate (blue line), RBF estimate (cyan line).

See also Fig. 5.30. Clearly these cases affect the computation of the index E_{ind}. Fig. 5.28 also shows a critical case at low SNR. In fact, all the three techniques provide not very good estimates, even if the two Bayesian methods deviate from the prominent oscillations due to the EEG noise. Note that the performances improve when the SNR increases, see middle and bottom panels. Analogous considerations can be done for the sweep represented in Fig. 5.29. Finally, it is

worth to notice that the estimates given by the two Bayesian approaches are quite similar even if, as already discussed in the previous section, the estimates given by the MTL method is better in tracking some peaks, see for example the bottom panel of Fig. 5.26 or Fig. 5.29.

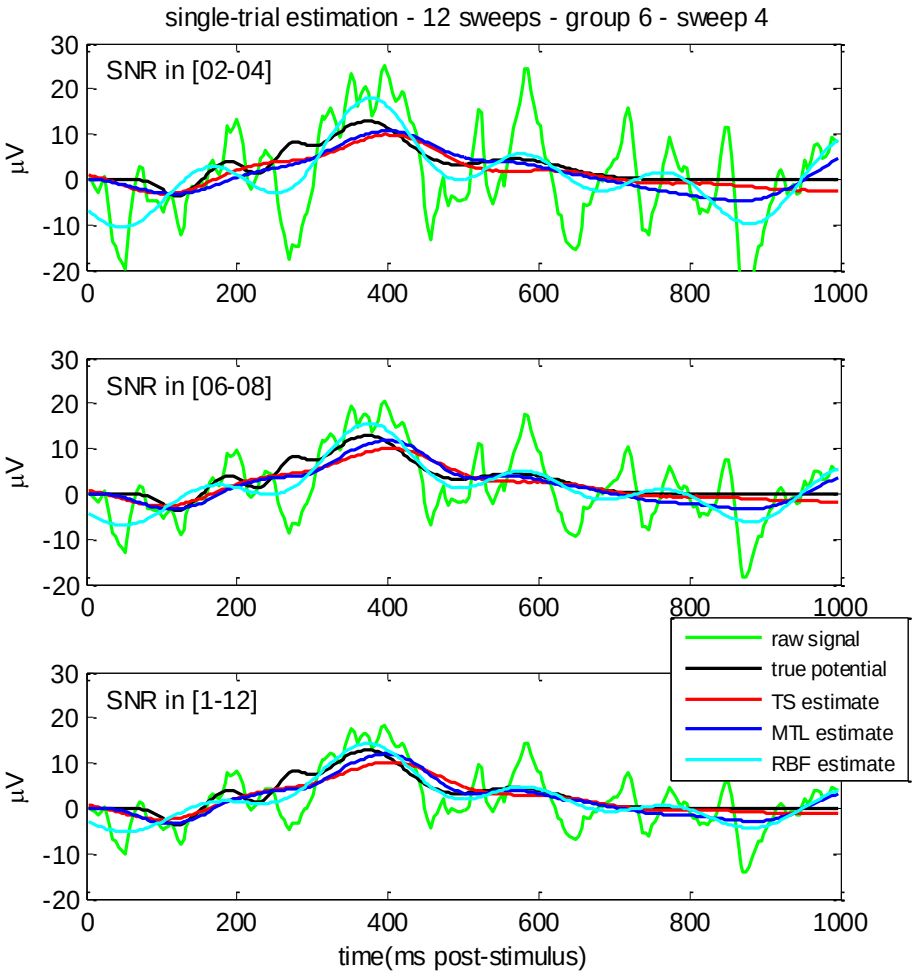

Figure 5.30. Single-trial ERP estimation for the sweep 4 of the group 6. Top Panels: SNR level in the range [0.2-0.4]. Central Panels: SNR level in the range [0.6-0.8]. Bottom panels: SNR level in the range [1-1.2]. Raw signal (green line), true single-trial ERP (black line), TS estimate (red line), MTL estimate (blue line), RBF estimate (cyan line).

5.5 Conclusions

Results on simulated data have demonstrated that the two new techniques are able to provide improved estimates of the average ERP and good single-trial profiles.

With regard to the average ERP response, the new approaches provide estimates significantly better with respect to the CA, for each SNR level. In particular, if few sweeps are available the TS method gives results significantly better of the MTL method. By using these Bayesian methods, less sweeps are needed (about 50 %) with respect to the CA technique in order to obtain the same error. This improvement allows to shorten the time of the experiments and this is important to keep participants under stationary conditions, above all if tasks involving attention are considered. Moreover, the reduction of the sweeps is needed for those subjects, such as patients or children, who do not tolerate long-lasting experiments. In terms of ERP profiles, the two proposed approaches provide average ERP estimates much more similar to the true signals. The profiles obtained by using the CA technique are characterized, above all in case of low SNR, by pronounced oscillations that are not present in the true signal. At higher SNR levels these oscillations become less evident even if they can still be misleading in the determination of latency and amplitude of peaks, for example the P300 component.

As regards the single-trial estimation, the two procedures have been evaluated, in comparison with the RBF technique and the MAX method, both in terms of errors in estimating the ERPs profiles and in determining the P300 latency and amplitude. In terms of errors in the estimating the ERPs profiles, the proposed methods provide a significantly better reconstruction of the single-trial responses in comparison with the RBF method. No significant differences have been found between the two new methods. The better performance of the two Bayesian methods with respect the RBF methodology is more evident if the

number of available sweeps increases. This is because the two Bayesian techniques are positively influenced by the increasing of the available sweeps: the first method makes use of the estimated average ERP in order to obtain the single-trial profiles; the second method uses all the available data in a population analysis context. On the other hand, the RBF methodology, conceived for on-line applications, provides the single-trial estimate sweep by sweep, without exploiting any kind of information deriving from the other sweeps. With regard the determination of the P300 parameters, the MAX method gives in general the worst performance while the two Bayesian approaches and the RBF technique give similar results. In particular, the values of E_a provided by the MAX method are significantly larger than those provided by the other three approaches for each SNR level. The MAX method, in fact, is very positively biased in the determination of P300 amplitude. At low SNR, significant differences have been found between the two new methods and the RBF approach that gives the best performance in terms of median E_a. For higher SNR, instead, significant differences have been found between the MTL and the TS method while no significant difference between the MTL and the RBF method have been found. At middle and high SNR, in fact, the performance of the MTL method becomes similar to that of the RBF approach, while the TS method seems to be positively biased. With regard to the AE_a index, the performance of the MAX method still results the worst while significant differences have been found between the RBF and the MTL method. The latter, in particular, gives the best estimates in terms of absolute amplitude error. With regard to determination of the P300 latency, all the methods give comparable performances. Significant differences have been found only between the MAX method and the two proposed approaches, above with low SNR. A different trend characterizes the AE_l index. At low SNR the two new approaches give results significantly better with respect to the other techniques while the MAX method gives the worst results. At higher levels of SNR, all the techniques seems to give similar results even if a significant

difference has been found between the MAX technique and the TS approach, that gives the lowest values of AE_l.

6 ASSESSMENT ON REAL DATA

This chapter is focused on the results obtained by applying the proposed techniques to real data. In the first sections a description of the real database and of the experimental test to which the participants have been subjected is given; moreover, the pre-processing procedure is described. In the following sections the estimates of the average profile and of the single-trial ERPs obtained on these data are shown. Interesting results regarding the estimation of the P300 parameters in cirrhotic patients are discussed.

6.1 Database and preprocessing

6.1.1 Subjects

Data here used were collected at the Department of Clinical and Experimental Medicine of the University of Padua, by using a digital electroencephalograph (System Plus, Micromed, Mogliano Veneto, Italy). EEG was continuously recorded with Ag/AgCl electrodes positioned on 29 standard locations according to the International 10/20 system [99] using an elastic cup. The Fpz electrode was used as ground while the two earlobe electrodes shorted together were used as reference. The horizontal and vertical electro-oculogram were recorded by means of two electrodes placed on the outer cantus and under the left eye. Impedance was kept below 5 kΩ. Each channel had its own analogical-to-digital converter; the EEG signals were digitalized online with a sampling frequency of 512 Hz and a conversion resolution of 0.19 μV/digit.

Participants comprised 29 cirrhotic patients with an age of 51 ± 9 (mean ± standard deviation), 14 healthy aged-matched control subjects (51 ± 9 years) and 11 young control subjects (24±3 years). None of the subjects had history of past or current alcohol misuse or reported history of neurological disorders, diabetes, cardiovascular, respiratory or renal insufficiency, neuropsychiatric disorders or

dementia; none had uncorrected impairment of visual acuity or was color blind. The diagnosis of cirrhosis was made on the basis of historical, clinical, laboratory, endoscopic and radiological findings. None of the patients had evidence of overt hepatic encephalography (HE) at the time of the study. Briefly, HE is a complex neuropsychiatric syndrome that develops in patients with severe liver disease and/or portal-systemic shunting [100,101]. The term "hepatic encephalopathy" is used for a wide range of different situations in which the cerebral function is altered as a consequence of a previous failure of hepatic function [102]. The main alterations regard cognitive and motor function and circadian rhythms. Cognitive impairment may affect attention, memory, learning; the motor alterations include motor coordination, hypokinesia and bradykinesia; alterations in sleep/waking are also often present [102]. HE may be acute or chronic and may present different grades from minimal HE to coma and death. Minimal HE (MHE) is the mildest form of HE, it is characterized by brain dysfunctions without recognizable signs on clinical examination [103]. MHE is detectable in 20-60% of cirrhotic patients [100,104] and the neuropsychological dysfunctions that characterize it concern visual-constructive abilities, orienting of visual attention, psychomotor speed, inhibitory processes and executive functions [105]. Among the cirrhotic subjects of the database 16 patients resulted to have MHE, whereas the remaining 15 patients did not show marks of MHE. The presence of MHE was assessed on the basis of spectral EEG analysis [106-108] and performance on several paper and pencil psychometric tests [100]. The EEG was considered to be abnormal if the mean dominant frequency was ≤7.3 Hz and/or the theta relative power ≥35% [107]. Patients were considered to have MHE if at least one of measures (paper and pencil tests and/or EEG) was abnormal [100,106].

6.1.2 Experimental protocol

The database employed to test the applicability of the proposed techniques in real cases consists in EEG signals recorded on human subjects during an experiment based on the "Simon paradigm" [109]. The Simon task consists in a

two-choice paradigm in which the subject is required to evaluate which stimulus, between the two possible target stimuli, has been presented; the target stimuli are shown on either the left or on the right side of a monitor. The task of the subject is to respond as fast as possible by pressing a key of the keyboard on either the left or on the right side according to prefixed instructions. The subjects performing this task include cirrhotic patients with and without minimal hepatic encephalopathy. The analysis of the ERPs evoked during such a task in normal and abnormal subjects can help to discover and better understand the processes underlying these abnormalities.

In the present experiment, a Compaq 80386 Proline interfaced to a 14 in. monitor controlled stimuli presentation by means of the software package E-Prime 1.0 (Psychology Software Tools, Inc., 2002). Participants were seated in front of the computer screen at a distance of 80 cm with their head positioned in an adjustable head-and-chin rest; they were encouraged to maintain fixation from the presentation of a fixation cross to response execution, avoiding saccadic eye movement and blinks as much as possible. The monitor background was held constantly white. The stimuli consisted in red-and-black or green-and-black 4x4 chessboards. Each stimulus was presented at 3.3° to the left or right of a central fixation cross and subtending a visual angle of 1.4°. In order to avoid asymmetries in the event-related potentials a 4x4 black-and-white chessboard was used as distracter and projected on the side opposite to which of the stimulus. One half of the participants were instructed to press the left button, in our case the ‘Z’ letter of the keyboard, if the stimulus was a red-and-black chessboard and to press the right button, the ‘M’ letter of the keyboard, if the stimulus was a green-and-black chessboard. Opposite instructions were given to the remaining subjects. Four combinations of color-position were possible: red-and-black chessboard on the left side of the monitor, red-and-black chessboard on the right side of the monitor, green-and-black chessboard on the left side of the monitor, green-and-black chessboard on the right side of the monitor. After a warm-up session of 40 trials, participants received, in a completely randomized

sequence, a total of 300 stimuli (75 for each combination of hand and stimulus position) with an inter-trial interval ranging from 800 to 1200 ms. Each stimulus was displayed for 176 ms and a maximum of 1200 ms was given for the response.

The four conditions of the above described task can be grouped in corresponding and non-corresponding. The corresponding conditions take place when the stimulus occurs of the side of the monitor associated with the button to be pressed, non corresponding conditions happen in the other cases. For example, if the 'Z' letter is associated to the red-and-black chessboard, a corresponding condition takes place if the red-and-black chessboard appears in the left side of the monitor. Fig. 6.1 shows a schematic representation of the four conditions of the Simon task. Characteristic of the Simon task is that the decision about which button must be pressed has to be taken only on the basis of the stimulus characteristics and not on its spatial position. The "Simon effect" is defined as the increment of the reaction times and the reduction of the accuracy in the non corresponding conditions. Several theories have been proposed in order to explain the mechanisms underlying the Simon effect, see [110], but it is a common opinion that this effect is due to an automatic activation of the ipsilateral response. Namely, there is a natural tendency to respond with the hand whose relative position is corresponding to that of the stimulus on the screen. In case of non corresponding conditions, this automatic tendency has to be inhibited and this produced longer reaction times.

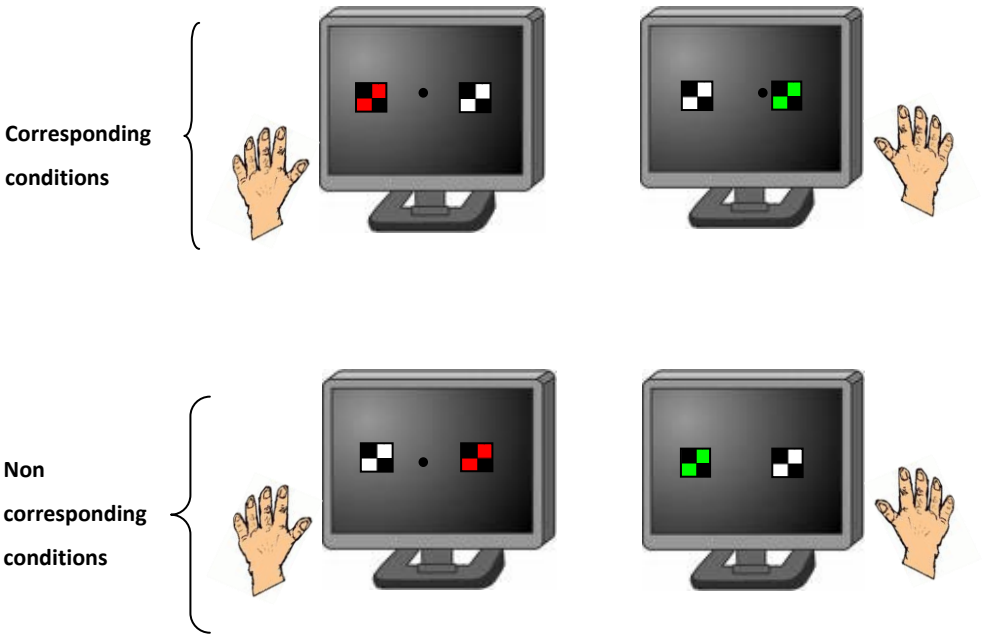

Figure 6.1. Schematic representation of the Simon task. In the top part of the figure the two corresponding conditions are shown. By assuming that the left button of the keyboard has been associated to the red-and-black chessboard and the right button to the green-and-black one, the two conditions are characterized by a correspondence between the relative position of the stimulus on the screen and the relative position of the corresponding hand. In the bottom part of the figure the non corresponding conditions are shown.

6.1.3 Pre-processing

The EEG signals, obtained as described in the previous section, were digitally pass-band filtered (0.7-30 Hz) utilizing a cascade of a high pass and a lowpass linear phase FIR filters. Filtered signals were resampled to 256 Hz and then segmented into trials time-locked to the stimulus onset spanning from −0.8 to 1.5 s, baseline correction was carried out by using the interval [-0.2 – 0] ms. Trials without response or with erroneous response were excluded from further analysis. For each subject, trials were divided in 4 groups on the basis of the color-position combination. In each group, artifact removal was carried out by first visual inspecting the data and discarding the badly distorted epochs; then,

the contribute of the artifact was removed in EEGLAB [111] by using the Independent Component Analysis. In order to give an example, a brief discussion about the removal of the ocular blink artifact will follow. Fig. 6.2 shows five trials of a subject.

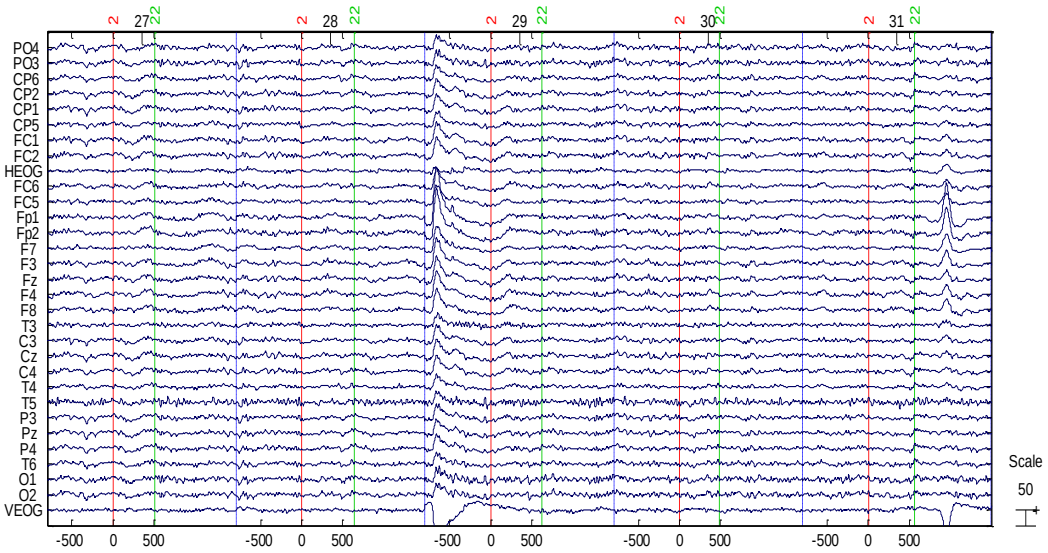

Figure 6.2. Five trials of a representative subject. Note the ocular blinks at about -600 ms in trial 29 and at about 800 ms in trial 31. All the 31 electrodes are shown.

These trials belong to the condition characterized by a green-and chessboard appearing on the left side of the monitor and are shown after the filtering procedure. As visible from the figure, trials 29 and 31 are contaminated by an artifact which seems to be due to an ocular blink. In fact, it is present in the VEOG electrode that records the vertical eye movements and, with opposite polarity, on the frontal sites [7]. Moreover, the amplitude of the artifact decreases quickly with greater distance from the orbits. Fig. 6.3 shows the 31 components obtained after ICA decomposition. As clearly evident from the figure, the second component seems to resample the artifacts present in trial 29 and trial 31. Fig. 6.4 shows the scalp map projection of the component (top- left), the ERP image with the activity of the component among trials (top-right), the power spectrum of the component (bottom).

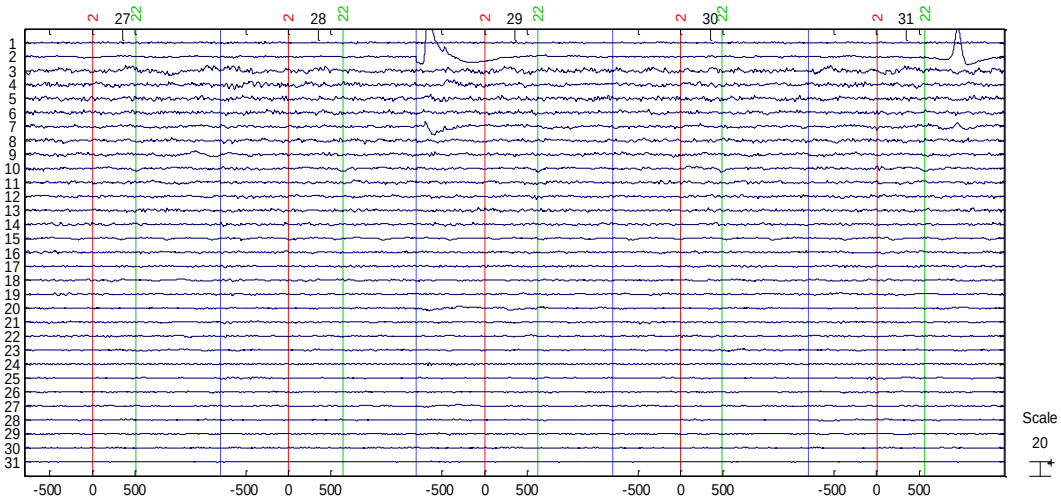

Figure 6.3. The 31 components obtained after ICA decomposition. Their temporal progress during the five trials of Fig. 6.2. Note the ocular blinks at about -600 ms in trial 29 and at about 800 ms in trial 31 clearly isolated in the second component.

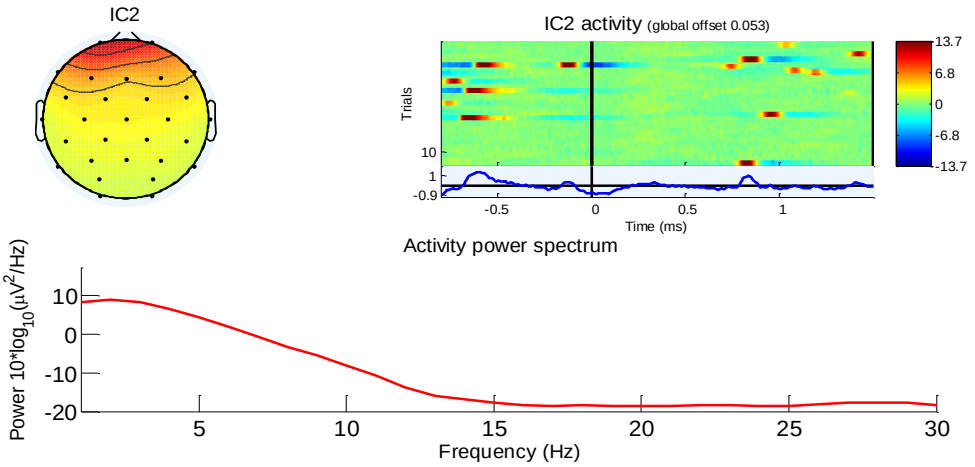

Figure 6.4. Scalp map projection of the component (top- left), ERP image with the activity of the component among trials (top-right), power spectrum of the component (bottom).

These characteristics are typical of the eye blink artifact: the spectrum is smoothly decreasing, the scalp map shows a strong frontal distribution, individual eye movements can be seen in the component ERP image (top-right panel). These considerations have brought to the removal of the third

component together with those identified as artifacts. Fig. 6.5 shows the five trials after the removal of the artifactual components.

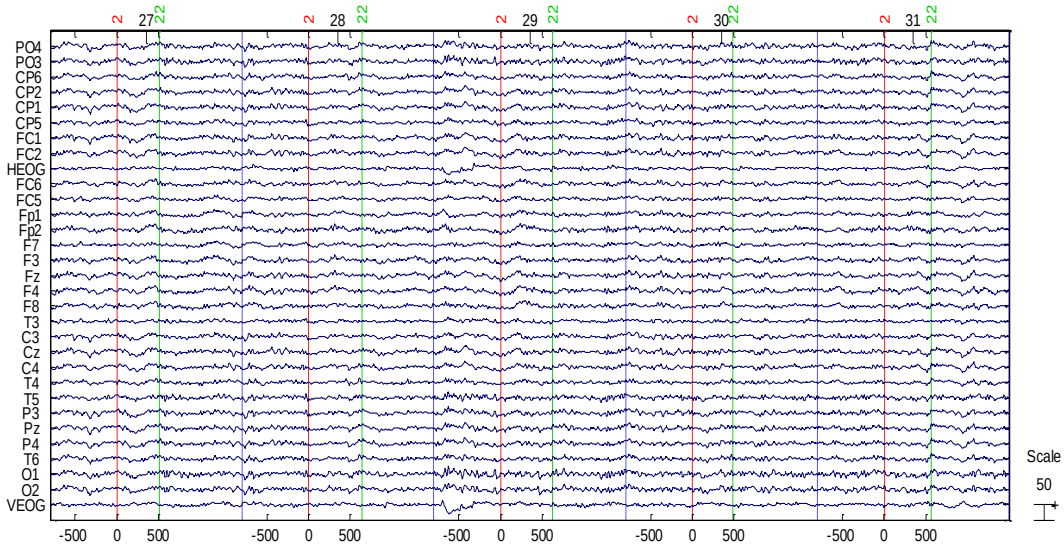

Figure 6.5. The five trials after the removal of the artifactual components. Note the absence of the peaks identified as artifacts and the cleaning of all the interested channels.

It is evident the absence of the peaks identified as ocular artifacts and the cleaning of all the interested signals.

6.2 Results

6.2.1 Rationale

EEG trials pre-processed as above described have been used to test the applicability of the two proposed estimation techniques. The possibility of studying the intra-subject variability of the ERP components by the way of single-trial estimation techniques, in particular, will be useful to investigate if and how the cirrhosis, with and without MHE, influences the P300 parameters.

In the following only the results regarding the Pz electrode will be shown and discussed. It is of significant importance keeping in mind that only 12 sweeps will

be used in order to evaluate the effectiveness of the two techniques when a very limited number of sweeps is available.

6.2.2 Average ERP estimation

In addition to the estimates provided by the two proposed approaches, the CA profiles will be shown for comparison. Fig. 6.6, 6.7, 6.8, and 6.9 report some results for the young normal subjects, the elderly normal subjects, the cirrhotic patients without MHE, and the cirrhotic patients with MHE, respectively.

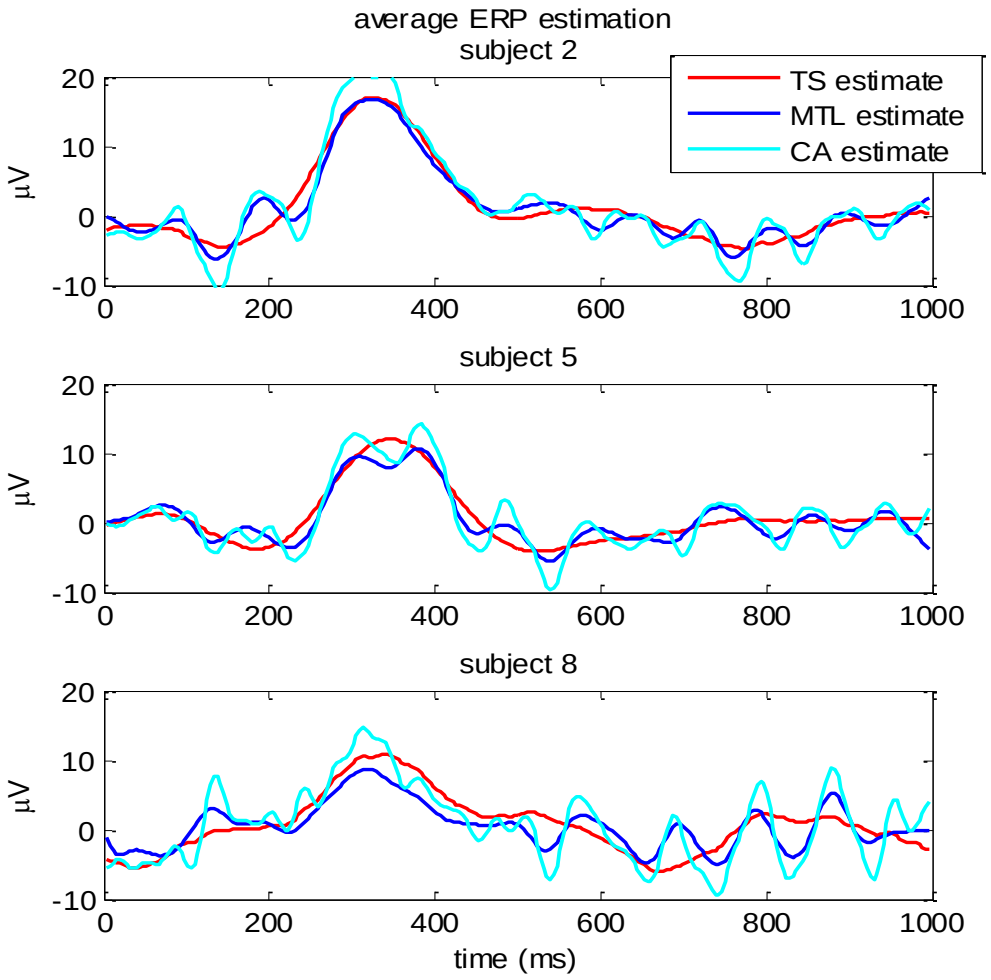

Figure 6.6. Average ERP estimation in three representative young control subjects obtained by using 12 sweeps. Time 0 denotes stimulus delivery. Top, central and bottom panel show the results for three different subjects of the group. TS estimate (red line), M2 estimate (blue line), CA estimate (cyan line).

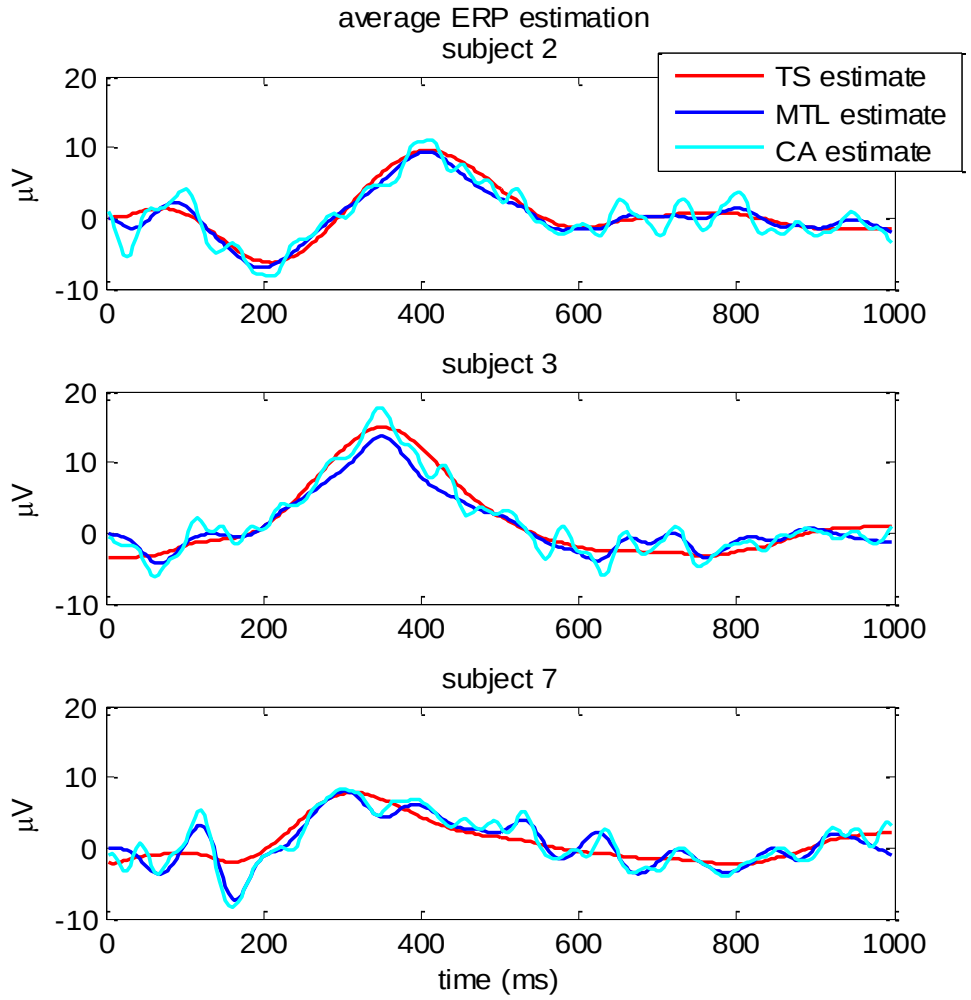

Figure 6.7. As in Fig. 6.6 in three representative elderly control subjects.

By determining, for example, the P300 amplitude (as the maximum of the estimated profile in 250-600 ms) by using the estimate provided by the CA technique a higher value will be obtained in comparison with the two Bayesian methods, see for example Fig. 6.7. This trend can be found in the simulations results too. In fact, above all in cases in which few sweeps were available, the estimates given by the CA technique presented many spurious oscillations misleading for the estimation of P300 amplitude, see for example Fig. 5.8 and 5.9. In the estimation of the average P300 latency there are cases in which the estimates by the three approaches are quite different. See for example the central and bottom panels of Fig. 6.6. In these cases the estimate of the P300

latency given by the TS method will be different from those given by the other two methods. It is worth to remember that the true P300 latency of the average ERP is not known but in this situation the small number of sweeps is determinant. By remembering the simulations results, it is reasonable to suppose that the estimate given by the TS approach is closer to the actual value. Moreover, if a higher number of sweeps is employed the estimates given by the MTL method and the CA techniques become stable and the two peaks (at times 300 and 380 ms) of the central panel of Fig. 6.6 merge into one giving only one peaks with latency closer to that estimated by the TS method.

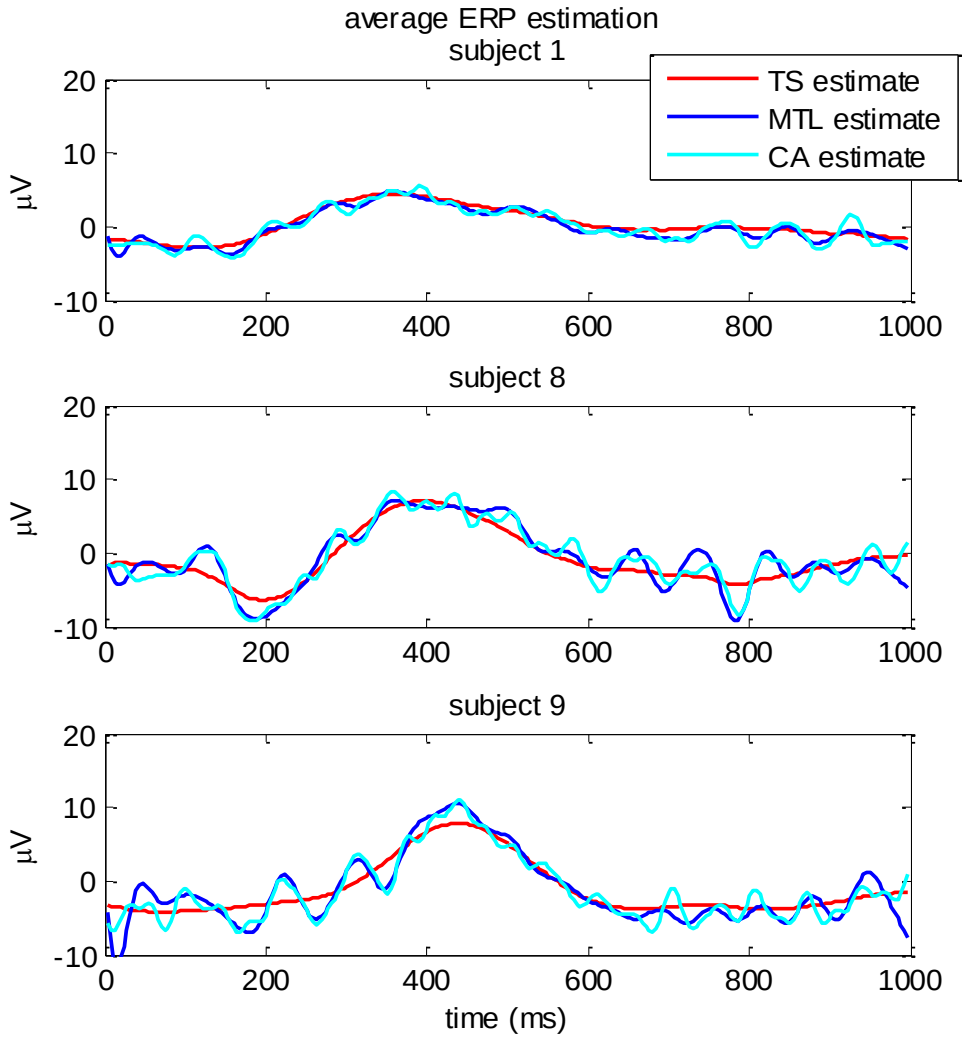

Figure 6.8. As in Fig. 6.6 in three representative cirrhotic patients without MHE.

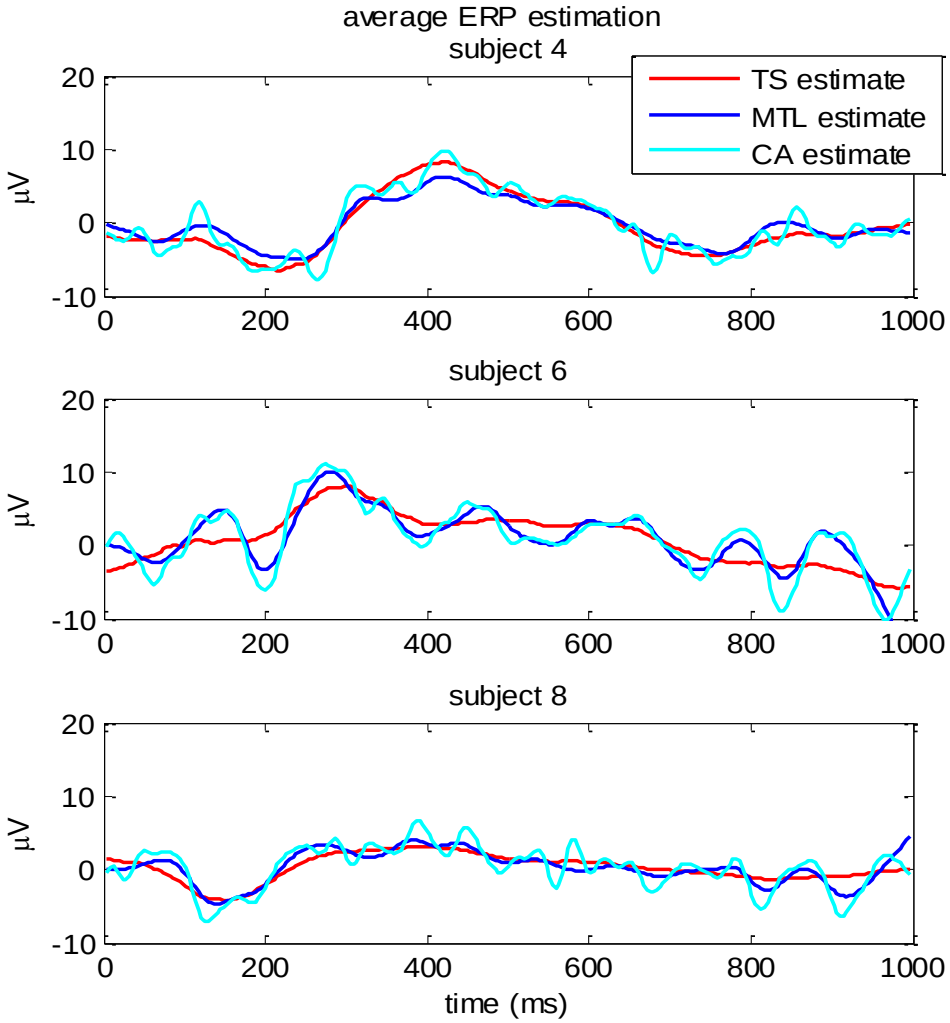

Figure 6.9. As in Fig. 6.6 in three representative cirrhotic patients with MHE.

Although, given the purpose of the work, only three subjects for group have been shown, we can notice as, in some cases among those reported, the estimate of the average ERP in cirrhotic patients can result in a signal of smaller amplitude in comparison with those obtained in control subjects. See the top panel of Fig. 6.8 and the bottom panel of Fig. 6.9. In particular, note as the amplitude of the P300 component can be strongly reduced. As will be discussed in the following section through single trial analysis, this reduction is a typical and well characterized feature in hepatic cirrhosis.

6.2.3 *Single-trial ERP estimation*

In the following the estimates obtained by using only 12 sweeps will be discussed. In addition to the estimates provided by the two new approaches, also those obtained by using the RBF method will be shown for comparison. For each of the four groups a representative subject has been selected. In Fig. 5.10 the results regarding a representative young control subject are shown, two representative sweeps have been reported. Results on the top panel are referred to the first sweep while those on the bottom panel to the second one.

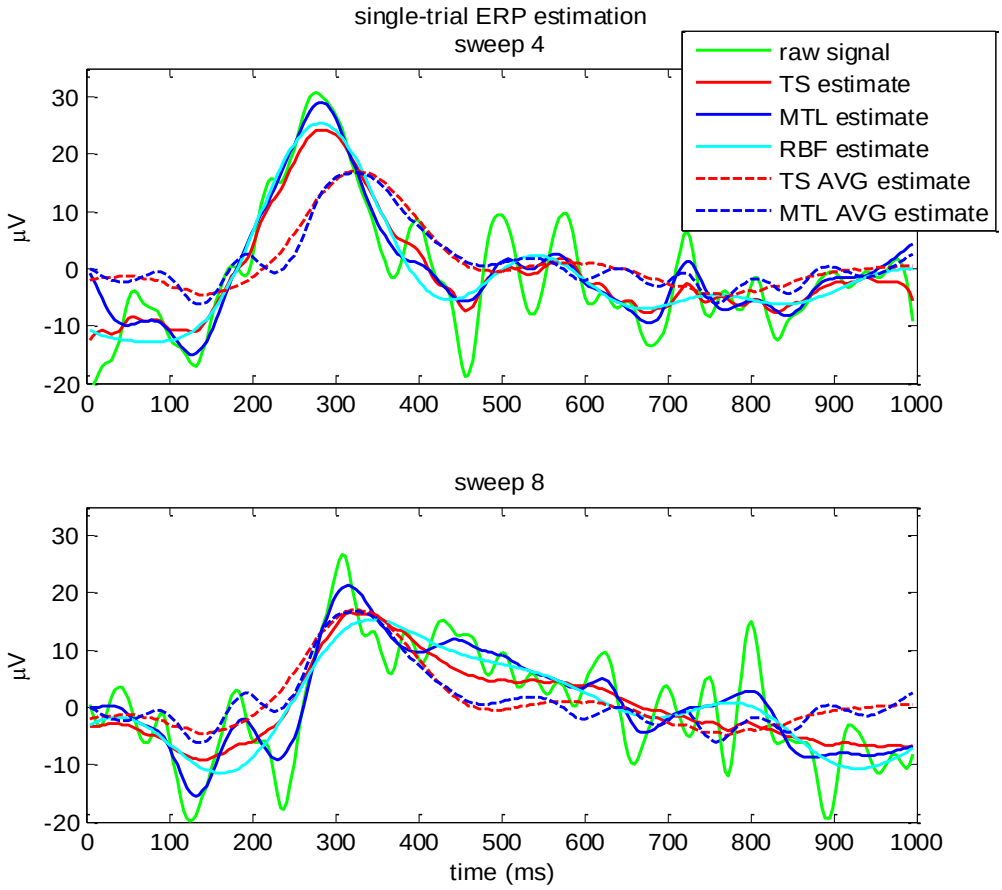

Figure 6.10. Single-trial ERP estimation for a representative young normal subject (#2). Top panel: results obtained for the sweep #4. Bottom panel: results obtained for the sweep #8. Raw signal (green line), TS single-trial estimate (red line), MTL single-trial estimate (blue line), RBF estimate (cyan line), TS average estimate (dashed red line), MTL average estimate (dashed blue line).

In the same way, the results regarding a representative elderly control subject, a representative cirrhotic patient without MHE and a representative cirrhotic patient with MHE are represented in Fig. 6.11, 6.12, 6.13, respectively. The raw single trial sweep is represented by a green line, the estimate given by the TS method by a red line, that provided by MTL method by a blue line while a cyan line is used for the RBF estimate. In addition, the estimates of the average ERP given by the TS and the MTL approaches have been added for comparison, they are shown by dashed red lines and dashed blue lines respectively.

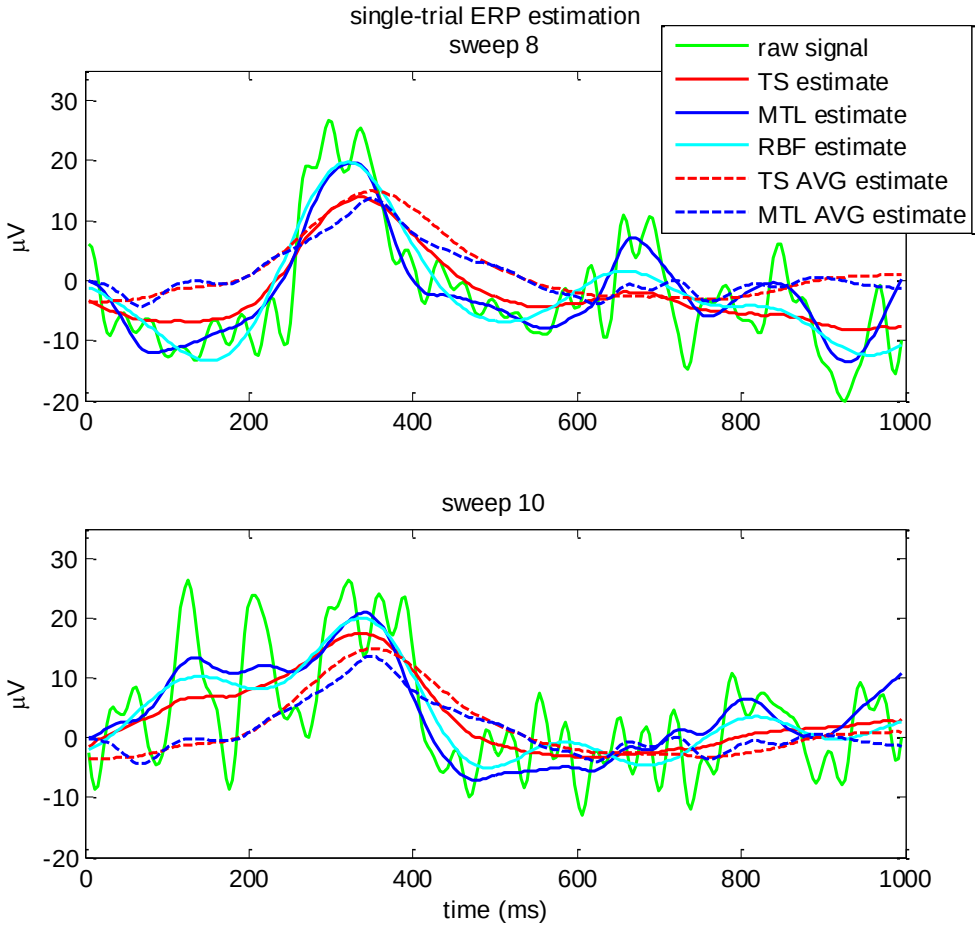

Figure 6.11. Single-trial ERP estimation for a representative elderly subject (#3). Top panel: results obtained for the sweep #8. Bottom panel: results obtained for the sweep #10. Raw signal (green line), TS single-trial estimate (red line), MTL single-trial estimate (blue line), RBF estimate (cyan line), TS average estimate (dashed red line), MTL average estimate (dashed blue line).

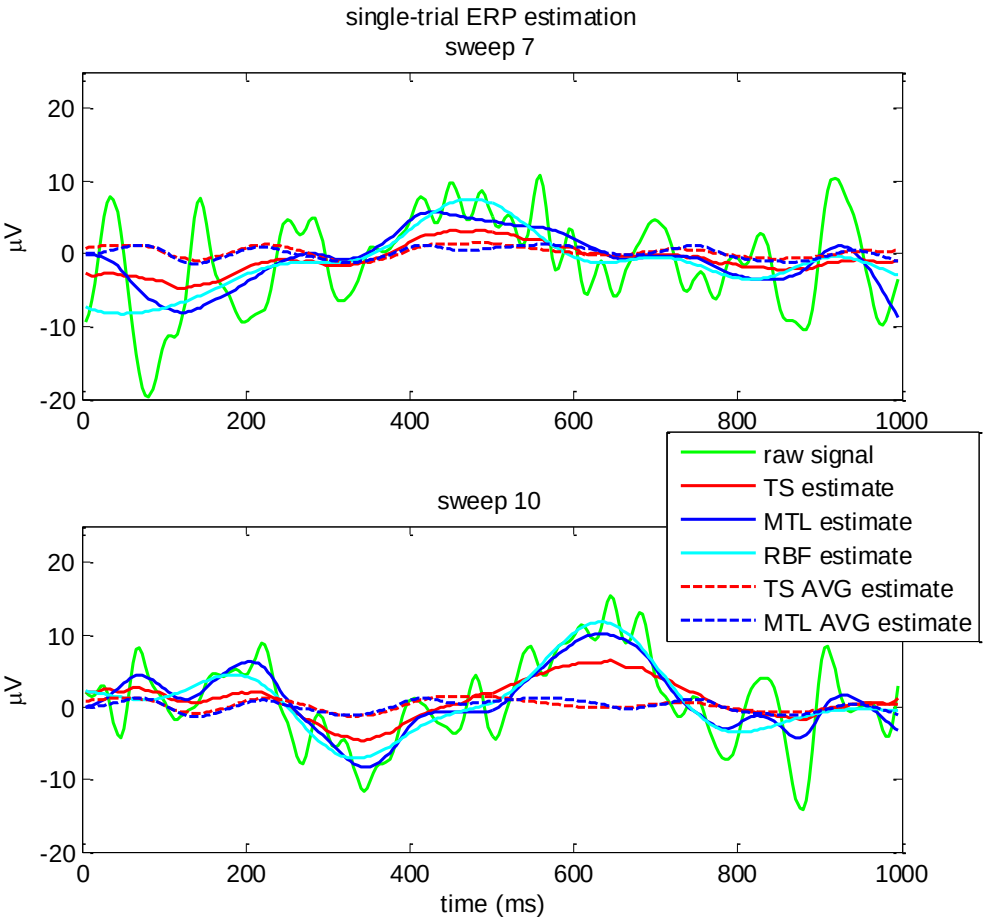

Figure 6.12. Single-trial ERP estimation for a representative cirrhotic subject without MHE (#7). Top panel: results obtained for the sweep #7. Bottom panel: results obtained for the sweep #10. Raw signal (green line), TS single-trial estimate (red line), MTL single-trial estimate (blue line), RBF estimate (cyan line), TS average estimate (dashed red line), MTL average estimate (dashed blue line).

Let us consider the healthy subjects. In many cases the estimates given by the three approaches are quite similar, see for example the top panel of Fig. 6.10 and the bottom panel of Fig. 6.11. Both the RBF methodology that the two Bayesian techniques provide plausible estimates of the single-trial ERP. The two proposed approaches seem to be able to describe the ERP variability by giving single-trial estimates that are a good compromise between the estimate of the average ERP and the data available for the current sweep. See the top panel of Fig. 6.10 or the bottom panel of Fig. 6.11. The single trial estimates diverge from the average

estimate to follow the data. In other cases the single trial estimate is much more similar to the average ERP, see the bottom panel of Fig. 6.10. As regards the comparison between the two Bayesian techniques, the estimates given by the TS method are, as seen in the results regarding the simulated data, smoother than those provided by the MTL method. Moreover, the MTL estimate seems to be more influenced by the data of the current sweep. In general, it seems that, in comparison with the TS method, latencies and amplitudes of the single trial estimates given by the MTL method more easily diverge from those of the average ERP.

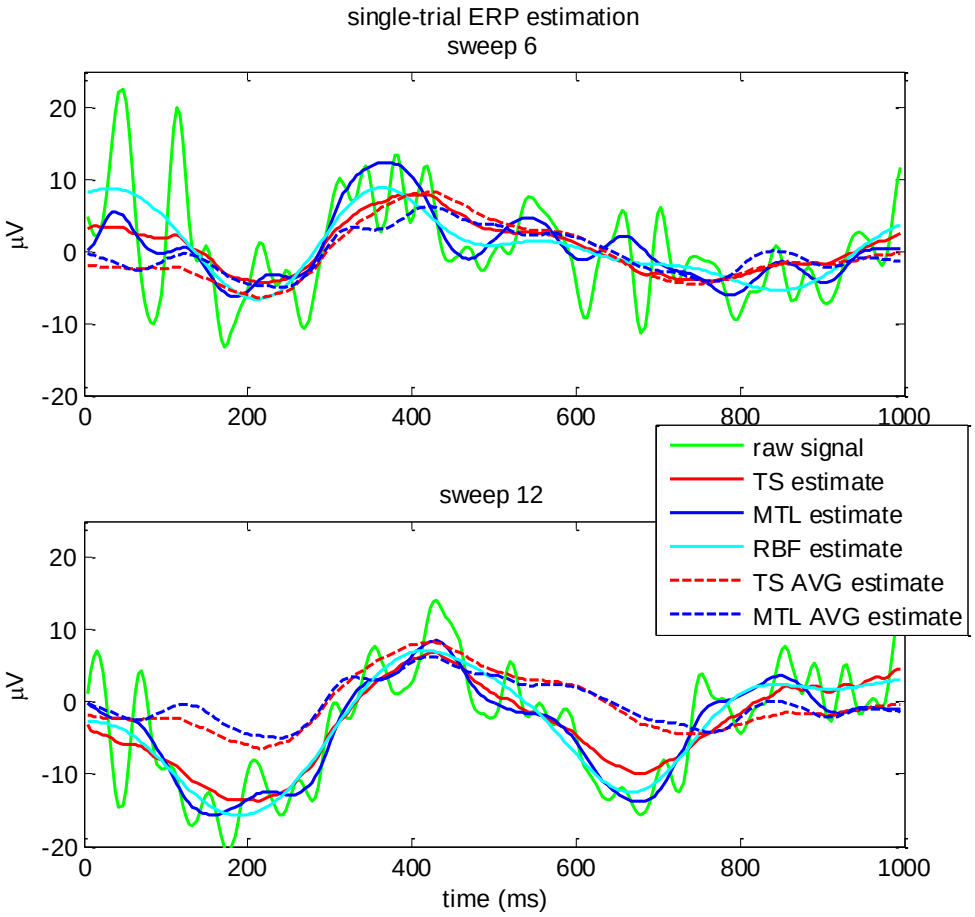

Figure 6.13. Single-trial ERP estimation for a representative cirrhotic subject with MHE (#4). Top panel: results obtained for the sweep #6. Bottom panel: results obtained for the sweep #12. Raw signal (green line), TS single-trial estimate (red line), MTL single-trial estimate (blue line), RBF estimate (cyan line), TS average estimate (dashed red line), MTL average estimate (dashed blue line).

In cirrhotic patients, the ERP signals are smaller in amplitude in comparison with the estimates obtained for the control subjects; see Fig. 6.12 and 6.13 and note the different scale used for the cirrhotic patients. Moreover, the latency of the P300 component seems to be more variable in patients. See for example Fig. 6.12: in two different sweeps of the same subject the P300 latency differs of about 200 ms. These considerations, together with the evidences of the increased intra-individual variability of the reaction times in cirrhosis and of the well-known behavior of the P300 parameters obtained by the CA technique on patients, have encouraged to investigate the variability of the P300 component among trials. These clinical aspects will be discussed in the following section.

6.3 Physiological interpretation of the results

In the following the main results regarding the single-trial estimation of P300 parameters on real data are briefly discussed, see [112] for more details. These results have been obtained by using only the two-stage Bayesian approach of Chapter 3 and by employing all the sweeps available after the pre-processing step, as described in section 6.1. Results in the previous section have been obtained by using only 12 sweeps and only the data recorded from Pz electrode. This case has been studied in order to evaluate, on real data too, the capability of the two new approaches in extracting the ERPs when few sweeps are available. In this section all the sweeps have been used and the data of three electrodes (Pz, Cz and Fz) have been considered, being the interest in the clinical importance of the P300 parameters. In particular, the aim is twofold. It concerns, on the one hand, the investigation of the reasons of the reduction of the average-based P300 amplitude in cirrhosis, on the other hand the study of the connection between the intra-individual variability of the reaction times (RTs) and the individual variability of the P300 parameters.

6.3.1 Average-based P300 amplitude reduction

From several studies it is known that the CA-based P300 amplitude in cirrhotic patients is smaller than that of control subjects [44]. ANOVA analysis of the P300 parameters provided by the CA on the present data and reported in [112], has revealed significantly smaller average-based P300 amplitude in patients with liver cirrhosis compared to control subjects. Here, the availability of single-trial P300 parameters have been used in order to evaluate if this reduction of the P300 amplitude is due to a reduction of the P300 response in each trial, to an increased P300 latency or on both the reasons. The standard deviation (SD) of the P300 latency has been found greater in patients compared to control subjects above all on Pz in the non corresponding conditions. A linear multivariate regression analysis, reported in [112], has revealed that the reduction of the P300 amplitude in cirrhotic patients is related to both an increased latency variability and to a reduced amplitude of the single-trial P300 components. Moreover, the SD of the P300 latencies has been found to negatively correlate with the P300 amplitude provided by the CA, both in normal subjects and in cirrhotic patients without MHE while this correlation is absent in patients with MHE.

6.3.2 Intra-individual variability of RTs and P300 parameters

In a previous study [113] that included a subset of the patients here analyzed, it was reported that the intra-individual variability of the reaction times is higher in patients with MHE in comparison with those without MHE and with healthy control subjects. As regards the behavioral data, ANOVA results on the present data show that an increased intra-individual variability of the RTs have been found in patients with and without MHE. With regard to the relationship between the RTs distribution and single-trial P300 parameters results have shown that in normal subjects P300 latency increases and P300 amplitude decreases with increasing RTs. This pattern is weaker in cirrhotic patients without MHE while it is completely absent in patients with MHE.

These results reveal that the increased intra-individual variability in cirrhosis can be partially related to an alteration of the brain functions involved in the information processing. Moreover, this interesting finding has given value to the hypothesis of [114] that the P300 component is not only related to the stimulus evaluation process but it is also implied in the first phase of response selection.

7 CONCLUSIONS

ERPs represent the brain responses related to sensory, cognitive and motor events and they are a very useful tool in cognitive neuroscience. Particular attention is addressed to quantitative evaluation of latency and amplitude of the principal peaks of the ERP waveform; one of the most addressed components in experimental and clinical studies is the P300. The main problem associated to the study of the P300 component, and of all the ERPs in general, is the difficult extraction procedure. The traditionally used approach, the CA technique, presents well-known limitations. It assumes that the ERPs are identical and the EEG stationary among trials. Moreover, a high number of sweeps is often required in order to obtain a stable ERP waveform. These drawbacks have encouraged the development of more sophisticated methodologies in order to reduce the number of sweeps necessary to obtain an interpretable average estimate and to provide a single-trial description of the ERPs. None of the proposed techniques is become a standard and the CA techniques is still the most commonly used method in clinical practice. So, the problem of the ERP extraction remains an open issue.

In this thesis, two Bayesian techniques have been proposed in order to improve the estimate of the average ERP and to provide a single-trial description of the ERPs at the same time. The first method is based on a two-stage procedure. In the first stage each raw sweep is processed by an individual optimal filter by exploiting a 2^{nd} order *a priori* statistical information on the background EEG and on the unknown ERP, then, an average ERP is estimated as weighted averaging of the N filtered sweeps. In the second stage, single-sweep estimation is dealt with within the same framework, by using the average ERP estimated in the previous stage as *a priori* expected response. The second method is based on a one-stage multi task learning Bayesian procedure. Differently from the most estimation approaches, the method provides the estimation of the average and the single-trial responses by processing just once all the N sweeps simultaneously. The

method assumes that the generic sweep can be modelled as the sum of three independent stochastic processes: an average curve of population that is common to all the sweeps, an individual shift that differentiates each sweep from the others, a background EEG noise component varying sweep by sweep. At our best knowledge, this is the first time that a multi-task learning approach has been applied to the ERPs estimation problem.

These methods have been assessed by using simulated data at different SNR levels and compared with three literature methods, the CA technique, the RBF methodology, and the MAX method. With regard the estimation of the average response, results demonstrate that the two techniques provide an significantly improved estimate with respect to that given by the CA. In particular, with the new approaches, the number of sweeps needed for the average ERP estimation can be reduced of about 50 %. This improvement allows to shorten the time of the experiments and this is important to keep participants under stationary conditions, above all if tasks involving attention are considered. Moreover, the reduction of sweeps is needed for those subjects, such as patients or children, who do not tolerate long-lasting experiments. As regards the single-trial estimation, the two procedures have been evaluated, in comparison with the RBF technique and the MAX method, both in terms of errors in estimating the ERPs profiles and in determining the P300 latency and amplitude. In terms of errors in the estimating the ERPs profiles, the two Bayesian techniques have a significantly better performance with respect the RBF methodology, and the difference is more evident if the number of available sweeps increases. This is because the two Bayesian techniques are positively influenced by the increasing of the available sweeps. With regard the determination of the P300 amplitude latencies, the two proposed techniques and the RBF approach give similar results, while the worst performance is given by the MAX method.

Satisfactory average and single-trial estimates have been obtained also on real data. In particular, interesting results regarding the estimation of the P300 parameters have been obtained with regard the comparison between cirrhotic

patients and control subjects. It has been shown that the P300 amplitude in cirrhotic patients is related to both an increased latency variability and to a reduced amplitude of the single-trial P300 components. Moreover, the negative correlation between the SD of the P300 latencies and the P300 amplitude provided by the CA was absent in patients with MHE. An increased intra-individual variability of the P300 latency in patients compared to control subjects has been found, together with the increased intra-individual variability of the reactions times. With regard to the relationship between the RTs distribution and single-trial P300 parameters results have shown that in normal subjects P300 latency increases and P300 amplitude decreases with increasing RTs. This pattern is weaker in cirrhotic patients without MHE while it is completely absent in patients with MHE. So, these results have revealed that the increased intra-individual variability in cirrhosis can be partially related to an alteration of the brain functions involved in the information processing.

Further developments of the present work will regard the assessment of the techniques on EEG data recorded during brain-computer interface sessions, where the available trials are often few and the application to the study of signals different from the ERPs, such as the hemodynamic responses recorded by functional near-infrared spectroscopy.

REFERENCES

[1] M.A. Patestas and L.P. Gartner, *A textbook of Neuroanatomy*, Malden, MA, USA: Blackwell Publishing Ltd, 2006.

[2] V.S. Ramachandran, ed., *Encyclopedia of the Human Brain*, San Diego, CA, USA: Academic Press, 2002.

[3] D. Purves, G.J. Augustine, D. Fitzpatrick, W.C. Hall, A. LaMantia, J.O. McNamara, and L.E. White, eds., *Neuroscience*, Sunderland, MA, USA: Sinauer Associates Inc., 2008.

[4] S. Sanei and J.A. Chambers, *EEG Signal Processing*, Chichester, West Sussex, England: John Wiley & Sons Inc., 2007.

[5] P. Nunez and R. Srinivasan, *Electric Fields of the Brain. The Neurophysics of EEG.*, New York, NY, USA: Oxford University Press, 2006.

[6] S. Tong and N.V. Thakor, eds., *Quantitative EEG Analysis Methods and Clinical Applications*, Norwood, MA, USA: Artech House Publishers, 2009.

[7] W.O. Tatum, A.M. Husain, S.R. Benbadis, and P.W. Kaplan, *Handbook of EEG interpretation*, New York, NY, USA: Demos Medical Publishing, 2008.

[8] S. Makeig, A.J. Bell, T. Jung, and T.J. Sejnowski, "Independent Component Analysis of Electroencephalographic Data," *Advances in neural information processing systems 8*, D. Touretzky, M. Mozer, and M. Hasselmo, eds., Cambridge, MA, USA: The MIT Press, 1996, pp. 145-151.

[9] G.C. Filligoi, L. Capitanio, F. Babiloni, L. Fattorini, A. Urbano, and S. Cerutti, "Reduction of ocular artefacts in source current density brain mappings by ARX2 filtering," *Med. Eng. Phys.*, vol. 17, 1995, pp. 282-290.

[10] A. Nait-Ali, ed., *Advanced Biosignal Processing*, Berlin - Heidelberg, Germany: Springer Berlin Heidelberg, 2009.

[11] T. Yamada and E. Meng, *Practical Guide for Clinical Neurophysiologic Testing: EEG*, Philadelphia, PA, USA: Lippincott Williams & Wilkins, 2009.

[12] T.C. Handy, ed., *Brian Signal Analysis - Advances in Neuroelectric and Neuromagnetic Methods*, Cambridge, MA, USA: The MIT Press, 2009.

[13] A. Mouraux and G.D. Iannetti, "Across-trial averaging of event-related EEG responses and beyond.," *Magn. Reson. Imaging*, vol. 26, 2008, pp. 1041-54.

[14] S.J. Luck, *A Introduction to the Event-Related Potential Technique*, Cambridge, MA, USA: The MIT Press, 2010.

[15] J. Polich and K.L. Herbst, “P300 as a clinical assay: rationale, evaluation, and findings.,” *Int. J. Psychophysiol.*, vol. 38, 2000, pp. 3-19.

[16] J.D. Kropotov, *Quantitative EEG, Event-Related Potentials and Neurotherapy*, San Diego, CA, USA: Academic Press, 2009.

[17] A.M. Halliday, ed., *Evoked Potentials in Clinical Testing*, Edinburgh, UK: Churchill Livingstone, 1993.

[18] J.M. Guérit, “Evoked potentials in severe brain injury,” *Progress in Brain Research*, vol. 150, 2005, pp. 415-426.

[19] G.D. Dawson, “A summation technique for detecting small signals in a large irregular background,” *J. Physiol.*, vol. 115, 1951, pp. 2-3.

[20] L. Sörnmo and P. Laguna, *Bioelectrical signal processing in cardiac and neurological applications*, San Diego, CA, USA: Academic Press, 2005.

[21] H. Riedel, M. Granzow, and B. Kollmeier, “Single-sweep-based methods to improve the quality of auditory brain stem responses Part II : Averaging methods,” *Z Audiol*, vol. 40, 2001, pp. 62-85.

[22] M. Hoke, B. Ross, R. Wickesberg, and B. Lütkenhöner, “Weighted averaging — theory and application to electric response audiometry,” *Electroencephalogr Clin Neurophysiol*, vol. 57, 1984, pp. 484-489.

[23] C.E. Davila and M.S. Mobin, “Weighted averaging of evoked potentials,” *IEEE Trans. Biomed. Eng.*, vol. 39, 1992, pp. 338-45.

[24] J.M. Łęski and A. Gacek, “Computationally Effective Algorithm for RobustWeighted Averaging,” *IEEE Trans. Biomed. Eng.*, vol. 51, 2004, pp. 1280-1284.

[25] J.M. Łęski, “Robust weighted averaging.,” *IEEE Trans. Biomed. Eng.*, vol. 49, 2002, pp. 796-804.

[26] B. Lütkenhöner, M. Hoke, and C. Pantev, “Possibilities and limitations of weighted averaging,” *Biol. Cybern.*, vol. 52, 1985, pp. 409-416.

[27] R. Mühler and H. von Specht, “Sorted averaging – principle and application to auditory brainstem responses,” *Scand Audiol*, vol. 28, 1999, pp. 145-149.

[28] T. Rahne, H. von Specht, and R. Mühler, “Sorted averaging--application to auditory event-related responses.,” *J. Neurosci. Methods*, vol. 172, 2008, pp. 74-8.

[29] C.D. Woody, “Characterization of an adaptative filter for analysis of variable latency neuroelectric signals,” *Med Biol Eng Comput*, vol. 5, 1967, pp. 539-554.

[30] D. Pham, J. Möcks, W. Köhler, and T. Gasser, “Variable latencies of noisy signals: estimation and testing in brain potential data,” *Biometrika*, vol. 74, 1987, pp. 525-533.

[31] L. Gupta, D.L. Molfese, R. Tammana, and P.G. Simos, “Nonlinear Alignment and Averaging for Estimating the Evoked Potential,” *IEEE Trans. Biomed. Eng.*, vol. 43, 1996, pp. 348-356.

[32] R.P. Borda and J.D. Frost, “Error reduction in small sample averaging through the use of the median rather than the mean,” *Electroencephalogr Clin Neurophysiol*, vol. 25, 1968, pp. 391-392.

[33] H. Yabe, F. Saito, and F. Y, “Median method for detecting endogenous event-related brain potentials,” *Electroencephalogr Clin Neurophysiol*, vol. 87, 1993, pp. 403-407.

[34] H. Yabe, “Median method for eliminating infrequent artifacts and identifying the signals blurred by latency jitter and uncertain occurrence,” *Behav Res Meth Instrum Comput*, vol. 30, 1998, pp. 68-77.

[35] Z. Leonowicz, J. Karvanen, and S.L. Shishkin, “Trimmed estimators for robust averaging of event-related potentials.,” *J. Neurosci. Methods*, vol. 142, 2005, pp. 17-26.

[36] D.O. Walter, “A posteriori ``Wiener filtering" of average evoked responses,” *Electroencephalogr Clin Neurophysiol (Suppl.)*, vol. 27, 1969, pp. 61-70.

[37] G. Sparacino, S. Milani, E. Arslan, and C. Cobelli, “A Bayesian approach to estimate evoked potentials.,” *Comput. Meth. Programs Biomed.*, vol. 68, 2002, pp. 233-48.

[38] N.V. Thakor, “Adaptive filtering of evoked potentials.,” *IEEE Trans. Biomed. Eng.*, vol. 34, 1987, pp. 6-12.

[39] C. a Vaz and N.V. Thakor, “Adaptive Fourier estimation of time-varying evoked potentials.,” *IEEE Trans. Biomed. Eng.*, vol. 36, 1989, pp. 448-55.

[40] P. Laguna, R. Jané, O. Meste, P.W. Poon, P. Caminal, H. Rix, and N.V. Thakor, “Adaptive filter for event-related bioelectric signals using an impulse correlated reference input: comparison with signal averaging techniques.,” *IEEE Trans. Biomed. Eng.*, vol. 39, 1992, pp. 1032-44.

[41] M. Furst and A. Blau, “Optimal a Posteriori Time Domain Filter for Average Evoked Potentials,” *IEEE Trans. Biomed. Eng.*, vol. 38, 1991, pp. 827-833.

[42] G.D. Iannetti, L. Zambreanu, G. Cruccu, and I. Tracey, “Operculoinsular cortex encodes pain intensity at the earliest stages of cortical processing as indicated by amplitude of laser-evoked potentials in humans.,” *Neuroscience*, vol. 131, 2005, pp. 199-208.

[43] A.M. Purves and S.G. Boyd, “Time-shifted averaging for laser evoked potentials.,” *Electroencephalogr Clin Neurophysiol*, vol. 88, 1993, pp. 118-122.

[44] A.F. Kramer, D.L. Strayer, and B. J, “Task versus component consistency in the development of automatic processing: a psychophysiological assessment,” *Psychophysiology.*, vol. 28, 1991, pp. 425-437.

[45] J.M. Ford, P. White, O.L. Kelvin, and A. Pfefferbaum, “Schizophrenics have fewer and smaller P300s: a single-trial analysis.,” *Biol. Psychiatry*, vol. 35, 1994, pp. 96-103.

[46] G. Fein and B. Turetsky, “P300 latency variability in normal elderly: effects of paradigm and measurement technique,” *Electroencephalogr Clin Neurophysiol*, vol. 72, 1989, pp. 384-394.

[47] P. Jaśkowski and R. Verleger, “Amplitudes and latencies of single-trial ERP ’s estimated by a maximum-likelihood method.,” *IEEE Trans. Biomed. Eng.*, vol. 46, 1999, pp. 987-93.

[48] A.M. Fjell, H. Rosquist, and K.B. Walhovd, “Instability in the latency of P3a/P3b brain potentials and cognitive function in aging.,” *Neurobiol. Aging*, vol. 30, 2009, pp. 2065-79.

[49] W. Truccolo, K.H. Knuth, A. Shah, S.L. Bressler, C.E. Schroeder, and M. Ding, “Estimation of single-trial multicomponent ERPs: differentially variable component analysis (dVCA).,” *Biol. Cybern.*, vol. 89, 2003, pp. 426-38.

[50] L. Xu, P. Stoica, J. Li, S.L. Bressler, X. Shao, and M. Ding, “ASEO: A Method for the Simultaneous Estimation of Single-Trial Event-Related Potentials and Ongoing Brain Activities.,” *IEEE Trans. Biomed. Eng.*, vol. 56, 2008, pp. 111-121.

[51] H.J. Heinze, H. Kunkel, and W. Massing, “Selective filtering of single evoked potentials by high performance ARMA methods,” *Recent Advances in EEG and EMG Data Processing*, Amsterdam, Holland: Elsevier-North-Holland Biomedical Press, 1981.

[52] H. Rauner, W. Wolf, and U. Appel, “New perspectives to noise reduction in evoked potential processing,” *Signal Processing II: Theory and Applications*, Amsterdam, Holland: Elsevier-North-Holland Biomedical Press, 1983.

[53] S. Cerutti, G. Baselli, D. Liberati, and G. Pavesi, “Single sweep analysis of visual evoked potentials through a model of parametric identification,” *Biol. Cybern.*, vol. 56, 1987, pp. 111-120.

[54] S. Cerutti, G. Chiarenza, D. Liberati, P. Mascellani, and G. Pavesi, “A parametric method of identification of single-trial event-related potentials in the brain.,” *IEEE Trans. Biomed. Eng.*, vol. 35, 1988, pp. 701-11.

[55] D. Liberati, S. Cerutti, E. Di Ponzio, V. Ventimiglia, and L. Zaninelli, “The implementation of an autoregressive model with exogenous input in a single sweep visual evoked potential analysis,” *J Biomed Eng*, vol. 11, 1989, pp. 285-292.

[56] L. Capitanio, G. Filligoi, D. Liberati, S. Cerutti, F. Babiloni, L. Fattorini, and A. Urbano, “ARX filtering of single-sweep movement-related brain macropotentials in mono- and multi-channel recordings.,” *Meth Inform Med*, vol. 33, 1994, pp. 28-31.

[57] R. Magni, S. Giunti, A.M. Bianchi, G. Reni, F. Bandello, A. Durante, S. Cerutti, and R. Brancato, “Single-sweep analysis using an autoregressive with exogenous input (ARX) model,” *Doc. Ophthalmol.*, vol. 86, 1994, pp. 95-104.

[58] L.T. Mainardi, J. Kupila, K. Nieminen, I. Korhonen, a M. Bianchi, L. Pattini, J. Takala, J. Karhu, and S. Cerutti, “Single sweep analysis of event related auditory potentials for the monitoring of sedation in cardiac surgery patients.,” *Comput. Meth. Programs Biomed.*, vol. 63, 2000, pp. 219-27.

[59] P.A. Karjalainen, J.P. Kaipio, K.A. S, and M. Vauhkonen, “Subspace regularization method for the single trial estimation of evoked potential,” *IEEE Trans. Biomed. Eng.*, vol. 46, 1999, pp. 849-860.

[60] P.O. Ranta-aho, a S. Koistinen, J.O. Ollikainen, J.P. Kaipio, J. Partanen, and P. a Karjalainen, “Single-trial estimation of multichannel evoked-potential measurements.,” *IEEE Trans. Biomed. Eng.*, vol. 50, 2003, pp. 189-96.

[61] C.W. Groetsch, *Inverse Problems in the Mathematical Sciences*, Braunschweig, Germany: Vieweg, 1993.

[62] M. Hanke and P.C. Hansen, “Regularization methods for large-scale problems,” *Surv. Math. Ind.*, vol. 3, 1993, p. 253–315.

[63] R.Q. Quiroga and H. Garcia, “Single-trial event-related potentials with wavelet denoising,” *Clin. Neurophysiol.*, vol. 114, 2003, pp. 376-390.

[64] S. Mallat, *A wavelet tour of signal processing*, San Diego, CA, USA: Academic Press, 1989.

[65] L. Cohen, “A primer on time frequency distributions,” *Time–frequency signal analysis*, B. Boashash, ed., Melbourne, Australia: Longman Cheshire, 1992.

[66] E.A. Bartnik, K.J. Blinowska, and P.J. Durka, “Single evoked potential reconstruction by means of wavelet transform,” *Biol. Cybern.*, vol. 67, 1992, pp. 175-181.

[67] T. Demiralp, A. Ademoglu, M. Schürmann, C. Başar-Eroglu, and E. Başar, “Detection of P300 waves in single trials by the wavelet transform (WT).,” *Brain and language*, vol. 66, 1999, pp. 108-28.

[68] A. Effern, K. Lehnertz, G. Fernández, T. Grunwald, P. David, and C.E. Elger, “Single trial analysis of event related potentials: non-linear de-noising with wavelets.,” *Clin. Neurophysiol.*, vol. 111, 2000, pp. 2255-63.

[69] L. Hu, A. Mouraux, Y. Hu, and G.D. Iannetti, “A novel approach for enhancing the signal-to-noise ratio and detecting automatically event-related potentials (ERPs) in single trials.,” *Neuroimage*, vol. 50, 2010, pp. 99-111.

[70] S. Turner, P. Piction, and J. Campbell, “Extraction of short-latency evoked potentials using a combination of wavelets and evolutionary algorithms,” *Med. Eng. Phys.*, vol. 25, 2003, pp. 407-412.

[71] S. Makeig, T.P. Jung, a J. Bell, D. Ghahremani, and T.J. Sejnowski, “Blind separation of auditory event-related brain responses into independent components.,” *Proceedings of the National Academy of Sciences of the United States of America*, vol. 94, 1997, pp. 10979-84.

[72] D. Iyer and G. Zouridakis, “Single-trial evoked potential estimation: comparison between independent component analysis and wavelet denoising.,” *Clin. Neurophysiol.*, vol. 118, 2007, pp. 495-504.

[73] G. Zouridakis, D. Iyer, J. Diaz, and U. Patidar, “Estimation of individual evoked potential components using iterative independent component analysis.,” *Phys. Med. Biol.*, vol. 52, 2007, pp. 5353-68.

[74] T.P. Jung, S. Makeig, M. Westerfield, J. Townsend, E. Courchesne, and T.J. Sejnowski, “Analysis and visualization of single-trial event-related potentials.,” *Hum. Brain Mapp.*, vol. 14, 2001, pp. 166-85.

[75] J. a Rushby and R.J. Barry, “Single-trial event-related potentials to significant stimuli.,” *Int. J. Psychophysiol.*, vol. 74, 2009, pp. 120-31.

[76] R.M. Chapman and J.W. McCrary, “EP component identification and measurement by principal components analysis.,” *Brain Cogn.*, vol. 27, 1995, pp. 288-310.

[77] A.C. Merzagora, F. Bracchi, S. Cerutti, L. Rossi, A. Gaggiani, and A.M. Bianchi, “Evaluation and application of a RBF neural network for online single-sweep extraction of SEPs during scoliosis surgery.,” *IEEE Trans. Biomed. Eng.*, vol. 54, 2007, pp. 1300-8.

[78] C. D ’Avanzo, S. Schiff, P. Amodio, and G. Sparacino, “A Bayesian method to estimate single-trial event-related potentials with application to the study of the P300 variability,” *Accepted pending minor revisions for J. Neurosci. Methods*.

[79] G. Sparacino, S. Milani, V. Magnavita, and E. Arslan, “Electrocochleography potentials evoked by condensation and rarefaction clicks independently derived by a new numerical filtering approach.,” *Audiol Neurootol.*, vol. 5, 2000, pp. 276-91.

[80] S.M. Kay, *Fundamentals of Statistical Signal Processing - Estimation Theory*, Upper Saddle River, NJ, USA: Prentice Hall, Inc., 1993.

[81] G. De Nicolao, G. Pillonetto, M. Chierici, and C. Cobelli, "Efficient Nonparametric Population Modeling for Large Data Sets," *2007 American Control Conference*, Jul. 2007, pp. 2921-2926.

[82] G. Sparacino, G. De Nicolao, and C. Cobelli, "Deconvolution," *Modeling Methodology for Physiology and Medicine*, San Diego, CA, USA: Academic Press, 2001.

[83] W. Gersch, "Spectral analysis of EEGs by autoregressive spectral decomposition o time series," *Math. Biosci.*, vol. 7, 1970, pp. 205-222.

[84] P.B.C. Fenwick, P. Mitchie, J. Dollimore, and G.W. Fenton, "Mathematical simulation of the electroencephalogram using an autoregressive model," *Int J Bio Med Comput*, vol. 2, 1971, pp. 281-307.

[85] M. von Spreckelsen and B. Bromm, "Estimation of single-evoked cerebral potentials by means of parametric modeling and Kalman filtering.," *IEEE Trans. Biomed. Eng.*, vol. 35, 1988, pp. 691-700.

[86] S. Twomey, "The application of numerical filtering to the solution of integral equation of the first kind encountered in indirect sensing measurement," *J Franklin Inst*, vol. 279, 1965, pp. 95-109.

[87] G. De Nicolao, G. Sparacino, and C. Cobelli, "Nonparametric input estimation in physiological systems: Problems, methods, and case studies," *Automatica*, vol. 33, 1997, pp. 851-870.

[88] M. Neve, G. Denicolao, and L. Marchesi, "Nonparametric identification of population models via Gaussian processes," *Automatica*, vol. 43, 2007, pp. 1134-1144.

[89] G. Pillonetto, G. Denicolao, M. Chierici, and C. Cobelli, "Fast algorithms for nonparametric population modeling of large data sets," *Automatica*, vol. 45, 2009, pp. 173-179.

[90] L. Aarons, "Software for population pharmacokinetics and pharmacodynamics," *Clin. Pharmacokinet.*, vol. 36, 1999, pp. 255-264.

[91] L.B. Sheiner and J.L. Steimer, "Pharmacokinetic/pharmacodynamic modeling in drug development," *Annual Review of Pharmacology and Toxicology*, vol. 40, 2000, pp. 67-95.

[92] L.B. Sheiner, B. Rosenberg, and V.V. Marathe, "Estimation of population characteristics of pharmacokinetic parameters from routine clinical data," *J Pharmacokinet Biopharm*, vol. 5, 1977, pp. 445-479.

[93] D.J. Lunn, N. Best, A. Thomas, J.C. Wakefield, and D. Spiegelhalter, “Bayesian Analysis of Population PK/PD Models: General Concepts and Software,” *J. Pharmacokinet. Pharmacodyn.*, vol. 29, 2002, pp. 271-307.

[94] A. Bertoldo, G. Sparacino, and C. Cobelli, “"Population" approach improves parameter estimation of kinetic models from dynamic PET data.,” *IEEE Trans. Biomed. Eng.*, vol. 23, 2004, pp. 297-306.

[95] F. Ferrazzi, P. Magni, and R. Bellazzi, “Bayesian clustering of gene expression time series,” *Proceedings of 3rd international workshop on bioinformatics for the management, analysis and interpretation of microarray data*, 2003, pp. 53-55.

[96] G.M. Allenby and P.E. Rossi, “Marketing models of consumer heterogeneity,” *J. Econom.*, vol. 89, 1999, pp. 57-78.

[97] N. Arora, G.M. Allenby, and J. Ginter, “A hierarchical Bayes model of primary and secondary demand,” *Marketing Science*, vol. 171, 1998, pp. 29-44.

[98] Greene, *Econometric Analysis*, Upper Saddle River, NJ, USA: Prentice Hall, Inc., 2002.

[99] American Electroencephalographic Society, “American Electroencephalographic Society, Guideline thirteen: guidelines for standard electrode position nomenclature. American Electroencephalographic Society,” *J. Clin. Neurophysiol.*, vol. 11, 1994, pp. 111-113.

[100] P. Ferenci, A. Lockwood, K. Mullen, R. Tarter, K. Weissenborn, and A.T. Blei, “Hepatic encephalopathy--definition, nomenclature, diagnosis, and quantification: final report of the working party at the 11th World Congresses of Gastroenterology,” *Hepatology*, vol. 35, 2002, pp. 716-721.

[101] R.F. Butterworth, “Complications of cirrhosis III. Hepatic encephalophathy,” *J. Hepatol.*, vol. 32, 2000, pp. 171-180.

[102] V. Felipo, “Alterations in neurotransmission in hepatic encephalopathy,” *Hepatic encephalopathy*, Barcelona, Spain: Permanyer, 2008.

[103] J. Córdoba Cardona, “Minimal hepatic encephalopathy,” *Hepatic encephalopathy*, Barcelona, Spain: Permanyer, 2008.

[104] P. Amodio, S. Montagnese, A. Gatta, and M.Y. Morgan, “Characteristics of minimal hepatic encephalopathy,” *Metab. Brain Dis.*, vol. 19, 2004, pp. 253-267.

[105] S. Schiff, D. Mapelli, A. Vallesi, R. Orsato, A. Gatta, C. Umiltà, and P. Amodio, “Top-down and bottom-up processes in the extrastriate cortex of cirrhotic patients: an ERP study.,” *Clin. Neurophysiol.*, vol. 117, 2006, pp. 1728-36.

[106] J.C. Quero, I.J. Hartmann, J. Meulstee, W.C. Hop, and S.W. Schalm, “The diagnosis of subclinical hepatic encephalopathy in patients with cirrhosis using

neuropsychological tests and automated electroencephalogram analysis.," *Hepatology*, vol. 24, 1996, pp. 556-560.

[107] P. Amodio, P. Marchetti, F. Del Piccolo, M. de Tourtchaninoff, P. Varghese, C. Zuliani, G. Campo, A. Gatta, and J.M. Guerit, "Spectral versus visual EEG analysis in mild hepatic encephalopathy," *Clin. Neurophysiol.*, vol. 110, 1999, pp. 1334-1344.

[108] P. Amodio, F. Del Piccolo, E. Petteno, D. Mapelli, P. Angeli, R. Iemmolo, M. Muraca, C. Musto, G. Gerunda, C. Rizzo, C. Merkel, and A. Gatta, "Prevalence and prognostic value of quantified electroencephalogram (EEG) alterations in cirrhotic patients.," *J. Hepatol.*, vol. 35, 2001, pp. 37-45.

[109] J.R. Simon and A.P. Rudell, "Auditory S-R compatibility: the effect of an irrelevant cue on information processing.," *J Appl Psychol*, vol. 51, 1967.

[110] A. Vallesi, D. Mapelli, S. Schiff, P. Amodio, and C. Umiltà, "Horizontal and vertical Simon effect: different underlying mechanisms?," *Cognition*, vol. 96, May. 2005, pp. B33-43.

[111] A. Delorme and S. Makeig, "EEGLAB: an open source toolbox for analysis of single-trial EEG dynamics including independent component analysis.," *J. Neurosci. Methods*, vol. 134, 2004, pp. 9-21.

[112] S. Schiff, C. D 'Avanzo, G. Cona, S. Montagnese, A. Goljahani, P. Bisiacchi, G. Sparacino, and P. Amodio, "Variability of Response Speed and P300 single-trial parameters: Insight from minimal hepatic encephalopathy," *Submitted to Neuroimage*.

[113] S. Schiff, A. Vallesi, D. Mapelli, R. Orsato, A. Pellegrini, C. Umiltà, A. Gatta, and P. Amodio, "Impairment of response inhibition precedes motor alteration in the early stage of liver cirrhosis: a behavioral and electrophysiological study.," *Metab. Brain Dis.*, vol. 20, 2005, pp. 381-92.

[114] R. Verleger, P. Jaskowski, and E. Wascher, "Evidence for an Integrative role of P3b in linking reaction times to perception.," *J. Psychophysiol.*, vol. 19, 2005, pp. 165-181.